Study biofuel and plastic fuel derived from pyrolysis process

Dissertation

zur Erlangung des akademischen Grades eines
Doktors der Naturwissenschaften
– Dr. rer. nat. –

vorgelegt von

Yun Xu

Fakultät für Chemie
der Universität Duisburg-Essen

2020

DOI: 10.17185/duepublico/74408
URN: urn:nbn:de:hbz:465-20230704-123143-1

Die vorliegende Arbeit wurde im Zeitraum von September 2016 bis September 2020 im Arbeitskreis von Prof. Dr. Wolfgang Schrader am Max-Planck-Institut für Kohlenforschung im Mülheim an der Ruhr durchgeführt.

Tag der Disputation: 15.04.2021

Gutachter:	Prof. Dr. Wolfgang Schrader
	Prof. Dr. Oliver J. Schmitz
Vorsitzender:	Prof. Dr. Jochen Gutmann

Erklärung

Hiermit versichere ich, dass ich die vorliegende Arbeit mit dem Titel

“Study biofuel and plastic fuel derived from pyrolysis process”

selbst verfasst und keine außer den angegebenen Hilfsmitteln und Quellen benutzt habe, und dass die Arbeit in dieser oder ähnlicher Form noch bei keiner anderen Universität eingereicht wurde.

Essen, im October 2020

业精于勤而荒于嬉，

行成于思而毁于随。

韩愈

Kurzfassung

Der Verbrauch an fossilen Brennstoffen ist in den letzten 200 Jahren stetig zugenommen. Nach wie vor sind fossile Brennstoffe weltweit die dominierende Energiequelle. Deren übermäßige Verbrauch wirft die große Sorge nach deren Erschöpfung auf und trägt zur Umweltverschmutzung sowie der globalen Erwärmung bei. Darüber hinaus stellt die übermäßige Abhängigkeit von fossilen Brennstoffen auch für die meisten Nationen eine Bedrohung der Energieversorgung und somit der nationalen Sicherheit dar, da fossile Brennstoffe eine ungleichmäßig verteilte Ressource sind und sich hauptsächlich auf einige wenige bestimmte Regionen konzentrieren. Die Nutzung erneuerbarer Energiequellen (z.B. Biomasse) oder von Hausmüll für die Energieerzeugung und den Energieverbrauch trägt dazu bei, diese Probleme auf umweltfreundliche und nachhaltige Weise anzugehen. Unter den Energieerzeugungstechniken, Pyrolyse weckt weltweites Interesse bei Forschern und der Industrie, da sie eine einfach, aber vielversprechende Technik ist, mit der Verkehrskraftstoffe in großem Maßstab hergestellt werden können.

Ziel dieser Arbeit ist die Gewinnung hochwertiger Brennstoffe aus Abfällen mittels Pyrolyse, z.B. Biomasse und Plastikmüll, die in der Regel deponiert werden. Um dieses Ziel zu erreichen, erfordert dies ein detailliertes Verständnis der verschiedenen Pyrolyseölsysteme. Für ein besseres Verständnis des Umwandlungsprozesses muss eine anspruchsvolle Analysemethode entwickelt werden, die das Verstehen der komplexen chemischen Umwandlung ermöglicht. Besonders wichtig ist hierbei, dass die verschiedenen Arten von Verbindungen unterschiedliche Eigenschaften aufweisen.

Für Biobrennstoff, der aus Biomasse (Lignin) mittels Pyrolyse erzeugt wird, lässt sich mit Hilfe der hochauflösenden Massenspektrometrie (HRMS) in Kombination mit komplementären Ionisationstechniken bei Atmosphärendruck (API) ein hoher Anteil von sauerstoffhaltigen Verbindungen nachweisen, was auf die geringe Qualität des erzeugten Biobrennstoffs hindeutet. Von diesem ursprünglichen Biobrennstoff kann erdölartiger Brennstoff durch ein katalytisches Hydrotreating-Verfahren hergestellt werden, das überwiegend aus Kohlenwasserstoffen besteht. Im Vergleich zu Materialien auf Biomassebasis hat kohlenstoffhaltiger Plastikmüll einen höheren Brennwert, von dem einige rein Kohlenwasserstoff basierte Kunststoffe sind (z.B. Polyethylen, Polypropylen, Polystyrol). Eine hocheffiziente Umwandlung von Plastikmüll in Brennstoffe durch Pyrolyse kann nicht nur für einzelne Kunststoffe, sondern auch für komplexe Kunststoffmischungen erreicht werden. Der Reaktionsmechanismus wurde durch die Strukturstudie unter Verwendung von

Gaschromatographie (GC)-Elektronenstoßionisation (EI)-Orbitrap aufgeklärt. Die Semi-Quantifizierung des ursprünglichen Plastik-Pyrolyseöls zeigt, dass die Produkte mit einer breiten Verteilung von Kohlenwasserstoffen zu einem Gemisch aus Verbindungen des Benzin-, Diesel- und Wachsbereichs gehören. Ein Destillationsverfahren im Labormaßstab wurde eingeführt, um Plastik-Pyrolyseöl für unterschiedliche Verwendungszwecke zu trennen.

Abstract

The last 200 years saw an increased consumption of fossil fuel, which until now still remains the dominant energy source globally. Overconsumption of fossil fuel not only raises a big concern of depletion, but also causes a big issue of environment pollution and global warming. Moreover, over dependence on fossil fuel for economic growth poses a threat to energy and national security for most nations as well because fossil fuel is an unequal distributed resource and mainly concentrated on a few specific regions. Turning to renewable energy sources (e.g., biomass) or household waste for energy production and consumption helps address these concerns in an environmentally friendly and sustainable manner. Among energy production techniques, pyrolysis process raises a worldwide interest from researchers and industry as it is a simple but promising technique capable of producing transport fuels in a large scale level.

The aim of this work is to obtain high quality fuels derived from waste resources such as biomass or plastic waste, which are usually deposited, utilizing a pyrolysis process. To achieve this goal, a detailed understanding of different pyrolysis oil systems is required. Additionally, for a better understanding of the conversion process, a sophisticated analytical method needs to be developed that allows analyzing the complex chemical mixtures. The different types of compounds exhibit different properties, which stresses its special importance.

A wide range of oxygen containing compounds can be detected for biofuel derived from biomass or lignin pyrolysis process by using high resolution mass spectrometry (HRMS) in combination with complementary atmospheric pressure ionization (API) technique, indicating the low quality of initial produced bio-fuel. This can be upgraded through a catalytic hydrotreating process to produce petro-like fuel, with the most abundant class detected as hydrocarbon. In comparison to biomass-based materials, carbonaceous plastic waste has a higher heating value, some of which are pure hydrocarbon plastics (e.g., polyethylene, polypropylene, polystyrene). A highly efficient pyrolysis transformation of plastics to fuels can be obtained not only for single plastic, but for complex plastic mixtures as well. The reaction mechanism has been studied by using gas chromatography (GC)-electron ionization (EI)-Orbitrap for detailed analysis. Semi-quantification of initial plastic pyrolysis oil reveals products with a wide carbon atoms distribution, belonging to a mixture of gasoline, diesel and wax range compounds. A lab scale distillation process has been successfully introduced to separate pyrolysis plastic fuels for different purpose of usage.

Contents

Chapter 1 General introduction

1.1 Energy and energy sources

Energy is the driving force of human society and civilization. Nowadays, energy usage is very intensive since the vast invention of machines drives our economy and society. It has almost been incorporated to every part of daily activities, e.g., agriculture, manufacturing, transport, household utilities, which provide a more convenient and comfortable life for us. Lacking of access to affordable energy resources has a negative impact on the economic growth, which can further create a lot of social problems: the increase of unemployment rate, the decrease of life quality and region's instability. Energy security issue, association with national security and the availability to natural energy resources, raises a big concern around the world. Since in 1913, Winston Churchill claimed "…it is not a case of choosing this course against that. On no one quality, on no one process, on no one country, on no one company, and no one route, and on no one oil field must we be dependent. Safety and certainty in oil lie in variety, and in variety alone."[1]

In the 1970s, the world went through two energy crisis (1973 and 1979 oil crisis with the surging of oil price) since there was little substitution to the supply of oil from the Middle East, on which developed economies are highly dependent for economic development.[2] Nowadays, overpopulation, urbanization and economic development especially for developing nations require an increasing demand of energy consumption. On the other hand, fossil fuel still dominates the energy consumption in most countries, the depletion of fossil fuel is another big issue.[3] Furthermore, overusing of fossil fuel is a major contributor to environment pollution and global warming, it is expected to decrease in a foreseeable future. Using renewable energy sources (such as solar, wind power, hydropower and biomass resources) or waste sources (byproducts from biomass and fossil fuel) for energy production and consumption could be the solution to address this challenging problem in an environmental friendly and sustainable manner.[4]

1.2 Biomass to biofuel

1.2.1 Benefits of using renewable biomass

Biomass is an organic matter made up of plants or animals, including various forms: plant wood such as round wood, chips, saw dust, forest residues, agricultural residues such as straw, corn and cotton stover, et al., energy crops such as switchgrass, algae et al., food derived biowaste and recycled papers. The consumption of biomass releases CO_2, which can be

compensated by the production through photosynthesis process using CO_2 and H_2O, converting solar energy into chemical energy. The chemical energy can be stored into carbohydrate molecules such as sugar. It is estimated that a primary production of biomass around 100 billion metric tons of carbon per year is available for the whole world.[5] In addition, using biomass waste does not interfere with the production of plants used for food production.

Unlike fossil fuel unequally distributed and concentrated on several specific nations, biomass is available in various forms for almost every nation in the world and at a large scale level even for countries with the lack of fossil fuel. In developing nations, a significant amount of biomass is burned for cooking and heating. In comparison with other renewable energy sources such as hydropower, solar and wind power, the advantage of using biomass is that it can be used to generate transport liquid fuel (e.g., bioethanol, biodiesel) adaptable for current car industry, which is made up of a significant amount of gasoline and diesel engine cars. Furthermore, biomass generally contains less amounts of sulfur and nitrogen in comparison with conventional fossil fuels, therefore it releases less toxic gas such as SO_2, NO_x, which can lead to less environmental issues (e.g., global warming and acid rain). [6, 7]

1.2.2 Biomass conversion options

Biomass can be transformed into different forms of energy by various conversion processes, the choice of which can be relied on the biomass feedstock type and quantity, desired energy form, project oriented factors, environmental issues among others.[8] Biomass can be exploited in different ways for energy production:[9]

1) Direct combustion of biomass for producing heat, which can be utilized immediately for the purpose of heating and electric power generation. This approach has significant disadvantages such as low efficiency of energy production and undesired ashes accumulation in the air.
2) Transformation of biomass into different types of biofuels via mechanical/chemical, biological/biochemical and thermochemical processes, which are summarized in Figure 1-1.

Lipid-rich oil plants such as soybean, sunflower, rapeseed etc. are widely applied for biodiesel production. Mechanic pressing or squeezing is an efficient approach for extracting vegetable oils from these resources, which are always further processed by transesterification reaction with a small alcohol (normally methanol or ethanol) and a catalyst (KOH, NaOH, and H_2SO_4) to meet requirements of their usages as biodiesel.[10]

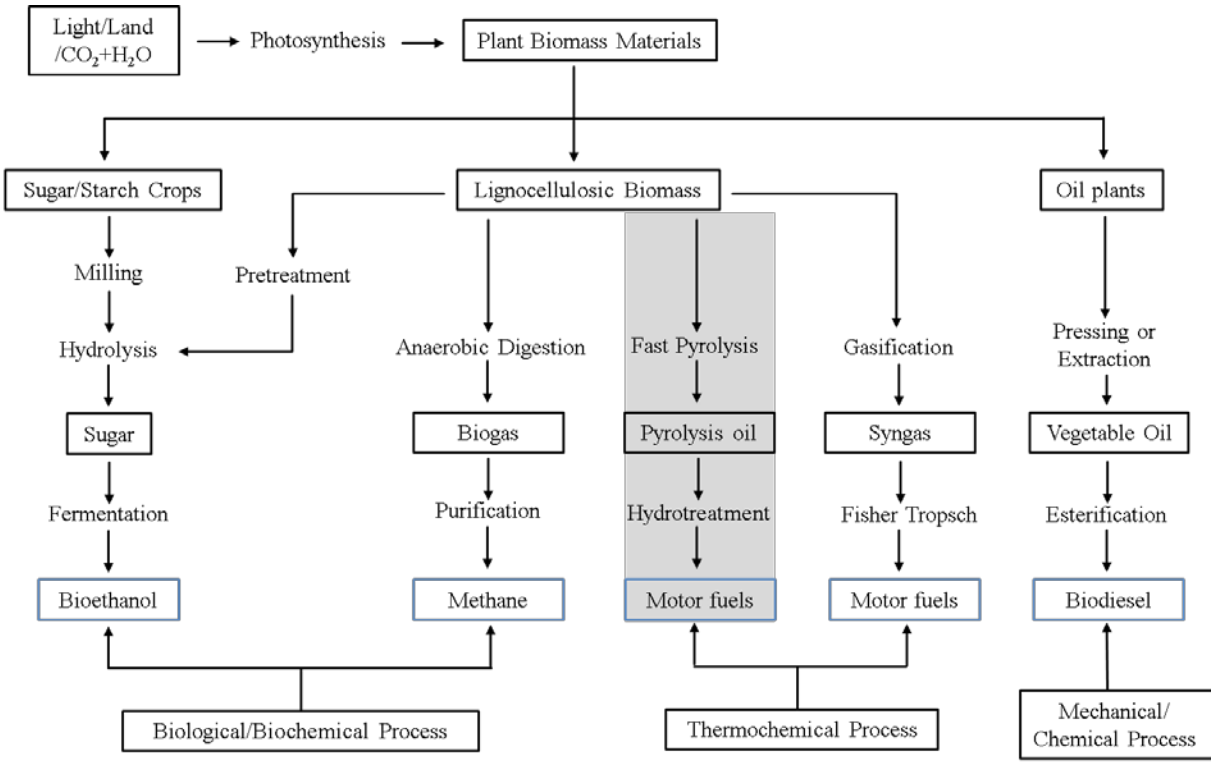

Figure 1-1. Overview of conversion processes for plant biomass materials into biofuel. The gray region highlights our focus in this work.

Biological/biochemical conversion is generally composed of two main processes, fermentation and anaerobic digestion that are often considered to be mature technologies. The complete biochemical conversion process would take a lot of time, which can last for several days. Fermentation is a conversion process for large scale bioethanol production typically by using sugar crops (e.g., sugarcane, sugar beet, etc.) and starch crops (e.g., corn, wheat, etc.) as feedstocks. Carbohydrates have to be initially converted into sugars (e.g., glucose) by hydrolysis process with enzymes, which is followed by microbial fermentation processes.[11] An affordable non-food biomass source, lignocellulosic biomass, can also be used as feedstock for fermentation, the commercial scale plant has already been developed. One disadvantage of using lignocellulose biomass is that lignin is not degradable in this process and has an impact on decreasing enzyme activity. Pretreatment of lignin separation prior to fermentation has to be applied, which raises the cost of the whole energy production process significantly.[12, 13] Anaerobic digestion is mainly used for the purpose of bio-waste management (e.g., municipal, agricultural, industrial biodegradable waste), converting organic materials into so called biogas, a mixture of methane and carbon dioxide. This process involves four key steps: hydrolysis, acidogenesis, acetogenesis and methanogenesis.[14]

Compared to the biological/biochemical conversion process, the thermochemical conversion process finishes in a short time (a few seconds or hours) and virtually can transform any forms of biomass and utilize the whole feedstock. Among thermochemical conversion processes, gasification and pyrolysis are the most investigated conversion technologies. Gasification uses a high temperature (>700 ^{o}C) with a controlled supply of oxygen to convert organic materials (e.g., biomass, coal) into syngas consisting of primarily carbon monoxide and hydrogen and very often some carbon dioxide.[15] Pyrolysis is a thermal decomposition process of organic matter in the absence of oxygen or air at a wide range of temperature. In our work, we mainly focused on the pyrolysis process.

1.2.3 Pyrolysis process for biofuel production

The pyrolysis process receives great attention from researches and industry as it is an easy but promising technique to produce biofuel from cheap biomass on a large scale level. The heart of this process is a pyrolysis reactor and several types of large capacity reactors have already been successfully established including fixed bed reactor, bubbling and circulating fluidized bed reactor, ablative reactor and auger reactor.[16] General changes associated with the pyrolysis process can be listed as follows:[17]

1) Heat transfer from a heater helps to increase the temperature inside the biomass;
2) Primary pyrolysis reaction initialized at a high temperature leads to the formation of char and volatiles;
3) Hot volatiles can be continuously removed and flow towards cooled fuel, which results in heat transfer between them;
4) Condensation of hot volatiles into liquid fuels accompany with the secondary reaction, which can further produce tar;
5) Autocatalytic secondary reactions happen in competition simultaneous during primary reactions due to the formation of catalyst such as carboxylic acid, phenol et al.

As a result, pyrolysis products from biomass contain three parts: condensable liquid, non-condensable gas and biochar. It is well understood from literatures that operating parameters (e.g., heating rate, temperature, residence time, feedstock type) have an impact on the distribution of pyrolysis products. A high temperature, high heating rate and short residence time favor the formation of liquid fuel while opposite conditions show preference for the formation of non-condensable gas. Based on this information, a general pyrolysis process can be classified into slow (carbonization and torrefaction) and fast pyrolysis.[18, 19] Depending on

the extra variant during pyrolysis process, pyrolysis technologies can be expanded to terms: vacuum pyrolysis, catalytic pyrolysis among others.[20-22]

Slow pyrolysis is a process performed at a low temperature and a slow heating rate. Therefore, the volatiles produced during heating do not escape quickly and compounds inside the volatiles generated from primary pyrolysis reaction can still react with each other. A long residence time favors the production of charcoal. Carbonization and torrefaction are widely being mentioned in the literature when discussing about the slow pyrolysis process. Carbonization of biomass is conducted at ~400 ^{o}C with a very low heating rate and the whole reaction time can last for days. The heating rate as low as 0.1-2 ^{o}C min^{-1} was reported.[23] Torrefaction is a mild pyrolysis process, with the aim of increasing the biomass energy density. It can be treated as incomplete carbonization reaction, which is carried out in the temperature range of 225-300 ^{o}C with a low heating rate. Because of the limitation of the low temperature, only water and low volatiles are lost during the process. The final product is dry, solid, blackened material, also termed as torrefied biomass. The drop of biomass weight and volume make it easier for biomass transport over long distance to power plants for further processing.[24, 25]

Fast pyrolysis gains more interest since it produces a high amount of liquid biofuel, which is easier to be stored and transported. To run a successful fast pyrolysis process of biomass, pyrolysis conditions need to be carefully controlled to give high liquid fuel yields. A finely grounding biomass feedstock is required to achieve a good heat transfer. A high heating rate (> 100 ^{o}C min^{-1}) and a high temperature (400-600 ^{o}C) is generally used for heating the feedstock. A short vapor residence time typically < 2 s is widely reported for fast pyrolysis process, which followed by a rapid cooling to prevent vapors further thermal cracking into non-condensable gases.[26-28]

1.2.4 Lignocellulosic biomass and pyrolysis biofuel compositions

Lignocellulosic biomass is most investigated feedstock for producing pyrolysis biofuel because it is cheap and available in a large scale of quantity for industrial process. A review of lignocellulose biomass components and corresponding structures is important to understand biofuel compositions and its physicochemical properties. Lignocellulosic biomass is mainly composed of three polymers: cellulose, hemicellulose and lignin in addition to some extractives such as tannins, fatty acids and resins, et al.[22] Elemental composition analysis on a

basis of 86 varieties of biomass revealed a decreasing order of elements abundance follows as: C, O, H, N, Ca, K, Si, Mg, Al, S, Fe, P, Cl, Na, Mn, and Ti.[29]

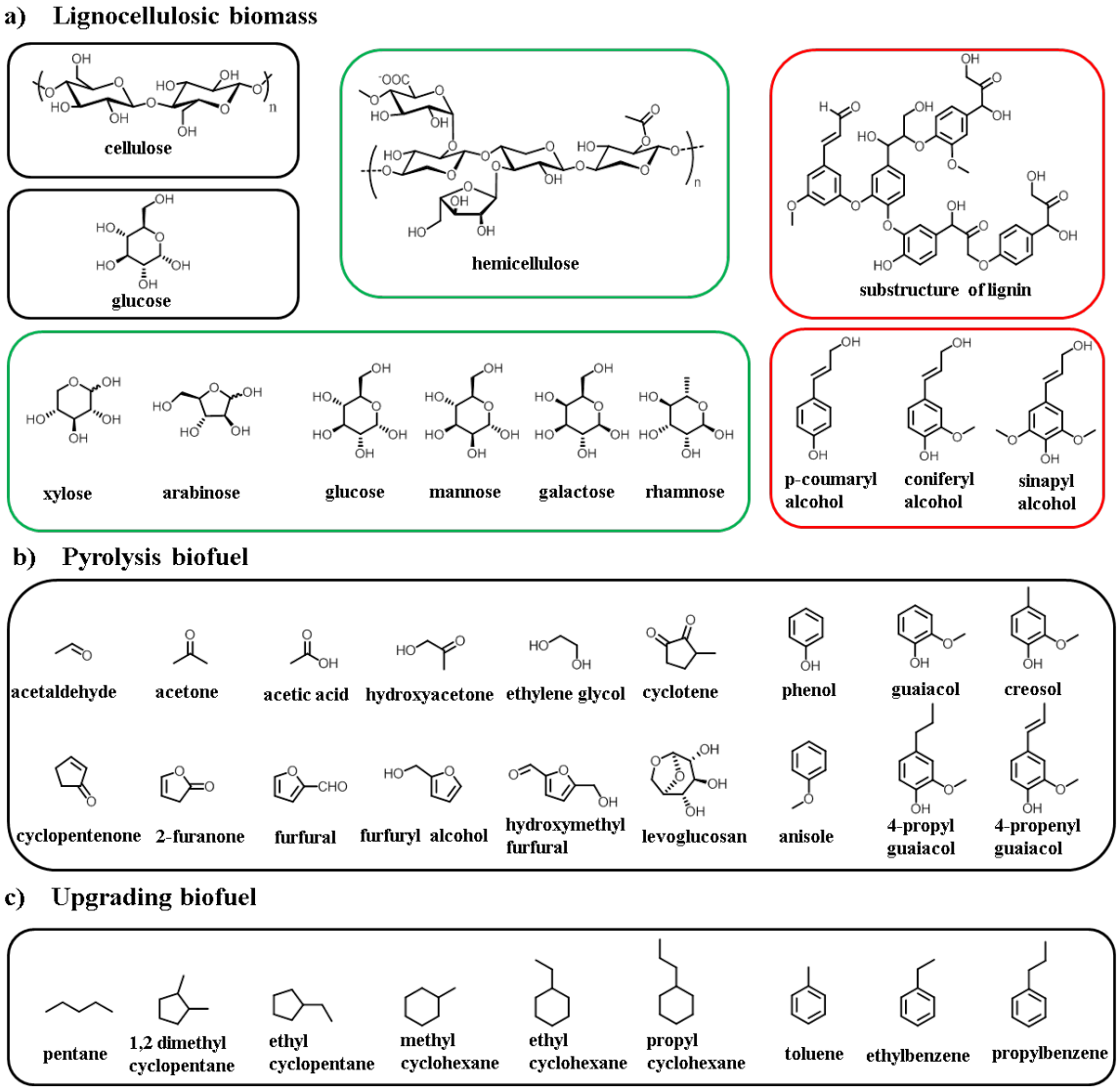

Figure 1-2. a) Three most abundant polymers and their corresponding construction units in lignocellulosic biomass. General identified compounds in pyrolysis biofuel (b) and upgrading biofuel (c) from literatures.[27, 28]

Figure 1-2a shows structures of cellulose, hemicellulose, lignin and their corresponding constructing monomers. Cellulose is a linear homopolysaccharide consisting of hundreds to thousands of glucose units connected by β−1,4-glycosidic bonds and is generally presented with the formula $(C_6H_{10}O_5)_n$.[30] Hemicellulose is a group of heteropolysaccharides and has more complex structures containing different types of sugar units: five carbon sugars (xylose, arabinose), six carbon sugars (mannose, galactose) and six carbon deoxy sugar rhamnose.[31, 32] Lignin is non-linear substituted phenolic polymer built with phenylpropane units, the

precursors of which are mainly composed of three monolignols such as p-coumaryl alcohol, coniferyl alcohol and sinapyl alcohol.[33]

At a high temperature, big polymers (cellulose, hemi-cellulose and lignin) can be cracked down into small fragments. Many studies have tried to reveal the structures of biomass pyrolysis products. As shown in Figure 1-2b, the compounds have a wide range of chemical classes, such as carboxylic acids, ketones, aldehydes, esters, ethers, alcohols, diols, furans, sugars and phenolic compounds. A study shows more than 300 compounds identified by gas chromatography-mass spectrometry (GC-MS) measurements are assigned to oxygenated species. Among these oxygenated compounds, most of the oxygenated aliphatic and furanic compounds are produced from pyrolysis process of cellulose and hemicellulose while the oxygenated phenolic compounds are generated from lignin pyrolysis.[34-36]

1.2.5 Pyrolysis biofuel physicochemical properties

Crude biofuel derived from lignocellulosic biomass pyrolysis process is a dark brown liquid that is made up of a highly complex oxygenated compounds mixture. Table 1-1 makes a comparison of the physicochemical properties between crude biofuel and crude oil.[37] Elemental analysis of a typical pyrolysis biofuel shows a range of 28-40 wt% oxygen, which gives it a high O/C ratio and a low heating value in comparison with fossil fuel. On the other hand, high oxygen content in pyrolysis biofuel is harmful and restricts its direct application as motor fuel. Water is the most abundant component inside pyrolysis biofuel with typical amount of 15-30 wt%, which generally does not separate into organic and aqueous phase. A low pH value of 2.8-3.8 in biofuel is attributed to a remarkable quantity of carboxylic acids, making its corrosiveness to storage materials as well as sealing parts. Also, acid can act as a good catalyst to activate chemical reactions among highly reactive oxygenated compounds and thus crude biofuel is an unstable fuel. These reactions include condensation and polymerization of aldehydes, ketones and phenols which continuously happen and lead to a high viscosity of pyrolysis biofuel as well. [38-40]

1.2.6 Pyrolysis biofuel upgrading

Upgrading process is a necessary step for pyrolysis biofuel to meet motor fuel specification. This includes physical and chemical upgrading processes. Physical upgrading involves hot vapor filtration to remove ash, alkali metals from biofuel, or associates with blending alcohol (or diesel) to increase heating value and biofuel stability. Chemical upgrading is a more effective way as it fundamentally addresses disadvantages of pyrolysis biofuel

physicochemical properties over fossil fuel by removing high oxygen content from the fuel.[9] One of the most widely used approach for chemical upgrading process is called catalytic hydrotreating process which is typically conducted at a high H_2 pressure (up to 20 MPa) and moderate temperature (up to 400 ^{o}C).[41] Two different reactions, hydrogenation and hydrodeoxygenation (HDO), are associated with upgrading process, and as a result, an efficient upgrading process produces a high yield of aromatic and saturated hydrocarbons (Figure 1-2c). Numerous heterogeneous catalysts including metal oxide, microporous materials, supported transition metal catalyst et al. have been exploited for catalytic hydrotreating.[22, 42] Model compounds based on the biomass polymer structures (e.g., phenol) are widely investigated for selectivity study of a specific catalyst and this can helps to improve the upgrading process efficiency of pyrolysis biofuel.[43] Other chemical upgrading approach by using catalytic pyrolysis has also been interested by some researchers and proved to be effective.[44, 45]

Table 1-1. Typical elementary composition and physicochemical properties of crude biofuel and crude oil, adapted from Dickerson et al.[37]

Composition	Biofuel	Crude oil
Water (wt%)	15-30	0.1
pH	2.8-3.8	–
Density (kg L^{-1})	1.05-1.25	0.86-0.94
Viscosity 50 ^{o}C (cP)	40-100	180
HHV (MJ kg^{-1})	16-19	44
C (wt%)	55-65	83.86
O (wt%)	28-40	<1
H (wt%)	5-7	11-14
S (wt%)	<0.05	<4
N (wt%)	<0.4	<1
Ash (wt%)	<0.2	0.1
H/C	0.9-1.5	1.5-2.0
O/C	0.3-0.5	~0

1.3 Plastic waste to fuel

1.3.1 Plastics

Human has a long history of using plastics, dating back to 1284 with first recorded mention of using horn and tortoiseshell as natural plastic.[46] The rapid evolution of plastics happened until 19th century, exploiting from using natural materials (e.g., chewing gum) to chemically modified natural materials (e.g., nitrocellulose, galalite). The invention of bakelite by Leo Beekland in 1907 defined a new era of synthesizing plastics by using no molecules found in nature.[47] Hermann Staudinger in 1920 proposed a fundamental understanding of polymers, which generally have a high molecular weight and is linked by successive small molecule units.[48, 49] Since then, a variety of plastics including polypropylene (PP), low/high density polyethylene (L/HDPE), polyester (PET), polystyrene (PS), polyvinyl chloride (PVC), et al., have been invented and commercialized. Plastics generally have a good durability, heat resistance, being capable for mechanical mass production and being shaped or molded into almost any form, thus, it provides endless possibilities. Every year, an average 4% of fossil fuel consumption is used for producing plastic feedstocks and another 3-4% is consumed to provide energy for making plastic products. These plastics have been manufactured into diverse products, such as packages, soft bottles, textiles, toys, electronic devices, et al.

1.3.2 Plastics waste disposal

Figure 1-3 shows a life cycle of plastic products. Plastics are not easily degraded since they are mainly made up of hydrocarbons. The natural degradation time can range from decades to even centuries.[50] Therefore, the recycling process is essential for plastic waste disposal. In 1988, the society of plastics industry (SPI) adopts to use the resin identification codes (RIC) as an industry-wide standard, aiming to make it easier for identifying and sorting recyclable plastic. Seven RIC are defined by SPI, with PET, HDPE, PVC, LDPE, PP and PS assigned from 1 to 6, respectively.[51] The sorting process can be conducted by manual sorting or by automatic sorting systems to differentiate resins, using a various detection sensors that depend on near-infrared, laser spectroscopy, et al.[52] Generally, plastic recycling process can be categorized into two major types: 1) mechanical recycling, where plastic is sorted, cleaned and regenerated; 2) chemical recycling, where plastic is degraded into basic components.[53] In reality, the recycling process is a more complicated issue. The additives, including functional additives, colorants, fillers and reinforcements, are added in plastic to make a defined color, shape and texture in final products.[54] As well, the material properties of polymers limit the

number of times that products can be recycled. Therefore, even the same type plastic waste cannot be easily combined to directly make new products. Nowadays recycling facilities prefer to recycle PET beverage bottles and HDPE containers like milk jugs as they are relatively clean and homogeneous. It makes extraction worthwhile for recyclers to handle a large quantity of them.[55]

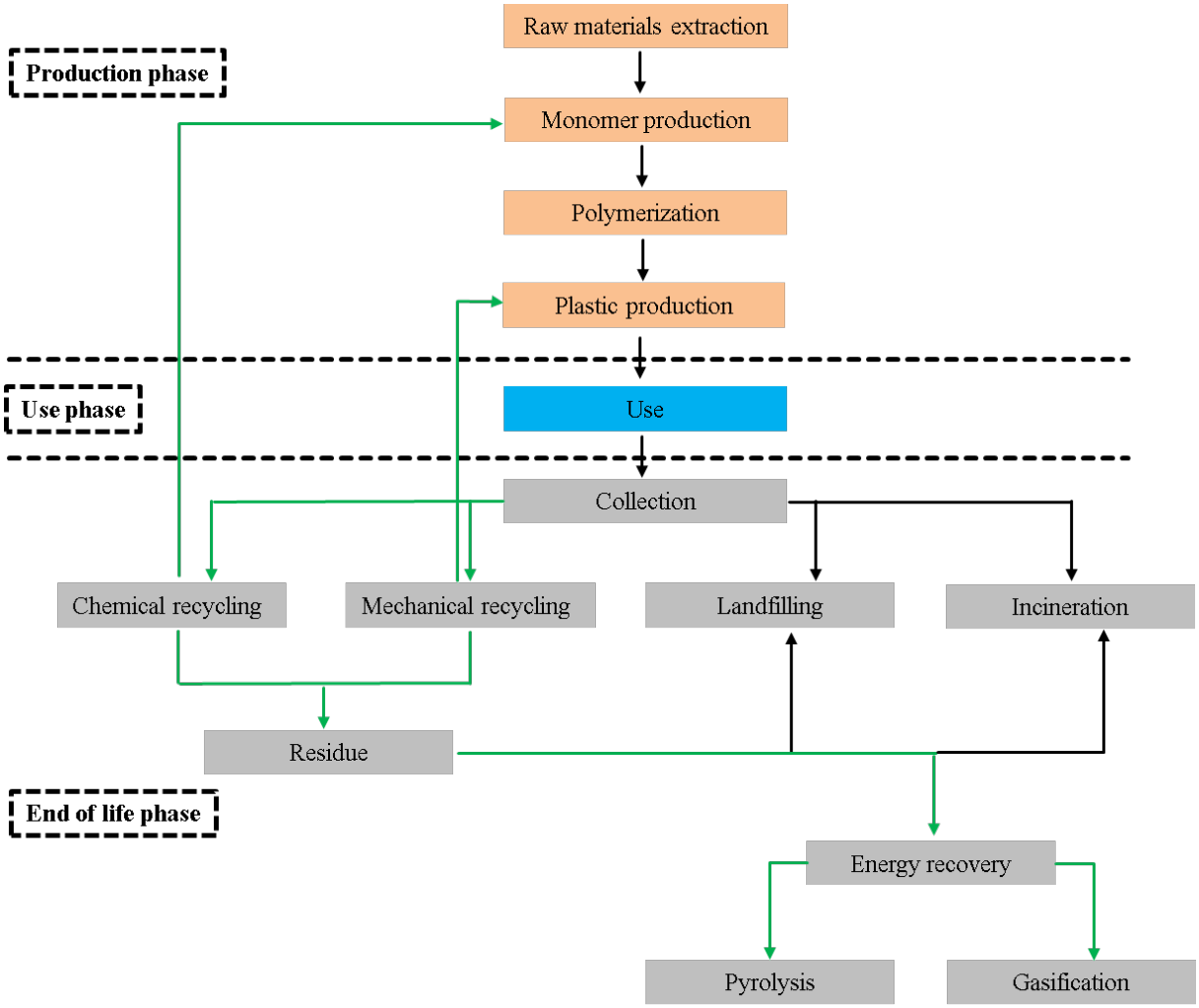

Figure 1-3. The lifecycle of plastic products. A preferred waste management is highlighted in green color.

Wide applications of plastics also cause wide global environmental, health and economic issues. Decreasing quality of plastics and plastics waste mismanagement leads to a large amount of plastics waste that typically ends up landfilling, dumping into oceans and incineration. Ingestion of plastics or entanglement harms marine wildlife, which has a negative impact on ecosystem health and fisheries sustainability. The consumption of plastic contaminated seafood also poses a health risk for human through chemical bio-accumulation. Coastal tourism can be negatively affected since tourists turn to get away from those beaches

that are highly plastic polluted.[56] Incineration of plastics waste releases toxic gases and metal in the smoke, although it generates heat and electricity.[57, 58] Last but not least, new plastic production filling the market demand requires fossil fuel input. This process is energy-intensive and releases a significant amount of greenhouse gas emissions.

In the past, for developed nations, it is a more cost-effective way to export low value plastics waste into developing nations. In 2016, around 14.1 million tones (or 4%) out of the total 355 million tons of plastics were exported outside the original country.[59] China, the largest import market of plastics waste, accounts for around 7.35 million tons (or 52%) of global imports.[60] In 2017, a notification was sent from China to WTO and Basel Convention to restrict the import of hazardous wastes and disposals due to protection of human health and environment.[60] Considering the lack of effective waste disposal infrastructures and the significant amount of waste, diverting exports to other developing nations (e.g., India, Indonesia, Viet Nam) is not a feasible solution. Stockpiles of waste calls for a stricter, more effective waste management and seek alternative solutions to address this issue locally as well.

1.3.3 Pyrolysis process for plastic fuel production

Plastics derived from fossil fuel industry have a high content of hydrocarbons containing high calorific value (CV) and are definitely good energy resources. Production of fuels from plastics waste can simultaneously tackle the challenging issue of increasing energy demand and plastic waste management. Pyrolysis process of plastics waste provides such an option to transform plastics waste into fuels. Not all plastics are suitable for energy recovery. Pyrolysis of plastic PVC containing a high content of chloride (theoretically 56.8 wt%) leads to the formation of HCl gas (around 57.1 wt%) at a low temperature range of 220-360 ^{o}C, which shows corrosion to the pyrolysis equipment.[61] For non-heteroatom containing plastics (PP, PS and L/HDPE), pyrolysis process at a temperature higher than 500 ^{o}C generally has high energy transformation efficiency, producing little char or almost no char. The condensed fuel is typical a mixture of gasoline, diesel and sometimes also wax. In respect of compositions, condensed liquid fuel or wax is mainly composed of toluene, styrene and their oligomers from PS, as well as aliphatic compounds from PP and L/HDPE.[62] Catalytic pyrolysis process is also exploited to achieve a high density jet fuel or to obtain a complete full gasoline range fuel.[63-65]

1.3.4 Plastic fuel distillation

Distillation is an essential developed fraction method based on boiling points to generate high quality fuels for different application purposes (e.g., liquefied petroleum gas, gasoline,

kerosene, diesel oil) in crude oil refinery process. Hydrocarbons in crude oil with boiling points lower than 350 ^{o}C is distillated through a crude oil distillation unit operated at atmospheric pressure. The residue with compounds that have even higher boiling points is further transferred to a vacuum distillation tower for distillation.[66] This method can also be applied for improving the fuel quality from pyrolysis derived plastic fuel. Plastic pyrolysis volatiles escape from the reactor at a high temperature, which was later condensed. This indicates that compounds with a wide range of boiling points coexist in the condensed products. Many literatures reported that a mixture of gasoline range, diesel range and wax fuels can be obtained from almost all variety types of plastics during this process. To improve the fuel quality from pyrolysis derived plastic fuel, similar distillation procedure should be conducted and then it can be used separately or be blended into similar types of fossil fuel.[67, 68] Generally, the pyrolysis and distillation process are carried out separately due to different operating parameters. A setup with integration of pyrolysis process with distillation process was also been investigated to separate the pyrolysis fuel into different types of fuel.[69]

1.4 Instrumentation

It is a challenging task to understand complex processes such as pyrolysis process of organic polymers (biomass and plastic) or upgrading process of initial pyrolysis fuel as thousands of different chemical compositions are present in the mixtures. A powerful technique for the analysis of such a mixture is to use high resolution mass spectrometry (HRMS). This method is capable of detecting each compound with high mass accuracy. The generation of ions in mass spectrometer is highly selective depending on the ionization technique. Coupling diverse atmospheric pressure ionization (API) techniques with HRMS generates a comprehensive database of compounds' present, and thus it deepens our understanding of the complex reaction systems. Additionally, the application of complementary analytic techniques (e.g., GC-MS) is also important, enabling to achieve more specific information (e.g., compounds' structures, semi-quantification).

1.4.1 Ionization techniques

1.4.1.1 Electron ionization

Electron ionization (EI) is a unique and fundamental ionization technique generally applied in GC-MS for analyzing chemical structures of volatile compounds. It is a hard ionization technique, typically using an electron energy with 70 eV. Vaporized analytes are transferred into gas phase, interacting with high energy electrons emitted by a heated metal coil in

vacuum. Electron-molecule collisions knock out one electron from the analyte to form singly charged radical ion $M^{+\cdot}$. However, due to the excess energy distributed to the ions, single or multiple fragments are being formed. The fragments information for a chemical is well explained based on the functional group in the structure. The fragment fingerprint mass spectra libraries for a wide range of compounds have already been effectively established, which can be used for analyzing an unknown compound.

1.4.1.2 Electrospray ionization

Electrospray ionization (ESI) is probably the most widely used soft ionization method in mass spectrometry. Both single charged and multiple charged quasimolecular ions can be formed and thus ESI can ionize molecules in a wide mass range from low molecular weight chemicals to large molecules up to intact proteins.[70-72] The generated ions can contain protonated cations ($[M+H]^+$, $[M+nH]^{n+}$) and sodium cation ($[M+Na]^+$) ionized in positive mode or deprotonated anions ($[M-H]^-$) in negative mode. ESI is capable of ionizing polar compounds containing heteroatoms N and O. In principle, a liquid solution is loaded into the electrospray nozzle needle applied with a spray voltage of 3-5 kV. Two forces (electrostatic force and surface tension) play an important role in holding the liquid in the needle. The electrostatic force pulls the liquid out of the needle while the surface tension retracts it to minimize the surface area. A so called Taylor cone is formed as a static equilibrium between electrostatic force and surface tension on the surface of the liquid, forming an elliptic shape. Further increasing needle potential breaks this stable state resulting in the ejection of liquid droplets from the Taylor cone tip. Initially, droplets with um size are formed, that undergo solvent evaporation and droplet fission into nm size charged particles assisted by drying gas and heated capillary.[73-75] Two major models explain for this ionization process: one is ion evaporation model (IEM) and the other one is charge residue model (CRM). In the ion evaporation model, droplets shrink by rapid solvent evaporation leads to high surface charge densities, followed by Coulomb explosion until molecular ions are formed in the gas phase.[76] In the charge residue model, ion is repeatedly released accompanying with solvent evaporation and at some point, there is no more solvent with the charge residing on a single molecule.[77]

1.4.1.3 Atmospheric pressure chemical ionization

Atmospheric pressure chemical ionization (APCI) is another soft ionization technique, primarily being capable of detecting low molecular weight compounds with nonpolar and less polar properties, especially useful for ionizing alkyl hydrocarbons. But it is not suitable for

thermally labile compounds' analysis. Typically it produces single charged molecular ions with the form of $[M+H]^+$ or $M^{+\cdot}$ in a positive mode. In APCI, the analyte is dissolved in the solvent and introduced into a silica capillary at a higher flow rate than ESI. The analyte solution evaporates into gases at a high heating temperature (300-500 ^oC), and is ionized by a corona discharge (3-5 kV) at the end of a heated quartz tube with the aid of a high flow rate of nebulizer gas N_2. The ionization mechanism associates with solvent mediated gas phase ion molecule reactions depicted in Scheme 1-1. The reaction is initiated with ionization of N_2^+, N_4^+ as primary ions, activating a cascade reaction to create secondary ions such as H_3O^+ and $[(H_2O)_nH]^+$. The last step involves the collision of analyte with $[(H_2O)_nH]^+$ to form $[M+(H_2O)_mH]^+$, which losses the neutral water clusters form $[M+H]^+$ in the high vacuum of mass analyzer. Depending on the solvent, it can also form protonated solvent clusters $[(ROH)_nH]^+$ for alcohols or radicals for benzene or still protonated water clusters $[(H_2O)_nH]^+$ for chloride solvents. Further reactions with analyte through proton transfer or charge transfer produce protonated or radical ions.[78, 79]

$$N_2 + e \rightarrow N_2^{+\cdot} + 2e$$

$$N_2^{+\cdot} + 2N_2 \rightarrow N_4^{+\cdot} + N_2$$

$$N_4^{+\cdot} + H_2O \rightarrow H_2O^{+\cdot} + 2N_2$$

$$H_2O^{+\cdot} + H_2O \rightarrow H_3O^+ + OH^{\cdot}$$

$$H_3O^+ + (H_2O)_{n-1} \rightarrow [(H_2O)_nH]^+$$

$$[(H_2O)_nH]^+ + M \rightarrow [M + (H_2O)_mH]^+ + (n-m)H_2O$$

$$[M + (H_2O)_mH]^+ \rightarrow [M+H]^+ + mH_2O$$

Scheme 1-1. Reaction mechanism of APCI in a positive mode.[80-82]

1.4.1.4 Atmospheric pressure photo ionization

Similar as APCI, atmospheric pressure photo ionization (APPI) is suitable for ionizing low molecular weight compounds with low polarity and nonpolar character, mainly containing aromatics and double bonds. Those compounds with atoms such as oxygen having lone pair electron, can also be detected. In APPI, the introduction of the sample is injected into the same ion source probe as APCI with similar parameter settings. The big difference is that instead of using a corona discharge for ionization process, a noble gas discharge lamp

(typically Krypton) is installed at the end of probe to emit a photo at 124 nm and 117 nm with the ionization energy (IE) of 10.0 and 10.6 eV, respectively. Also researchers published the use of a hydrogen discharge lamp (IE: 10.2 eV) or an argon discharge lamp (IE: 11.2 eV) as a light source for APPI.[83, 84] As most organic molecules have ionization potentials in the range of 7-10 eV, and thus analyte molecular ions can be directly generated by using a Krypton discharge lamp.[83] Scheme 1-2 depicts the corresponding ionization mechanism. In this process, a photon emitted takes off an electron from a molecule to produce a radical cation. In most cases, the use of a dopant (e.g., toluene, acetone) improves the ionization efficiency. In dopant assisted process, the dopant that has a low ionization potential below the ionization energy provided by discharge lamp, can initially be ionized. The produced dopant radical further undergoes the charge transfer or proton transfer with analyte. Additionally, the dopant radical first reacts with solvent cluster to generate a protonated form of solvent cluster, which then ionize the analyte molecules through proton transfer.[85-87]

$$M + hv \rightarrow M^{+\cdot} + e^-$$

$$M^{+\cdot} + S \rightarrow [M + H]^+ + [S - H]^\cdot$$

$$D + hv \rightarrow D^{+\cdot} + e^-$$

$$D^{+\cdot} + M \rightarrow D + M^{+\cdot}$$

$$D^{+\cdot} + M \rightarrow [M + H]^+ + [D - H]^\cdot$$

$$D^{+\cdot} + S_n \rightarrow [S_n + H]^+ + [D - H]^\cdot$$

$$M + [S_n + H]^+ \rightarrow [M + H]^+ + S_n$$

Scheme 1-2. Reaction mechanism of APPI and dopant assisted APPI in a positive mode. S and D stand for solvent and dopant, respectively.[86]

1.4.2 High resolution mass spectrometry

1.4.2.1 Mass resolution and mass accuracy

After the generation of charged particles from neutral analytes in the ionization source, ions have to be separated based on their mass-to-charge ratio (*m/z*). This task is conducted by a mass analyzer, the two important parameters of which are mass resolution and mass accuracy determining its capability of analyzing a complex sample. Mass resolution is defined by its ability to separate two adjacent peaks in a mass spectrum. It can be calculated with the equation as: $R = m/\Delta m$, where m is the mass of a selected ion peak and Δm is the mass

difference of two adjacent peaks. The minimum peak separation Δm in mass spectrometry can be represented by two different ways: (a) valley definition with either 10% or 50%; (b) peak width definition, which is mostly based on full width at half maximum (FWHM).[88] Mass accuracy of a mass spectrometer refers to how close a mass instrument measurement is close to the true value. In mass spectrometry, mass accuracy is presented in a unit of parts per million (ppm). It can be calculated with the formula as: Mass accuracy (ppm) = $(m_{calculated} - m_{observed}) / m_{observed} \times 10^6$.

1.4.2.2 Fourier transform analyzers

Currently, an ultra-high resolving power and mass accuracy can only be achieved by using Fourier transform (FT) based mass analyzers such as Orbitrap or ion cyclotron resonance (ICR).[89, 90] These two instrument types store the ions into either Penning trap or Orbitrap cell. In the cell, these ions are forced to make periodic oscillations and form distinct ion packets in a magnetic field or an electrostatic field. Each ion packet has a distinct frequency which is only depending on mass to charge ratio, regardless of kinetic energy. Once ion packets for all ions pass close to detection electrodes, they induce image current periodically which is further digitalized to a complex time domain signal (the transit). This complex domain signal can be resolved into frequency spectrum by using FT algorithm, resulting in typical mass spectrum with ion abundance versus *m/z*.

1.4.2.3 Hybridization with a linear ion trap

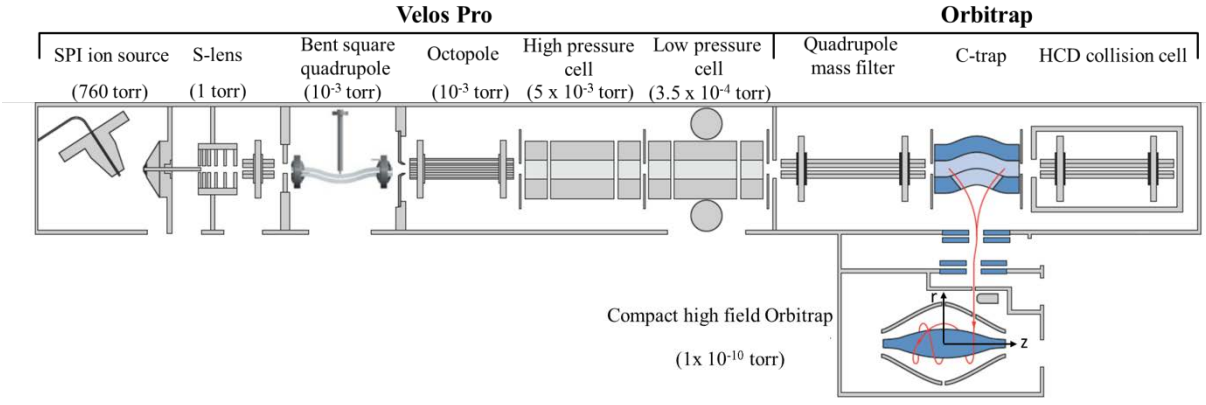

Figure 1-4. Schematic view of Orbitrap Elite mass spectrometer.[91, 92]

In our work, a hybrid mass spectrometer (research-type Orbitrap Elite from Thermo Fisher Scientific) was used and the scheme is shown in Figure 1-4. It combines two different mass

analyzers, dual linear ion trap quadrupole (LTQ, Velos Pro) and high field Orbitrap analyzer. In this instrument, LTQ adopts a dual pressure technology for the process of trapping, storing, selecting, fragmenting ions (high pressure cell) and detecting ions (low pressure cell). A helium gas is present in the high pressure cell, functioning in two ways: a) reduce kinetic energy of ions before their ejection for scanning out, which helps to enhance sensitivity and mass resolution significantly, b) act as a collision activation partner to interact with selected ions for fragmentation process. The resolving power for using ion trap as mass analyzer is limited, typically. In order to run a high mass accuracy measurement, the Orbitrap analyzer has to be used. A key development associated with practical implementation of the Orbitrap as a high resolution mass analyzer is to use an external forcusing device, so called C-trap which is radiofrequency (RF)-only bent quadrupole. Ions are stopped and accumulated to a certain volume in the C-trap by a gentle collision with N_2 gas. As the RF voltage is ramped down and a high voltage puzzle is applied across the trap, the ions were squeezed into short ion packets with different m/z and ejected onto the entrance aperture of the analyzer with an offset from its equator.

Orbitrap analyzer is a modified 'Knight-style' Kingdon trap with two well shaped coaxial electrodes, an outer barrel-like electrode (split in half at z = 0) and an inner spindle-like electrode.[93] Ramping the voltage on the inner electrode, the radius of ions get squeezed further a few percent and the ions starts to move towards the center. The ions thus are rotating around the central spindle electrode, and additionally perform radial as well as axial oscillations. With only a period of 50-100 oscillations in the Orbitrap, the ions of a given *m/z* uniformly distribute along a thin ring shaped ion packet. The ion packets for all ions distinctly oscillate back and force along the z-axis of the Orbitrap in an electrostatic field. The ion axial motion is a harmonic oscillation, the angular frequency ω_z of which is given by $\omega_z = \sqrt{\frac{k}{m/z}}$, only depending on *m/z* and instrument constant *k*. Image current produced by axial oscillation is collected continuously when the ion packets pass by the middle of outer electrode.[94]

The Orbitrap used here is a research type Orbitrap Elite, which has several specific features: 1) using a compact high field Orbitrap (radius of inner electrode R1 = 5 mm, radius of outer electrode R2 = 10 mm) instead of a standard Orbitrap (R1 = 6 mm, R2 = 15 mm) 2) using enhanced FT algorithm (absorption mode) instead of fast FT algorithm (magnitude mode) for signal processing.[91, 95] These two improvements allow this instrument to achieve a higher resolving power at a same transit time or a faster scanning speed at a same resolution. As a

result, a resolving power even in excess of 960, 000 at *m/z* 400 can be available at a transit time of 3.04 s.

1.4.3 Gas chromatography

Gas chromatography (GC) is a simple but quite useful technique for the separation of volatile compounds based primarily on compounds' boiling points. In the area of crude oil and pyrolysis derived plastic oil, it has been successfully applied for the simulation of distillation profiles. This developed method allows evaluate a fuel quality achieved from a distillation process according to the retention time.[67, 96] A typical method used in analytic chemistry is to couple gas chromatography with mass spectrometry using electron ionization method available to study the structural information of unknown compounds. GC-MS was widely used for the identification of pyrolysis derived plastic oil, biofuel and its upgrading products.[43, 97] A two dimensional separation technique GC x GC sometimes was also used for a better separation, and results in more compounds can be identified.[98]

1.5 The scope of study

The aim of this work is to study the conversion of municipal solid waste including biomass and plastic materials into hydrocarbon-based transport fuels by using pyrolysis and to gain a detailed understanding of the reaction using sophisticated analytical methods.

Chapter 2 is forcused on the development of analytical method to analyze pyrolysis fuels. Biofuel derived from biomass obtained through pyrolysis comprise of a highly complex mixture was analyzed by using HRMS in combination with complementary API ionization technique (APPI, APCI and ESI). A wide oxygen distribution with maximum of 24 oxygen atoms per molecule was detected in a pyrolysis produced biofuel. A high oxygen content limits its fundamental usage as fuels, and therefore needs to be upgraded to produce petro-like fuel.

Chapter 3 is focusing on the development of a pyrolysis reactor, using it for the pyrolysis of lignin, a very persistent part of biomass. The complex chemical transformation of lignin to fuels through pyrolysis and the following catalytic upgrading process were studied by using HRMS in combination with APCI. This work further addresses the high oxygen content in pyrolysis biofuel derived from lignin. To address this problem and to make a high quality fuel, a catalytic hydrotreating reaction was developed that can significantly remove oxygen.

In Chapter 4, the development of a method to study the pyrolysis of different types of plastic waste is described. This chapter acts as a starting point for the investigation of most commonly used plastic waste in our daily life including PET, L/HDPE, PVC, PP and PS to obtain pyrolysis plastic fuel. The obtained plastic fuels were studied by using GC-EI-Orbitrap. The compositions of the obtained fuels were studied and the corresponding structure of the most important compounds was elucidated for different plastic fuel, enabling us to gain a fundamental understanding of the transformation mechanism.

In Chapter 5, the study conducted both single type plastic and plastic mixture pyrolysis study. A high efficient transformation of plastic into fuel can not only be achieved for single type plastic, but for plastic mixture as well. It is important to understand if there are any interacting effects when different types of waste materials are being used. The obtained plastic fuels were studied by using GC-EI-Orbitrap, which enables to check the fuel quality through semi-quantification. Results show a wide carbon number distribution covering from gasoline range to wax range compounds, and therefore a distillation process was conducted aiming for different fuel-types.

In Chapter 6, studies were applied to gain a deeper understanding of the pyrolysis mechanism of polystyrene through the chemical composition and structural studies. High resolution mass spectrometry allows the determination of detailed compositions with a high mass accuracy. Two different types FT based Orbitrap instruments, GC-EI-Orbitrap and APCI Orbitrap, were applied for this study. Unlike GC-EI-Orbitrap which is more suitable for small, volatile compounds analysis, APCI Orbitrap can provide detailed information for the heavier compounds generated during the pyrolysis process, which has been rarely covered in previous studies.

Finally, a summary of this research is demonstrated in Chapter 7.

Overall, the detailed experimental studies were carried out here to help understand if pyrolysis can be a suitable tool for the production of transport fuels from different types of municipal waste.

1.6 References

1. Branko Terzic Energy Independence and Security: A Reality Check. https://www2.deloitte.com/us/en/insights/industry/power-and-utilities/energy-independence.html (accessed Oct. 26, 2012).
2. Kilian, L., Oil price shocks: Causes and consequences. *Annu. Rev. Resour. Econ.* **2014,** *6,* 133-154.

3. Shafiee, S.; Topal, E., When will fossil fuel reserves be diminished? *Energy Policy* **2009,** *37* (1), 181-189.
4. Jacobson, M. Z.; Delucchi, M. A., Providing all global energy with wind, water, and solar power, Part I: Technologies, energy resources, quantities and areas of infrastructure, and materials. *Energy Policy* **2011,** *39* (3), 1154-1169.
5. Field, C. B.; Behrenfeld, M. J.; Randerson, J. T.; Falkowski, P., Primary Production of the Biosphere: Integrating Terrestrial and Oceanic Components. *Science* **1998,** *281* (5374), 237-240.
6. Vassilev, S. V.; Baxter, D.; Andersen, L. K.; Vassileva, C. G., An overview of the chemical composition of biomass. *Fuel* **2010,** *89* (5), 913-933.
7. Demirbas, A., Biofuels sources, biofuel policy, biofuel economy and global biofuel projections. *Energy Convers. Manage.* **2008,** *49* (8), 2106-2116.
8. McKendry, P., Energy production from biomass (part 2): conversion technologies. *Bioresour. Technol.* **2002,** *83* (1), 47-54.
9. Dhyani, V.; Bhaskar, T., A comprehensive review on the pyrolysis of lignocellulosic biomass. *Renew. Energy* **2018,** *129*, 695-716.
10. Ma, F.; Hanna, M. A., Biodiesel production: a review1Journal Series #12109, Agricultural Research Division, Institute of Agriculture and Natural Resources, University of Nebraska–Lincoln.1. *Bioresour. Technol.* **1999,** *70* (1), 1-15.
11. Rosales-Calderon, O.; Arantes, V., A review on commercial-scale high-value products that can be produced alongside cellulosic ethanol. *Biotechnol. Biofuels* **2019,** *12* (1), 240.
12. Lee, J., Biological conversion of lignocellulosic biomass to ethanol. *J. Biotechnol.* **1997,** *56* (1), 1-24.
13. Limayem, A.; Ricke, S. C., Lignocellulosic biomass for bioethanol production: current perspectives, potential issues and future prospects. *Prog. Energy Combust. Sci.* **2012,** *38* (4), 449-467.
14. Mata-Alvarez, J.; Macé, S.; Llabres, P., Anaerobic digestion of organic solid wastes. An overview of research achievements and perspectives. *Bioresour. Technol.* **2000,** *74* (1), 3-16.
15. Taylor, R.; Howes, J.; Bauen, A., Review of technologies for gasification of biomass and wastes: final report. *NNFCC Project 09* **2009,** *8*.
16. Bridgwater, A. V.; Peacocke, G. V. C., Fast pyrolysis processes for biomass. *Renew. Sust. Energ. Rev.* **2000,** *4* (1), 1-73.
17. Mohan, D.; Pittman Jr, C. U.; Steele, P. H., Pyrolysis of wood/biomass for bio-oil: a critical review. *Energy Fuels* **2006,** *20* (3), 848-889.
18. Crombie, K.; Mašek, O., Investigating the potential for a self-sustaining slow pyrolysis system under varying operating conditions. *Bioresour. Technol.* **2014,** *162*, 148-156.
19. Duman, G.; Okutucu, C.; Ucar, S.; Stahl, R.; Yanik, J., The slow and fast pyrolysis of cherry seed. *Bioresour. Technol.* **2011,** *102* (2), 1869-1878.
20. Garcìa-Pèrez, M.; Chaala, A.; Roy, C., Vacuum pyrolysis of sugarcane bagasse. *J. Anal. Appl. Pyrolysis* **2002,** *65* (2), 111-136.
21. French, R.; Czernik, S., Catalytic pyrolysis of biomass for biofuels production. *Fuel Process. Technol.* **2010,** *91* (1), 25-32.
22. Liu, C.; Wang, H.; Karim, A. M.; Sun, J.; Wang, Y., Catalytic fast pyrolysis of lignocellulosic biomass. *Chem. Soc. Rev.* **2014,** *43* (22), 7594-7623.
23. Antal, M. J.; Grønli, M., The art, science, and technology of charcoal production. *Ind. Eng. Chem. Res.* **2003,** *42* (8), 1619-1640.
24. Bridgeman, T.; Jones, J.; Shield, I.; Williams, P., Torrefaction of reed canary grass, wheat straw and willow to enhance solid fuel qualities and combustion properties. *Fuel* **2008,** *87* (6), 844-856.

25. Prins, M. J.; Ptasinski, K. J.; Janssen, F. J. J. J. o. a., Torrefaction of wood: Part 1. Weight loss kinetics. *J. Anal. Appl. Pyrolysis* **2006,** *77* (1), 28-34.
26. Fan, L.; Zhang, Y.; Liu, S.; Zhou, N.; Chen, P.; Cheng, Y.; Addy, M.; Lu, Q.; Omar, M. M.; Liu, Y.; Wang, Y.; Dai, L.; Anderson, E.; Peng, P.; Lei, H.; Ruan, R., Bio-oil from fast pyrolysis of lignin: Effects of process and upgrading parameters. *Bioresour. Technol.* **2017,** *241*, 1118-1126.
27. Tsai, W.; Lee, M.; Chang, Y., Fast pyrolysis of rice husk: Product yields and compositions. *Bioresour. Technol.* **2007,** *98* (1), 22-28.
28. Miao, X.; Wu, Q.; Yang, C., Fast pyrolysis of microalgae to produce renewable fuels. *J. Anal. Appl. Pyrolysis* **2004,** *71* (2), 855-863.
29. Vassilev, S. V.; Baxter, D.; Andersen, L. K.; Vassileva, C. G.; Morgan, T. J., An overview of the organic and inorganic phase composition of biomass. *Fuel* **2012,** *94*, 1-33.
30. Toor, S. S.; Rosendahl, L.; Rudolf, A., Hydrothermal liquefaction of biomass: A review of subcritical water technologies. *Energy* **2011,** *36* (5), 2328-2342.
31. Ebringerová, A., Structural diversity and application potential of hemicelluloses. *Macromol. Symp.* **2005,** *232* (1), 1-12.
32. Scheller, H. V.; Ulvskov, P., Hemicelluloses. *Annu. Rev. Plant Biol.* **2010,** *61*.
33. Vanholme, R.; Demedts, B.; Morreel, K.; Ralph, J.; Boerjan, W., Lignin biosynthesis and structure. *Plant Physiol.* **2010,** *153* (3), 895-905.
34. Mortensen, P. M.; Grunwaldt, J. D.; Jensen, P. A.; Knudsen, K. G.; Jensen, A. D., A review of catalytic upgrading of bio-oil to engine fuels. *Appl. Catal. A Gen.* **2011,** *407* (1-2), 1-19.
35. Azeez, A. M.; Meier, D.; Odermatt, J. r.; Willner, T., Fast pyrolysis of African and European lignocellulosic biomasses using Py-GC/MS and fluidized bed reactor. *Energy Fuels* **2010,** *24* (3), 2078-2085.
36. Sipilä, K.; Kuoppala, E.; Fagernäs, L.; Oasmaa, A., Characterization of biomass-based flash pyrolysis oils. *Biomass Bioenergy* **1998,** *14* (2), 103-113.
37. Dickerson, T.; Soria, J., Catalytic fast pyrolysis: a review. *Energies* **2013,** *6* (1), 514-538.
38. Oasmaa, A.; Kuoppala, E., Fast pyrolysis of forestry residue. 3. Storage stability of liquid fuel. *Energy Fuels* **2003,** *17* (4), 1075-1084.
39. Demirbas, A., Competitive liquid biofuels from biomass. *Appl. Energy* **2011,** *88* (1), 17-28.
40. Hwang, H.; Oh, S.; Cho, T.-S.; Choi, I.-G.; Choi, J. W., Fast pyrolysis of potassium impregnated poplar wood and characterization of its influence on the formation as well as properties of pyrolytic products. *Bioresour. Technol.* **2013,** *150*, 359-366.
41. Bridgwater, A. V., Review of fast pyrolysis of biomass and product upgrading. *Biomass Bioenergy* **2012,** *38*, 68-94.
42. Rinaldi, R.; Schüth, F., Design of solid catalysts for the conversion of biomass. *Energy Environ. Sci.* **2009,** *2* (6), 610.
43. Zhao, C.; Lercher, J. A., Upgrading pyrolysis oil over Ni/HZSM-5 by cascade reactions. *Angew. Chem. Int. Ed.* **2012,** *124* (24), 6037-6042.
44. Carlson, T. R.; Tompsett, G. A.; Conner, W. C.; Huber, G. W., Aromatic Production from Catalytic Fast Pyrolysis of Biomass-Derived Feedstocks. *Top Catal.* **2009,** *52* (3), 241.
45. Samolada, M.; Baldauf, W.; Vasalos, I., Production of a bio-gasoline by upgrading biomass flash pyrolysis liquids via hydrogen processing and catalytic cracking. *Fuel* **1998,** *77* (14), 1667-1675.
46. Gilbert, M., Plastics Materials: Introduction and Historical Development. In *Brydson's Plastics Materials*, Elsevier: 2017; pp 1-18.

47. Baekeland, L. H., The synthesis, constitution, and uses of Bakelite. *Ind Eng Chem.* **1909,** *1* (3), 149-161.
48. Weber, M.; Deussing, G., Courageous Questioning of Established Thinking: The Life and Work of Hermann Staudinger. *Adv. Polym. Sci.* **2013**, 81-138.
49. Staudinger, H., Über polymerisation. *Ber. Dtsch. Chem. Ges.* **1920,** *53* (6), 1073-1085.
50. Barnes, D.; Milner, P., Drifting plastic and its consequences for sessile organism dispersal in the Atlantic Ocean. *Mar. Biol.* **2005,** *146* (4), 815-825.
51. Berins, M., *Plastics engineering handbook of the society of the plastics industry*. Springer Science & Business Media: 1991.
52. Bruno, E. A., Automated sorting of plastics for recycling. *Infohouse. p2ric. org* **2000**.
53. Ragaert, K.; Delva, L.; Van Geem, K., Mechanical and chemical recycling of solid plastic waste. *Waste Manage.* **2017,** *69*, 24-58.
54. Hahladakis, J. N.; Velis, C. A.; Weber, R.; Iacovidou, E.; Purnell, P., An overview of chemical additives present in plastics: migration, release, fate and environmental impact during their use, disposal and recycling. *J. Hazard. Mater.* **2018,** *344*, 179-199.
55. Hopewell, J.; Dvorak, R.; Kosior, E., Plastics recycling: challenges and opportunities. *Philos. Trans. R. Soc. B: Biological Sciences* **2009,** *364* (1526), 2115-2126.
56. Gregory, M. R., Environmental implications of plastic debris in marine settings—entanglement, ingestion, smothering, hangers-on, hitch-hiking and alien invasions. *Philos. Trans. R. Soc. B: Biological Sciences* **2009,** *364* (1526), 2013-2025.
57. Jung, C.; Matsuto, T.; Tanaka, N.; Okada, T., Metal distribution in incineration residues of municipal solid waste (MSW) in Japan. *Waste Manage.* **2004,** *24* (4), 381-391.
58. Shibamoto, T.; Yasuhara, A.; Katami, T., Dioxin formation from waste incineration. In *Reviews of environmental contamination and toxicology*, Springer: 2007; pp 1-41.
59. Wang, W.; Themelis, N. J.; Sun, K.; Bourtsalas, A. C.; Huang, Q.; Zhang, Y.; Wu, Z., Current influence of China's ban on plastic waste imports. *Environ. Prog. Sustain. Energy* **2019,** *1* (1), 67-78.
60. Brooks, A. L.; Wang, S.; Jambeck, J. R., The Chinese import ban and its impact on global plastic waste trade. *Sci Adv* **2018,** *4* (6), eaat0131-eaat0131.
61. Miranda, R.; Pakdel, H.; Roy, C.; Darmstadt, H.; Vasile, C., Vacuum pyrolysis of PVCII: Product analysis. *Polym. Degrad. Stab.* **1999,** *66* (1), 107-125.
62. Muhammad, C.; Onwudili, J. A.; Williams, P. T., Thermal Degradation of Real-World Waste Plastics and Simulated Mixed Plastics in a Two-Stage Pyrolysis–Catalysis Reactor for Fuel Production. *Energy Fuels* **2015,** *29* (4), 2601-2609.
63. Sun, K.; Huang, Q.; Ali, M.; Chi, Y.; Yan, J., Producing Aromatic-Enriched Oil from Mixed Plastics Using Activated Biochar as Catalyst. *Energy Fuels* **2018,** *32* (4), 5471-5479.
64. Odjo, A. O.; García, A. N.; Marcilla, A., Refinery Nonconventional Feedstocks: Influence of the Coprocessing of Vacuum Gas Oil and Low Density Polyethylene in Fluid Catalytic Cracking Unit on Full Range Gasoline Composition. *Energy Fuels* **2014,** *28* (2), 1579-1593.
65. Zhang, X.; Lei, H., Synthesis of high-density jet fuel from plastics via catalytically integral processes. *RSC Advances* **2016,** *6* (8), 6154-6163.
66. Gary, J. H.; Handwerk, G. E.; Kaiser, M. J., *Petroleum refining: technology and economics*. CRC press: 2007.
67. Sharma, B. K.; Moser, B. R.; Vermillion, K. E.; Doll, K. M.; Rajagopalan, N., Production, characterization and fuel properties of alternative diesel fuel from pyrolysis of waste plastic grocery bags. *Fuel Process. Technol.* **2014,** *122*, 79-90.
68. Kassargy, C.; Awad, S.; Burnens, G.; Kahine, K.; Tazerout, M., Gasoline and diesel-like fuel production by continuous catalytic pyrolysis of waste polyethylene and polypropylene mixtures over USY zeolite. *Fuel* **2018,** *224*, 764-773.

69. Miskolczi, N.; Angyal, A.; Bartha, L.; Valkai, I., Fuels by pyrolysis of waste plastics from agricultural and packaging sectors in a pilot scale reactor. *Fuel Process. Technol.* **2009,** *90* (7), 1032-1040.
70. Loo, J. A., Studying noncovalent protein complexes by electrospray ionization mass spectrometry. *Mass Spectrom. Rev.* **1997,** *16* (1), 1-23.
71. Smith, R. D.; Loo, J. A.; Edmonds, C. G.; Barinaga, C. J.; Udseth, H. R., New developments in biochemical mass spectrometry: electrospray ionization. *Anal. Chem.* **1990,** *62* (9), 882-899.
72. Kauppila, T. J.; Wiseman, J. M.; Ketola, R. A.; Kotiaho, T.; Cooks, R. G.; Kostiainen, R., Desorption electrospray ionization mass spectrometry for the analysis of pharmaceuticals and metabolites. *Rapid Commun. Mass Spectrom.* **2006,** *20* (3), 387-392.
73. Wilm, M. S.; Mann, M., Electrospray and Taylor-Cone theory, Dole's beam of macromolecules at last? *Int. J. Mass Spectrom. Ion Processes* **1994,** *136* (2), 167-180.
74. Kebarle, P.; Peschke, M., On the mechanisms by which the charged droplets produced by electrospray lead to gas phase ions. *Anal. Chim. Acta* **2000,** *406* (1), 11-35.
75. Wilm, M., Principles of Electrospray Ionization. *Mol. Cell. Proteom.* **2011,** *10* (7), M111.009407.
76. Iribarne, J.; Thomson, B., On the evaporation of small ions from charged droplets. *J. Chem. Phys.* **1976,** *64* (6), 2287-2294.
77. Dole, M.; Mack, L. L.; Hines, R. L.; Mobley, R. C.; Ferguson, L. D.; Alice, M. B., Molecular Beams of Macroions. *J. Chem. Phys.* **1968,** *49* (5), 2240-2249.
78. Carroll, D.; Dzidic, I.; Stillwell, R.; Haegele, K.; Horning, E., Atmospheric pressure ionization mass spectrometry. Corona discharge ion source for use in a liquid chromatograph-mass spectrometer-computer analytical system. *Anal. Chem.* **1975,** *47* (14), 2369-2373.
79. Horning, E.; Carroll, D.; Dzidic, I.; Haegele, K.; Horning, M.; Stillwell, R., Atmospheric pressure ionization (API) mass spectrometry. Solvent-mediated ionization of samples introduced in solution and in a liquid chromatograph effluent stream. *J. Chromatogr. Sci.* **1974,** *12* (11), 725-729.
80. Andrade, F. J.; Shelley, J. T.; Wetzel, W. C.; Webb, M. R.; Gamez, G.; Ray, S. J.; Hieftje, G. M., Atmospheric pressure chemical ionization source. 1. Ionization of compounds in the gas phase. *Anal. Chem.* **2008,** *80* (8), 2646-2653.
81. Byrdwell, W. C., Atmospheric pressure chemical ionization mass spectrometry for analysis of lipids. *Lipids* **2001,** *36* (4), 327-346.
82. Valadbeigi, Y.; Ilbeigi, V.; Michalczuk, B.; Sabo, M.; Matejcik, S., Study of atmospheric pressure chemical ionization mechanism in corona discharge ion source with and without NH3 dopant by ion mobility spectrometry combined with mass spectrometry: a theoretical and experimental study. *J. Phys. Chem. A* **2018,** *123* (1), 313-322.
83. Robb, D. B.; Covey, T. R.; Bruins, A. P., Atmospheric pressure photoionization: an ionization method for liquid chromatography− mass spectrometry. *Anal. Chem.* **2000,** *72* (15), 3653-3659.
84. Raffaelli, A.; Saba, A., Atmospheric pressure photoionization mass spectrometry. *Mass Spectrom. Rev.* **2003,** *22* (5), 318-331.
85. Kauppila, T. J.; Kersten, H.; Benter, T., The ionization mechanisms in direct and dopant-assisted atmospheric pressure photoionization and atmospheric pressure laser ionization. *J. Am. Soc. Mass Spectrom.* **2014,** *25* (11), 1870-1881.
86. Terrier, P.; Desmazières, B.; Tortajada, J.; Buchmann, W., APCI/APPI for synthetic polymer analysis. *Mass Spectrom. Rev.* **2011,** *30* (5), 854-874.

87. Klee, S.; Albrecht, S.; Derpmann, V.; Kersten, H.; Benter, T., Generation of ion-bound solvent clusters as reactant ions in dopant-assisted APPI and APLI. *Anal. Bioanal. Chem.* **2013,** *405* (22), 6933-6951.
88. Murray, K. K.; Boyd, R. K.; Eberlin, M. N.; Langley, G. J.; Li, L.; Naito, Y.; Tabet, J. C., IUPAC standard definitions of terms relating to mass spectrometry. *IUPAC MS Terms and Definitions, First Public Draft* **2005**.
89. Gross, M. L.; Rempel, D. L., Fourier transform mass spectrometry. *Science* **1984,** *226* (4672), 261.
90. Hu, Q.; Noll, R. J.; Li, H.; Makarov, A.; Hardman, M.; Graham Cooks, R., The Orbitrap: a new mass spectrometer. *J. Mass Spectrom.* **2005,** *40* (4), 430-443.
91. Michalski, A.; Damoc, E.; Lange, O.; Denisov, E.; Nolting, D.; Müller, M.; Viner, R.; Schwartz, J.; Remes, P.; Belford, M.; Dunyach, J.-J.; Cox, J.; Horning, S.; Mann, M.; Makarov, A., Ultra High Resolution Linear ion Trap Orbitrap Mass Spectrometer (Orbitrap Elite) Facilitates Top Down LC MS/MS and Versatile Peptide Fragmentation Modes. *Mol. Cell. Proteom.* **2011,** *11*, O111.013698.
92. Gross, J. H., Instrumentation. In *Mass Spectrometry: A Textbook*, Gross, J. H., Ed. Springer International Publishing: Cham, 2017; pp 151-292.
93. Knight, R., Storage of ions from laser-produced plasmas. *Appl. Phys. Lett.* **1981,** *38* (4), 221-223.
94. Makarov, A., Electrostatic Axially Harmonic Orbital Trapping: A High-Performance Technique of Mass Analysis. *Anal. Chem.* **2000,** *72* (6), 1156-1162.
95. Lange, O.; Damoc, E.; Wieghaus, A.; Makarov, A., Enhanced Fourier transform for Orbitrap mass spectrometry. *Int. J. Mass Spectrom. Ion Processes* **2014,** *369*, 16-22.
96. Roussis, S. G.; Fitzgerald, W. P., Gas chromatographic simulated distillation-mass spectrometry for the determination of the boiling point distributions of crude oils. *Anal. Chem.* **2000,** *72* (7), 1400-1409.
97. Miandad, R.; Barakat, M. A.; Aburiazaiza, A. S.; Rehan, M.; Ismail, I. M. I.; Nizami, A. S., Effect of plastic waste types on pyrolysis liquid oil. *Int. Biodeteriorat. Biodegradation* **2017,** *119*, 239-252.
98. Cao, Z.; Engelhardt, J.; Dierks, M.; Clough, M. T.; Wang, G. H.; Heracleous, E.; Lappas, A.; Rinaldi, R.; Schüth, F., Catalysis meets nonthermal separation for the production of (Alkyl) phenols and hydrocarbons from pyrolysis oil. *Angew. Chem. Int. Ed.* **2017,** *56* (9), 2334-2339.

Chapter 2 Studying the complexity of biomass derived biofuels

Redrafted from “Xu, Y.; Schrader, W., Studying the complexity of biomass derived biofuels”, will be submitted to *Energies*.

2.1 Abstract

Biofuel produced from biomass pyrolysis process presents a good model of a highly complex mixture. Detailed understanding of its composition is a necessary step for optimizing pyrolysis and further upgrading conditions. The major challenge in understanding the composition of biofuel derived from biomass is potential compounds with high diversity of polarities and dynamic range that can be present. In this work, a comprehensive analysis by applying different resolving power (120k, 240k, 480k and 960k), ionization methods (positive APPI, APCI, ESI and negative ESI) and scan techniques (full and spectra stitching method) was applied for studying the complexity of a pyrolysis biofuel. Using a mass resolution of 960k and spectra-stitching scan technique gave the assigned compositions of 21652 for positive APPI. And the total compositions were significantly expanded by the combination of different ionization methods. A total number of 34472 compositions were finally detected.

2.2 Introduction

The decrease of petroleum resources in combination with economic, environmental, and political concerns associated with a petroleum-based economy leads to the resurgence in the development of alternative substitutions for fossil fuels.[1] Among the renewable energy resources, biofuel derived from biomass feedstocks invokes the interests of scientific community because of the cheap price, high quantity availability and a good reproducibility of feedstocks which allows perform transformation processes in a large scale under industrial conditions. Lignocellulosic biomass is a complex material, mainly consists of cellulose, hemicellulose and lignin in addition to extractives (tannins, fatty acids, and resins) and inorganic salts.[2] The quantity of each component is highly dependent on the type of biomasses, typically containing about 40-47 wt% (weight%) cellulose, 25-35 wt% hemicellulose, and about 16-31 wt% lignin.[3]

One of the most efficient ways to generate bio-oils is fast pyrolysis process, generally carried out at relative high temperature (around 500 ^{o}C), short residence time (several seconds), non-oxydative condition and sometimes the use of a solid state catalyst.[4, 5] The mechanism behind this is called thermal cracking, which enables to break down organic biopolymer into small molecules. However, biomass derived oils usually contain a high amount of oxygen that can reach up to 60 wt%, which limits its fundamental use as energy source because of its low heating value, high corrosiveness, high viscosity and instability, and therefore needs to be upgraded.[2, 6]

For an optimized upgrading procedure, it is important to understand the molecular diversity of bio-oils since they are highly complex mixtures that at least contain thousands of different compounds. Therefore, it is of tremendous importance to use cutting-edge tools for its evaluation. Elemental analysis is a direct and efficient way to determine content of elements in pyrolysis oil. Michael et al.[3] summarized the elemental composition of fast pyrolysis oils for various biomass feedstocks (pine, poplar, oak et al.) from different regions, with the variation of C 37-61%, H 4-8%, O 32-52%, N 0.1-1.2%, S 0.02-0.15% and ppm levels of K, Na and Cl. IR and NMR have also been widely used for addressing the bulk features in complex pyrolysis oil.[7-9] However, these analytic techniques show incapability of revealing any information on a single molecule level. High resolution mass spectrometry (HRMS) is an effective tool for this kind of study since a lot of chemical compounds in pyrolysis oil show very similar molecular masses.[10-12] Separation techniques such as liquid-liquid extraction[13], liquid chromatography[14], et al. prior to mass spectrometry to generate fractions will simplify

the complex mixture for compositional analysis. One or two dimensional GC-MS, which enables to study structural information, has been widely used for mechanistic studies of bio-oil upgrading.[15, 16] However, both of these methods still show disadvantages on the separation efficiency of a wide variety of polar compounds with different volatilities, different response factors resulting a skewed abundance, which could be limiting factors for an in depth compositional analysis.

ESI (electrospray ionization) in negative mode was widely used for characterization of pyrolysis oils in consideration of its acidic property, while positive ESI is more suitable for the analysis of basic compounds. However, single ionization technique generally shows ionization discrimination and therefore, multiple ionization techniques should be considered.[17-19] In comparison with ESI, APCI (atmospheric pressure chemical ionization) and APPI (atmospheric pressure photo ionization) are additional methods for the analysis of non-polar compounds and are more suitable for ionizing aromatic moieties. Referring to the functional groups of the compounds in the pyrolysis derived biofuel, commonly both parts coexist: 1) polar sites including hydroxyl, ketone, aldehyde, carboxylic acid, and 2) non polar sites including phenyl group and aliphatic chains.[20] Based on the preferences provided by a single ionization technique, using diverse complementary ionization techniques in combination with ultra-high resolution mass spectrometry can help to enrich discovered compositions and therefore provides a basis for in-depth data analysis. Fourier transform analyzers, ICR (ion cyclotron resonance)[21] and Orbitrap[22], are the most powerful mass analyzers in terms of mass accuracy and resolving power. In the past, only limited scientific studies dealt with the use of Orbitrap for pyrolysis oil characterization resulting that only a small number of compositions were discovered.[23, 24]

Overall, in order to achieve a better understanding of the chemical components in bio-oil complex mixtures, complementary techniques need to be implemented to study the potential effects. These techniques include the application of different ionization techniques (APPI, APCI and ESI), scan techniques (full and spectra stitching mode) and transient times (0.38 s, 0.77 s, 1.53 s and 3.04 s at *m/z* 400). The 3 s transient time with a mass resolution of 960k at *m/z* 400 was first reported for pyrolysis biofuel characterization. While the structural characterization of fossil fuels is already well advanced, the same cannot be said about biofuel because both polar and non-polar compounds compete during the analysis, which may cause further discrimination. Here, we show a detailed study of molecular analysis of a biomass derived pyrolysis fuel.

2.3 Experimental section

2.3.1 Sample preparation

2.5 mg pyrolysis oil was diluted with 10 mL of methanol (UPLC-MS grade, Biosolve, Netherland) to achieve a final concentration of 250 μg mL^{-1} and used without further treatment.

2.3.2 Instrument and methods

Mass spectra were recorded on a research-type Orbitrap Elite mass spectrometer (Thermo Fisher Scientific, Bremen, Germany) equipped with commercially available ESI, APPI and APCI sources. The mass spectrometer was externally calibrated, resulting in mass accuracy of less than 1 ppm error prior to data collection. The spectra were collected in positive mode using ESI, APPI, APCI and negative mode using ESI. For ESI measurements, the sample was infused at a flow rate of 5 μL min^{-1}, and the ionization was performed with a electrospray ion source with a metal-ESI needle. Positive ESI settings were as follows: needle voltage = 4 kV (positive mode) or 3.5 kV (negative mode), sheath gas = 5 arbitrary units, auxiliary gas = 2 arbitrary units, capillary temperature = 275 ^{o}C, S-lens RF-level = 50%. In the case of APPI and APCI measurements, the sample was infused with a flow rate of 20 μL min^{-1}, evaporated at 350 ^{o}C with the sheath and auxiliary gas flow of 20 and 10 (arbitrary units), respectively. APCI current was set as 5 kV. Photoionization was achieved by a Kr VUV lamp at 10.0 and 10.6 eV for APPI (Syagen Technologies, Tustin, CA, U.S.A.). Several distinct resolutions, approximately 120k, 240k, 480k and 960k at *m/z* 400, were acquired for APPI with mass range of 100-1000 using the spectral stitching method (windows of 30 Da with 5 Da overlap).[25] Additionally, full scan mass spectra with a resolution of 480k were also collected using APPI. In respect of APCI and ESI, only the highest resolution 960k was collected for evaluation.

2.3.3 Data analysis

The acquired mass spectra were initially analyzed and converted by Xcalibur 2.2 (Thermo Fisher Scientific, Bremen, Germany). The converted file was imported and transformed into molecular formulas by Composer V1.5.0 (Sierra Analytics, Modesto, CA, U.S.A.). The applied parameters and chemical constraints were as follows: $C_{0-100}H_{0-1000}N_{0-3}O_{0-30}Na_{0-1}$, 1 ppm tolerance error, and a double bond equivalent (DBE) ranging from 0 to 40. The assignments of the most abundant ions were confirmed by their isotopic peaks. Radical cations and molecular adducts were distinguished and assigned as

X and X[Y] (in this case Y= H or Na). The calculated molecular formulas were sorted into compound classes. The obtained mass list was exported into Excel and later transferred to Origin for data evaluation and Figure preparation. Replicates analysis were carried on by online programmer VENNY 2.1[26] and associated plots were created by offline Venn Diagram Plotter (PNNL, Richland, WA, U.S.A.) [27]from calculated data.

2.4 Results and discussion

Study the complexity of pyrolysis biofuel is a challenging task. The combination of a rich C, H, O atoms with a minor N, S atoms results in an extreme complex elemental compositions mixture. These compositions have a wide range of polarity, abundance. The elucidation of elemental compositions in such a complex mixture by mass spectrometry requires a high resolving power and a good instrument sensitivity. The research type Orbitrap Elite applied in this study can achieve a resolving power with a maximum of 960k. The improved sensitivity can be additionally gained by using a spectra-stitching method. In comparison with full scan, on one hand, it reduces sample complexity in each scan to decrease ion-ion interactions. On another hand, it helps accumulate low abundant compositions and therefore make them being detected by mass spectrometry.

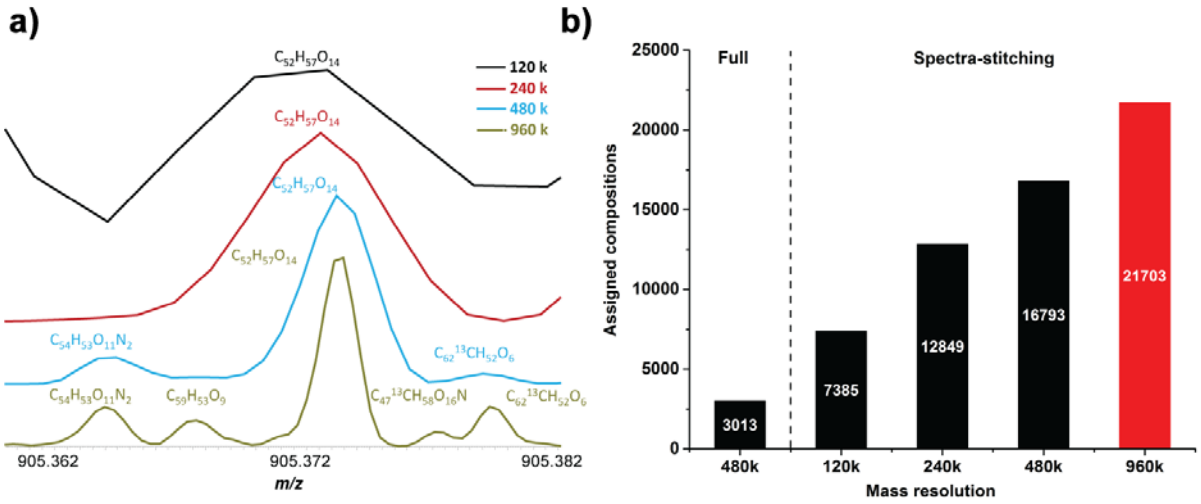

Figure 2-1. a) Zoom in mass spectra comparison from m/z 905.362.25 to 905.382 Da for resolution 120k, 240k, 480k and 960k (from top to down). **b)** Summarized population distribution of different resolution data, spectra-stitching scan for resolution 120k, 240k, 960k and both spectra-stitching and full scans for resolution 480k.

Here, a variety of resolution settings, including 120k, 240k, 480k and 960k at *m/z*= 400, were investigated for APPI by collecting the mass spectra from 100 to 1000 Da. First overview of the mass spectra, measured with different resolving power, shows a similar pattern

(Figure A2-1). However, as zooming into the mass spectra within the mass range of 905.322 to 905.344 Da (Figure 2-1a), a significant difference can be observed. A single mass peak at low resolving power 120k and 240k splits into three peaks at 480k and 5 peaks at 960k. Four more compositions were detected at 960k with two of them detected as isotopic signal.

Generally, using APPI(+) as ionization technique yields both radical and protonated cations at the same time by charge transfer or proton transfer. Figure 2-1b compares the number of assigned unique compositions among different resolving power and scan technique for APPI. The result at resolution 480k shows that spectra-stitching measurements (16793 compositions) gives 5 times more detected compositions in comparison with full scan with only 3013 compositions in total. Even by contrast with the unique composition number at lowest resolution 120k (7385 compositions) in this study, the full scan with much higher resolution 480k still shows significantly smaller number of pyrolysis oil composition detections with less than half of them detected. When using a higher resolution setting of 960k, around 30% higher number of detected compositions is obtained. Therefore, in order to achieve in depth understanding of pyrolysis oil compositions, mass spectra under ultrahigh resolution settings offers the best results to cover the conversion of energy materials. It has to be noted here, that mass spectrometry, although highly accurate and high resolving power, only provides elemental compositions and can alone not separate different isomers.

2.4.1 Ionization effects

The results of a complex mixture characterization by mass spectrometry are highly dependent on the ionization technique applied for the study. To cover a broader view of the sample, it has been shown that multiple ionization techniques are required due to the discrimination effect by using single ionization technique[12, 17]. In this study, four different ionization methods, APPI and APCI both in positive ionization mode and ESI in both positive and negative ionization modes were investigated. The corresponding mass spectra with a resolution of 960k for individual ionization method were compared. Although the same solution was used for these measurements, mass spectra of each ionization technique are completely different (Figure 2-2). The highest peak at individual ionization technique is observed at *m/z* 163.0756 Da for APPI(+), 113.0598 Da for APCI(+), 185.0423 Da ESI(+) and 161.0457 Da for ESI(-), corresponding to composition of $[C_{10}H_{10}O_2+H]^+$, $[C_6H_8O_2+H]^+$, $[C_6H_{10}O_5+Na]^+$ and $[C_6H_{10}O_5-H]^-$, respectively. A mass scale-expanded segment ranging from *m/z* 469.12 to 469.24 Da was selected to compare the detected compositions. The zoom in mass spectra for APPI(+) and APCI(+) shows somehow similar pattern and the major peaks

belong to O_x proton adducts. In ESI(+), the sodium adducts can be widely observed in the whole mass spectra and are the peaks with major intensity although there were no additional sodium-ions added to the sample solution. In ESI(-), major peaks are detected as deprotonated molecules.

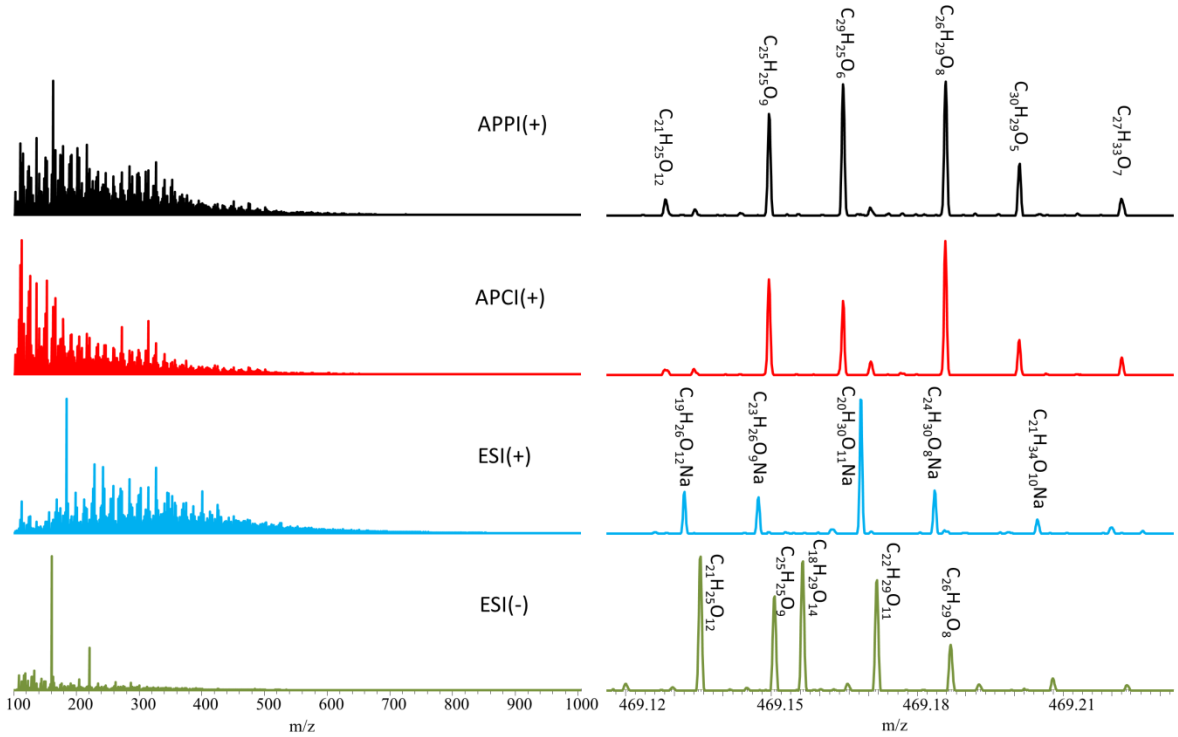

Figure 2-2. Mass spectra comparison using multiple ionization techniques (left graph) and corresponding zoom in mass spectra (right graph) from 409.12 to 409.24 Da at a resolution of 960k.

Due to the mass shift, a more reasonable way to compare these mass spectra is to align them for the same origin compositions according to the mass differences calculated between different types of ions formed at different ionization conditions. The difference of the chemical formulas between sodium adduct ($[M+Na]^+$) and proton adduct ($[M+H]^+$) for the same original composition is the mass difference between H^+ and Na^+, leading to a mass difference of 21.9819 Da. Similarly, the formulas difference of [2 * H^+] is corresponding to mass difference, 2.0146 Da. Based on these mass differences, the mass spectra were compared (Figure 2-3) at *m/z* 409 Da for APPI(+) and APCI(+), 431 Da for ESI(+) and 407 Da for ESI(-), respectively, with a mass window of 0.12 Da by aligning the original composition $C_{26}H_{16}O_5$. A clear difference could be observed for these mass spectra. Assigned compositions $C_{26}H_{16}O_5$, $C_{27}H_{20}O_4$ and $C_{28}H_{24}O_3$ are only detected in APPI(+) and APCI(+). These compositions contain a low oxygen number (5, 4 and 3, respectively) but show a high

DBE value (calculated as 18, 18 and 17, respectively). DBE is the number of ring closures and double bonds in a molecule and can be an indication of the aromaticity of a compound. Some compositions, $C_{16}H_{23}O_{12}$, $C_{17}H_{28}O_{11}$ and $C_{18}H_{32}O_{10}$ are only detected in ESI(+) and ESI(-) which consist of a high oxygen number (12, 11 and 10) and a low DBE (5, 4 and 3). A high oxygen number in the composition indicates a high polarity, ensuring them to have a high affinity to form sodium adducts to facilitate the ionization in ESI(+). Also, a high oxygen number means these compositions contain a high probability of acidic functionalities, such as phenolic, carboxyl acidic group, which allows them to easily lose a proton to form deprotonated molecules in ESI(-).

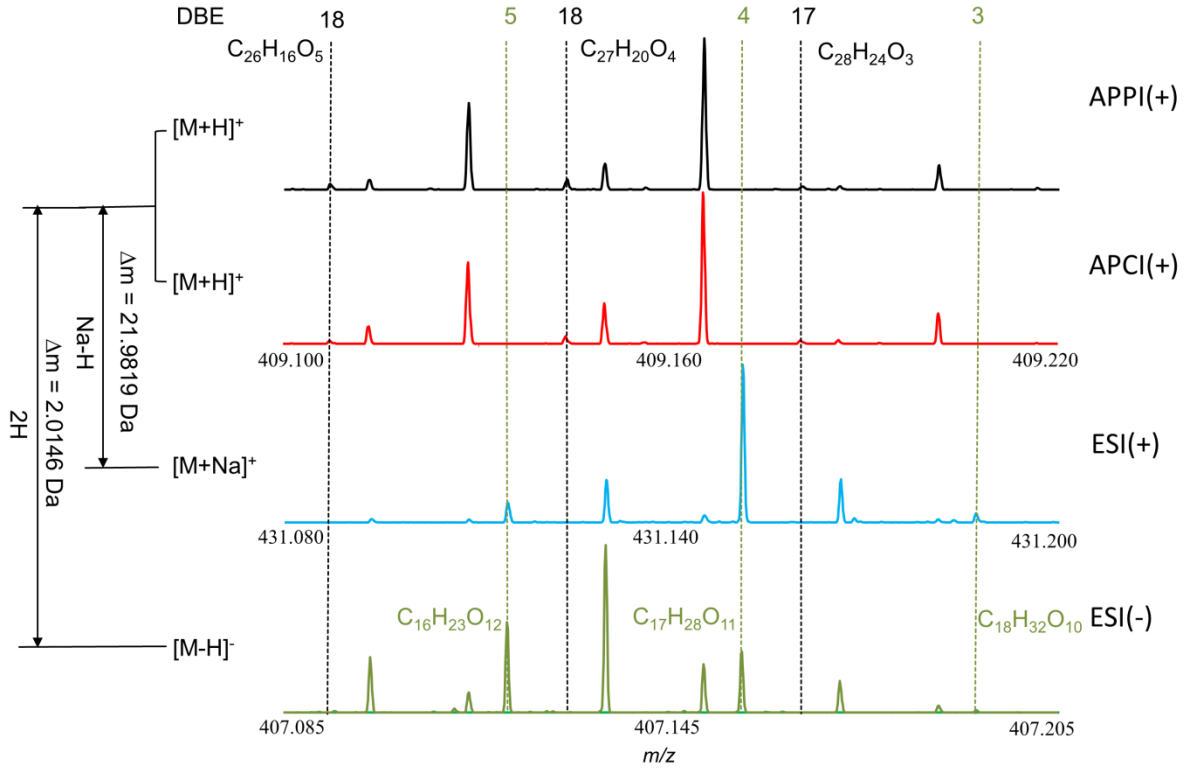

Figure 2-3. Adjusted mass scale mass spectra comparison for same elemental composition using different ionization techniques: *m/z* range from 409.100 to 409.220 Da for APPI(+), APCI(+), 431.080 to 431.200 Da for ESI(+) and 407.085 to 407.205 Da for ESI(-). The mass difference was calculated between different types of ion product for the same composition shown on the left.

The whole mass spectrometric information was summarized in intensity based classes distributions and displayed in Figure 2-4a. No matter which ionization method was applied, the oxygenated species was detected as the most abundant class. In ESI(-), a highest relative intensity of oxygenated species was detected with a contribution of 99.5%. For APPI(+) and APCI(+), the O_x species contributes to 87.2% (protonated adduct: 82.8%, radical: 4.4%) and 91.7% (protonated adduct: 89.9%, radical: 1.83%), respectively. For positive ESI, O_x species

are both detected as sodium and protonated molecules, which contribute to 89.0% (sodium adduct: 77.1%, protonated adduct: 11.9%). Non heteroatom hydrocarbons are easier to be detected at positive APPI (protonated adduct: 5.7%, radical: 3.8%) and APCI (protonated adduct: 4.8%, radical: 2.4%) than ESI (protonated adduct: 0.9%) which indicates lower aromatic structures that cannot easily being ionized by ESI. However, N_xO_y species (especially for NO_x) show the reversed case with contribution of total ion current equals to 2.7%, 0.9% and 8.6% for positive APPI, APCI and ESI.

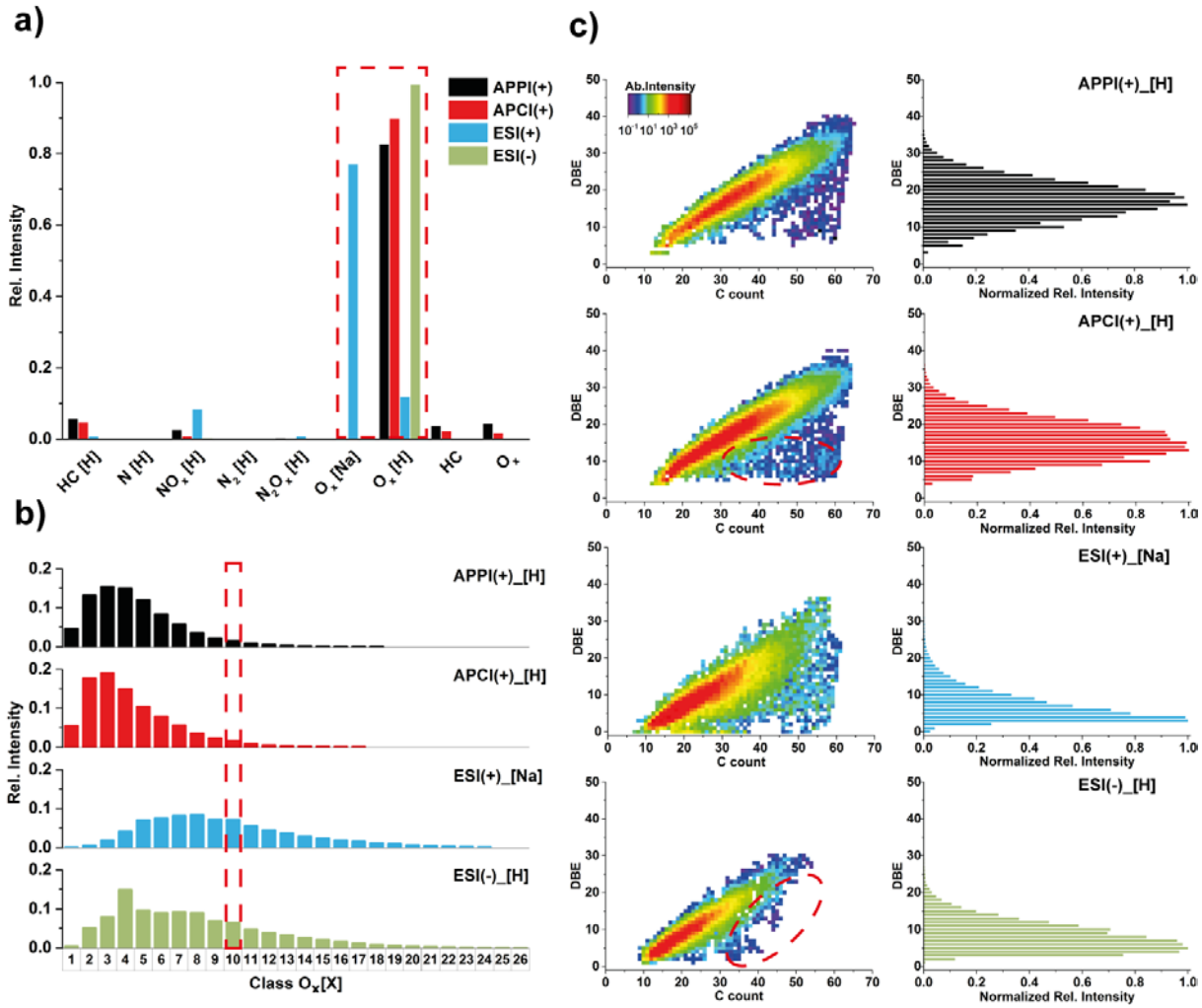

Figure 2-4. a) Relative intensity based class distribution for different ionization techniques. **b)** Relative intensity based class distribution for the most abundant class $O_x[X]$. The x shown as subscript represents the number of oxygen in each molecular formulas. The capital X in brackets represents protonated adduct in APPI(+), APCI(+), sodium adduct in ESI(+) and deprotonated adduct in ESI(-). **c)** The left graph shows the Kendrick plots for O_{10} class and the right graph presents the bar plots of DBE versus normalized intensity.

For the most abundant O_x species which contributes to around 90% of the total intensity, all of the ionization techniques provide data of a wide range of O_x distributions (Figure 2-4b). The

maximum number of oxygenated compositions in ESI is up to 24 (sodium adduct: 24, protonated adduct: 11) in positive and 26 in negative mode, while in APPI(+) and APCI(+), only up to 18 and 17 was available to be detected. Also, the intensity based O_x distribution shows that it shifts to higher oxygen number obviously and is more widely spread in ESI than APPI and APCI. These results show that ESI is more capable of detecting polar compositions than APCI and APPI. Moreover, a higher oxygen number was detected when comparing the data with recent reports [30] which is more likely to be contributed to spectra stitching scan method and ultra-high resolution technique applied in this study. Median and mean O/C values are also calculated for detected compositions and are shown in Table 2-1. Slight differences around 0.01-0.04 were observed between median and mean values. In consistent with previous discussion, significant differences were discovered for the most abundant O_x species among different ionization techniques. By comparison of the median O/C values, positive APPI and APCI presents the lowest value with 0.19 whereas ESI shows higher value with 0.29 (calculated by median of all O_x sodium and protonated adducts) for positive mode and the highest value with 0.35 for negative mode. O_x sodium adducts in positive ESI shows 0.06 higher O/C values than O_x protonated adducts.

Table 2-1. Calculated median and mean O/C values for detected compositions.

Median/Mean	**APPI(+)**	**APCI(+)**	**ESI(+)**		**ESI(-)**
All assigned compositions	0.21/0.24	0.20/0.23	0.26/0.29		0.37/0.40
O_x	0.19/0.22	0.19/0.22	0.29/0.33 [a] 0.23/0.28 [b]	0.29/0.33 [c]	0.35/0.39
NO_x	0.26/0.30	0.24/0.27	0.25/0.26		0.43/0.45
N_2O_x	0.24/0.26	0.23/0.25	0.24/0.27		0.33/0.42

Note: [a] indicates median and mean O/C values for sodium adducts, [b] for protonated adducts and [c] for the whole O_x species in positive ESI.

By checking individual class distribution, more detailed information can be gained to understand how different ionization method work for the same sample. Here, O_{10} class display an opposite intensity trend, with APPI(+), APCI(+) showing a low intensity and ESI(+), ESI(-) displaying a relative high intensity. And this detailed information of the O_{10} class was summarized in DBE versus C-count Kendrick plots and DBE versus normalized intensity bar plots for each ionization technique, shown in Figure 2-4c. When comparing APPI(+) and

APCI(+) results, APCI(+) contains slightly more compositions assigned at low DBE but with high carbon number, which is in agreement to the fact that APCI(+) is more likely to ionize alkyl hydrocarbons. Similar as APCI(+), ESI(+) also has a large amount of O_{10} compositions detected. This is because of a higher oxygen number contained in the compositions which attributes them a high polarity and shows a high affinity to sodium ion to improve ionization efficiency. In contrast, ESI(-) show less detected compositions. To compare O_{10} class DBE distribution, the relative intensity for DBE values at each ionization method was normalized into the range of 0 to 1. APCI(+) and APPI(+) show similar DBE distribution pattern for O_{10} class, with DBE value ranging from 4 to 40 for APPI(+) and 3 to 40 for APCI(+). The compositions ionized by APCI(+) present a DBE value with the highest intensity at 13, whereas the DBE value of compositions ionized by APPI (+) were centered at 16. In comparison, ESI shows a further significant DBE shift. ESI(+) and (-) both ionize compositions at a lower DBE value, which with the highest intensity are centered around 5 and 3, respectively. And the lowest DBE value achieved by using ESI(+) and (-) is 0 and 1, respectively. Biomass is mainly composed of three components, such as lignin, cellulose and hemicellulose. The pyrolytic biofuel can contain a large amount of phenolic and sugar like molecules. Based on our results, ionization efficiency using different ionization technique is associated with distinct chemical property in this complex mixture. APPI(+) and APCI(+) are more capable of ionizing phenolic compounds with high DBE originated from lignin. The sugar compositions derived from cellulose and hemicellulose are more easily to be ionized by ESI(+) and (-).

2.4.2 Total unique compositions with complementary ionization techniques

Through detailed analysis above, due to ionization selectivity effect by individual ionization technique, a number of distinct compositions can be distinguished using ultra-high resolution mass spectrometry, which improves the compositional coverage of pyrolysis based biofuels. As mentioned before, a single composition ionized by APPI(+) can be detected by both radical and protonated cations and therefore increases the complexity of unique composition analysis in a single ionization technique. Additionally, both radical and protonated cations can be obtained by using APCI(+). For ESI(+), composition can be both detected as protonated and sodium adducts. This further increases the complexity to count total unique composition. Here, in order to achieve total unique compositions to do further analysis, the strategy is to use two steps replicates overlap analysis procedure and this was done by using an open tool called ‘vennyl 2.1’[26]. The result is shown in Figure 2-5. First, an overlap analysis was applied

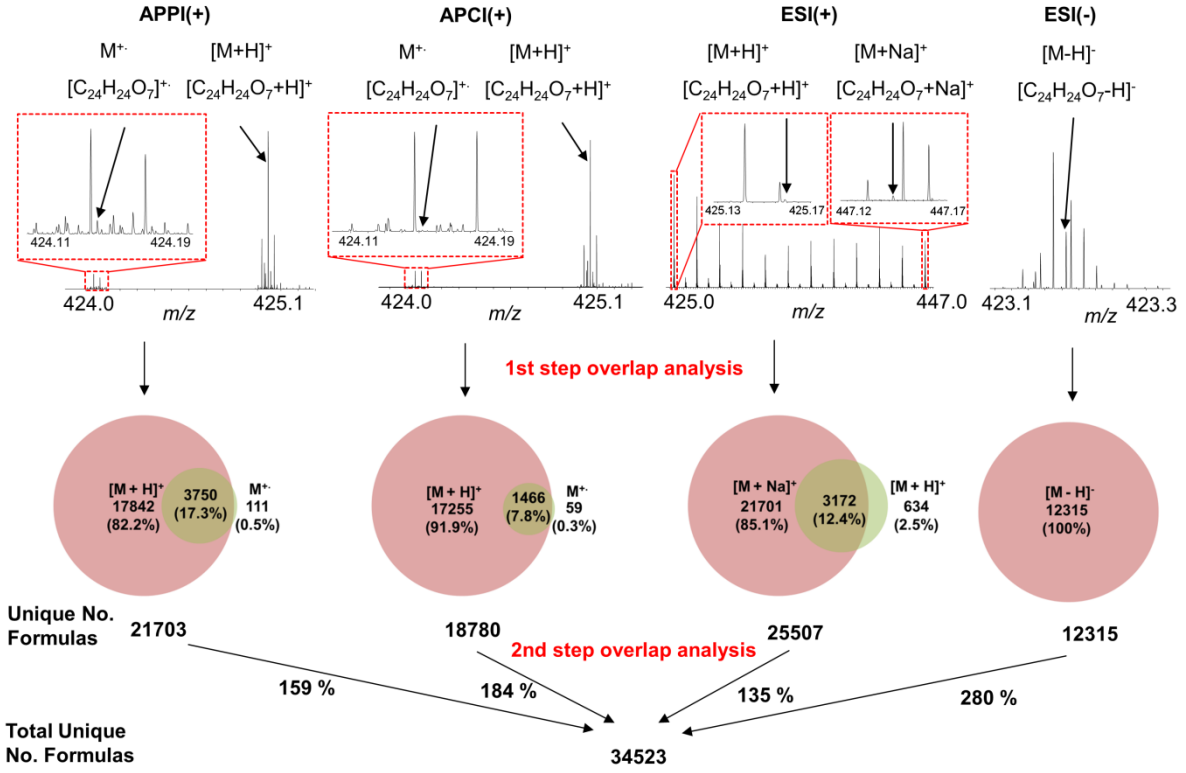

Figure 2-5. Two steps procedure to remove formulas replicates. The first step is to achieve unique number of formulas in a single ionization technique. An example with the composition of $C_{24}H_{24}O_7$ was shown in the zoom in mass spectra, which can be detected as multiple forms depending on the applied ionization technique. The second step is to remove composition replicates among multiple ionization techniques to obtain a total unique number of formulas.

to a single ionization technique which trims replicates to obtain unique compositions for each ionization method and this is shown in a venn diagram. For example, in APPI (+), 17842 and 111 compositions can be exclusively detected as protonated cations $[M+H]^+$ and radical cations $[M]^{+\cdot}$, respectively while 3750 compositions can be detected as both. In the final stage we only count the unique compositions with original molecular formula denoted as M and therefore if a composition is both detected as different ion types, it should only be counted once. In this step, a number of unique compositions, 21703, 18780, 25507 and 12315 were obtained by using APPI(+), APCI(+), ESI(+) and (-). In comparison of radical cations obtained by APPI(+) and APCI(+), more than double the number of compositions can be ionized by APPI(+) (3750 compositions) than that by APCI(+) (1466 compositions). However, the radical cations only show a very small part of contribution to the unique compositions (APPI(+): 0.5%, APCI(+): 0.3%). For ESI(+), protonated adducts contribute to slightly more unique compositions with 2.5%. In comparison with sodium adducts, the contribution to the unique compositions by protonated adducts are still limited. Further, a

second overlap analysis was applied to trim the replicates obtained by different ionizing techniques and finally a total number of 34523 unique compositions were detected by using complementary ionization techniques. And this number shows a significant composition coverage improvement of 159%, 184%, 135% and 280%, in comparison with that of single ionization technique APPI(+), APCI(+), ESI(+) and (-), respectively.

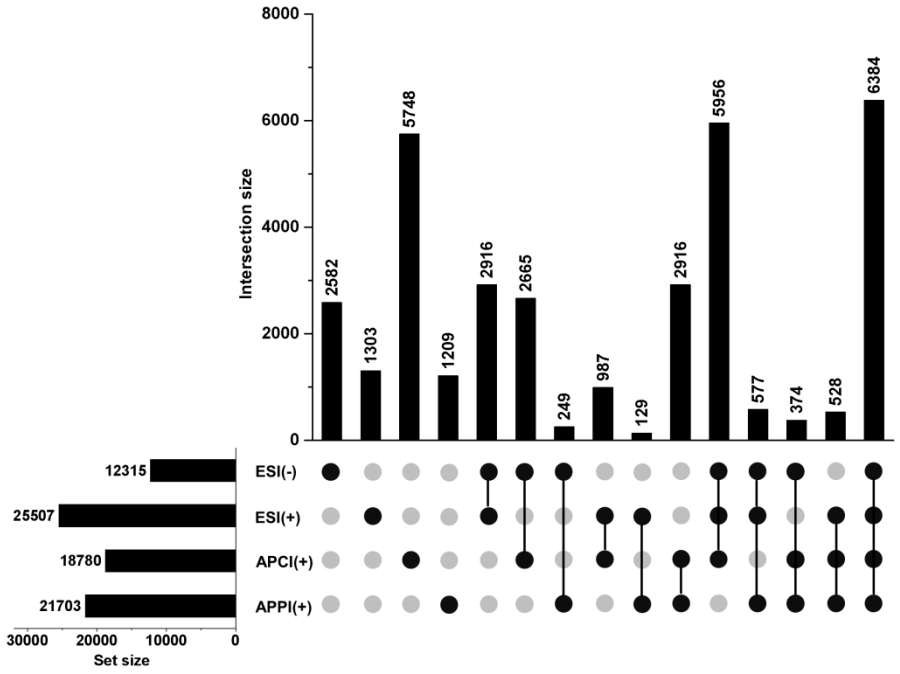

Figure 2-6. Set size bar plot on the left displays the unique No. formulas detected at individual ionization technique. The UpSet plot shows the intersection bar plot of detected formulas by using a combination of complementary ionization techniques.

Moreover, by applying a second overlap analysis it also allows us to investigate the intersections of assigned compositions among various ionization methods. Overlap analysis of datasets less than 3 datasets leads to a maximum number of 7 intersections. It is an extreme difficult task to show these areas proportionally in venn diagram graph with more than 3 datasets.[31, 32] One substitution is to represent the size of interactions across multiple datasets by using UpSet plots (see Figure 2-6) [33, 34] or displaying them in a Table (Table A2-1). Among all the ionization techniques, ESI(+) has the most exclusive compositions assigned, while ESI(-) gives the least assigned compositions (5748 versus 1209 compositions). APPI(+) and ESI(-) provides the least pairwise intersections with 129 compositions assignment. There are 6384 compositions that can be commonly achieved by all these ionization techniques. These compositions probably contain multiple functional groups such as phenols, sugar derivatives, et al. in a single composition, which make them capable to be ionized by different

ionization methods. Another reason is that these compositions may belong to different isomers with different functional groups fitting for individual ionization method. The limitation here is that fragmentation of a single peak was not carried out to prove this because separation of an individual composition (minimum isolation window is 0.1 Da) by Orbitrap Elite for this complex mixture is hard to be achieved.

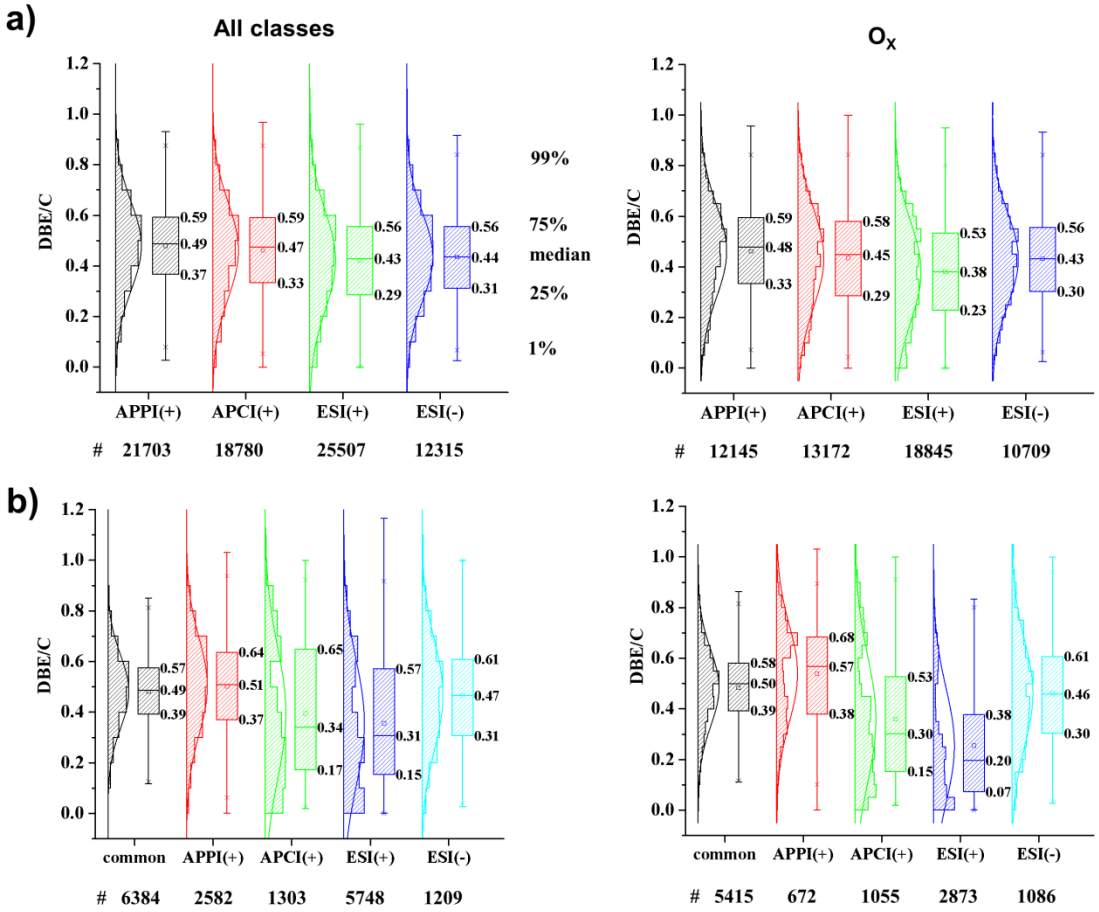

Figure 2-7. a) DBE/C distribution of all assigned classes compositions (top left) and O_x (top right) for individual ionization methods. **b)** DBE/C distribution of all assigned components (bottom left), O_x compositions (bottom right) for common (detected by all ionization methods) and exclusive compositions (detected only by one ionization method).

To further address method-dependent ionization selectivity issue, a normalization of the DBE to the number of carbons within the given molecule (DBE/C) has been carried out for common and exclusive compositions among various ionization methods. Before overlap analysis of detected compositions, all assigned compositions for individual ionization technique (Figure 2-7a) have a median DBE/C value of 0.49, 0.47, 0.43, 0.44, successively. Slight median DBE/C value difference was observed within the range of 0.01-0.06 among different ionization techniques. After overlap analysis, the DBE/C value difference for

exclusive compositions was widened into the range of 0.03-0.2 (Figure 2-7b). The common compositions still shows a relative high median DBE/C value of 0.49. APPI(+) (0.51) shows a significant higher median DBE/C value than that of APCI(+) (0.34). This is because, by comparison of these two methods, APPI is more capable of ionizing highly aromatic compositions, whereas APCI are more efficiently ionizing compositions containing alkyl chain. ESI(+) achieves the smallest median DBE/C value of 0.31, which is because of the formation of sugar sodium ions. Oxygen-containing species is the most abundant class in pyrolytic biofuel, showing the similar trend.

2.5 Conclusion

In this work, a comprehensive analysis by applying different resolving power (120k, 240k, 480k and 960k), ionization methods (positive APPI, APCI, ESI and negative ESI) and scan techniques (full and spectra stitching method) was achieved for studying the complexity of a pyrolysis biofuel. Using a mass resolution of 960k and spectra-stitching scan technique gave the highest assigned compositions (21652) for positive APPI. And the total compositions were significantly expanded by the combination of different ionization methods. A total number of 34472 compositions were detected. O_x species, detected with around 90% TIC, were the most abundant species, no matter which ionization technique was used. Sodium adducts is only detected at positive ESI, which leads to DBE shift to lower part, even to 0. The higher oxygen number and more widespread O_x distribution pattern was observed in ESI than APPI and APCI, which indicates ESI is more polar ionization method. The similar trend can also be observed by O/C median values evaluation for detected O_x compositions with higher value of 0.28 (positive ESI) and 0.35 (negative ESI) in comparison with positive APPI and APCI (both with 0.19).

This research successfully demonstrates the importance of utilizing complementary techniques, which helps to give an in-depth analysis of the pyrolysis oil. Ionization discrimination effect of single ionization methods can be compensated by using multiple ionization techniques. Additionally, the use of higher resolution and spectra stitching method give much bigger composition data, which allows researchers to dig data in depth and better to understand these discrimination effects.

2.6 References

1. Vispute, T. P.; Zhang, H.; Sanna, A.; Xiao, R.; Huber, G. W., Renewable chemical commodity feedstocks from integrated catalytic processing of pyrolysis oils. *Science* **2010,** *330* (6008), 1222-1227.

2. Liu, C.; Wang, H.; Karim, A. M.; Sun, J.; Wang, Y., Catalytic fast pyrolysis of lignocellulosic biomass. *Chem. Soc. Rev.* **2014,** *43* (22), 7594-7623.
3. Talmadge, M. S.; Baldwin, R. M.; Biddy, M. J.; McCormick, R. L.; Beckham, G. T.; Ferguson, G. A.; Czernik, S.; Magrini-Bair, K. A.; Foust, T. D.; Metelski, P. D.; Hetrick, C.; Nimlos, M. R., A perspective on oxygenated species in the refinery integration of pyrolysis oil. *Green Chem.* **2014,** *16* (2), 407-453.
4. Bridgwater, A.; Peacocke, G., Fast pyrolysis processes for biomass. *Renew. Sustain. Energy Rev.* **2000,** *4* (1), 1-73.
5. Rinaldi, R.; Schüth, F., Design of solid catalysts for the conversion of biomass. *Energy Environ. Sci.* **2009,** *2* (6), 610.
6. Czernik, S.; Bridgwater, A., Overview of applications of biomass fast pyrolysis oil. *Energy Fuels* **2004,** *18* (2), 590-598.
7. Biswas, B.; Pandey, N.; Bisht, Y.; Singh, R.; Kumar, J.; Bhaskar, T., Pyrolysis of agricultural biomass residues: Comparative study of corn cob, wheat straw, rice straw and rice husk. *Bioresour. Technol.* **2017,** *237*, 57-63.
8. Pu, Y.; Cao, S.; Ragauskas, A. J., Application of quantitative 31P NMR in biomass lignin and biofuel precursors characterization. *Energy Environ. Sci.* **2011,** *4* (9), 3154-3166.
9. Ben, H.; Ragauskas, A. J., NMR characterization of pyrolysis oils from kraft lignin. *Energy Fuels* **2011,** *25* (5), 2322-2332.
10. Xian, F.; Hendrickson, C. L.; Marshall, A. G., High resolution mass spectrometry. *Anal. Chem.* **2012,** *84* (2), 708-719.
11. Aebersold, R.; Mann, M., Mass spectrometry-based proteomics. *Nature* **2003,** *422* (6928), 198-207.
12. Vetere, A.; Schrader, W., Mass Spectrometric Coverage of Complex Mixtures: Exploring the Carbon Space of Crude Oil. *Chemistry Select* **2017,** *2* (3), 849-853.
13. Wei, Y.; Lei, H.; Wang, L.; Zhu, L.; Zhang, X.; Liu, Y.; Chen, S.; Ahring, B., Liquid–Liquid Extraction of Biomass Pyrolysis Bio-oil. *Energy Fuels* **2014,** *28* (2), 1207-1212.
14. Kanaujia, P. K.; Sharma, Y.; Agrawal, U.; Garg, M., Analytical approaches to characterizing pyrolysis oil from biomass. *TrAC, Trends Anal. Chem.* **2013,** *42*, 125-136.
15. Zhao, C.; Lercher, J. A., Upgrading pyrolysis oil over Ni/HZSM-5 by cascade reactions. *Angew. Chem., Int. Ed. Engl.* **2012,** *51* (24), 5935-40.
16. Zhao, C.; Kou, Y.; Lemonidou, A. A.; Li, X.; Lercher, J. A., Highly Selective Catalytic Conversion of Phenolic Bio-Oil to Alkanes. *Angew. Chem., Int. Ed. Engl.* **2009,** *121* (22), 4047-4050.
17. Gaspar, A.; Zellermann, E.; Lababidi, S.; Reece, J.; Schrader, W., Impact of different ionization methods on the molecular assignments of asphaltenes by FT-ICR mass spectrometry. *Anal. Chem.* **2012,** *84* (12), 5257-5267.
18. Brecht, D.; Uteschil, F.; Schmitz, O. J., Development of a fast-switching dual (ESI/APCI) ionization source for liquid chromatography mass spectrometry. *Rapid Commun. Mass Spectrom.* **2020**, e8845.
19. Lenzen, C.; Winterfeld, G. A.; Schmitz, O. J., Comparison of piracetam measured with HPLC-DAD, HPLC-ESI-MS, DIP-APCI-MS, and a newly developed and optimized DIP-ESI-MS. *Anal. Bioanal. Chem.* **2016,** *408* (15), 4103-4110.
20. Akalın, M. K.; Karagöz, S., Analytical pyrolysis of biomass using gas chromatography coupled to mass spectrometry. *TrAC, Trends Anal. Chem.* **2014,** *61*, 11-16.
21. Marshall, A. G.; Hendrickson, C. L.; Jackson, G. S., Fourier transform ion cyclotron resonance mass spectrometry: a primer. *Mass Spectrom. Rev.* **1998,** *17* (1), 1-35.
22. Hu, Q.; Noll, R. J.; Li, H.; Makarov, A.; Hardman, M.; Graham Cooks, R., The Orbitrap: a new mass spectrometer. *J. Mass Spectrom.* **2005,** *40* (4), 430-443.

23. Staš, M.; Chudoba, J.; Kubička, D.; Pospíšil, M., Chemical characterization of pyrolysis bio-oil: application of Orbitrap mass spectrometry. *Energy Fuels* **2015,** *29* (5), 3233-3240.
24. Staš, M.; Chudoba, J.; Auersvald, M.; Kubička, D.; Conrad, S.; Schulzke, T.; Pospíšil, M., Application of orbitrap mass spectrometry for analysis of model bio-oil compounds and fast pyrolysis bio-oils from different biomass sources. *J. Anal. Appl. Pyrolysis* **2017,** *124*, 230-238.
25. Gaspar, A.; Schrader, W., Expanding the data depth for the analysis of complex crude oil samples by Fourier transform ion cyclotron resonance mass spectrometry using the spectral stitching method. *Rapid Communications in Mass Spectrometry* **2012,** *26* (9), 1047-1052.
26. Oliveros, J. C. (2007-2015) Venny. An interactive tool for comparing lists with Venn's diagrams. https://bioinfogp.cnb.csic.es/tools/venny/index.html.
27. Littlefield, K.; Monroe, M., Venn Diagram Plotter. *PNNL, Richland, WA* **2008**.
28. Hertzog, J.; Carré, V.; Le Brech, Y.; Mackay, C. L.; Dufour, A.; Mašek, O.; Aubriet, F., Combination of electrospray ionization, atmospheric pressure photoionization and laser desorption ionization Fourier transform ion cyclotronic resonance mass spectrometry for the investigation of complex mixtures – Application to the petroleomic analysis of bio-oils. *Anal. Chim. Acta* **2017,** *969*, 26-34.
29. Gaspar, A.; Schrader, W. J. R. C. i. M. S., Expanding the data depth for the analysis of complex crude oil samples by Fourier transform ion cyclotron resonance mass spectrometry using the spectral stitching method. *Rapid Commun. Mass Spectrom.* **2012,** *26* (9), 1047-1052.
30. Ware, R. L.; Rowland, S. M.; Rodgers, R. P.; Marshall, A. G., Advanced Chemical Characterization of Pyrolysis Oils from Landfill Waste, Recycled Plastics, and Forestry Residue. *Energy Fuels* **2017**.
31. Chen, H.; Boutros, P. C., VennDiagram: a package for the generation of highly-customizable Venn and Euler diagrams in R. *BMC Bioinformatics* **2011,** *12* (1), 35.
32. Micallef, L.; Rodgers, P., eulerAPE: drawing area-proportional 3-Venn diagrams using ellipses. *PloS One* **2014,** *9* (7), e101717.
33. Lex, A.; Gehlenborg, N.; Strobelt, H.; Vuillemot, R.; Pfister, H., UpSet: visualization of intersecting sets. *IEEE Trans. Vis. Comput. Graph.* **2014,** *20* (12), 1983-1992.
34. Kew, W.; Mackay, C. L.; Goodall, I.; Clarke, D. J.; Uhrín, D., Complementary Ionization Techniques for the Analysis of Scotch Whisky by High Resolution Mass Spectrometry. *Anal. Chem.* **2018,** *90* (19), 11265-11272.

2.7 Appendix

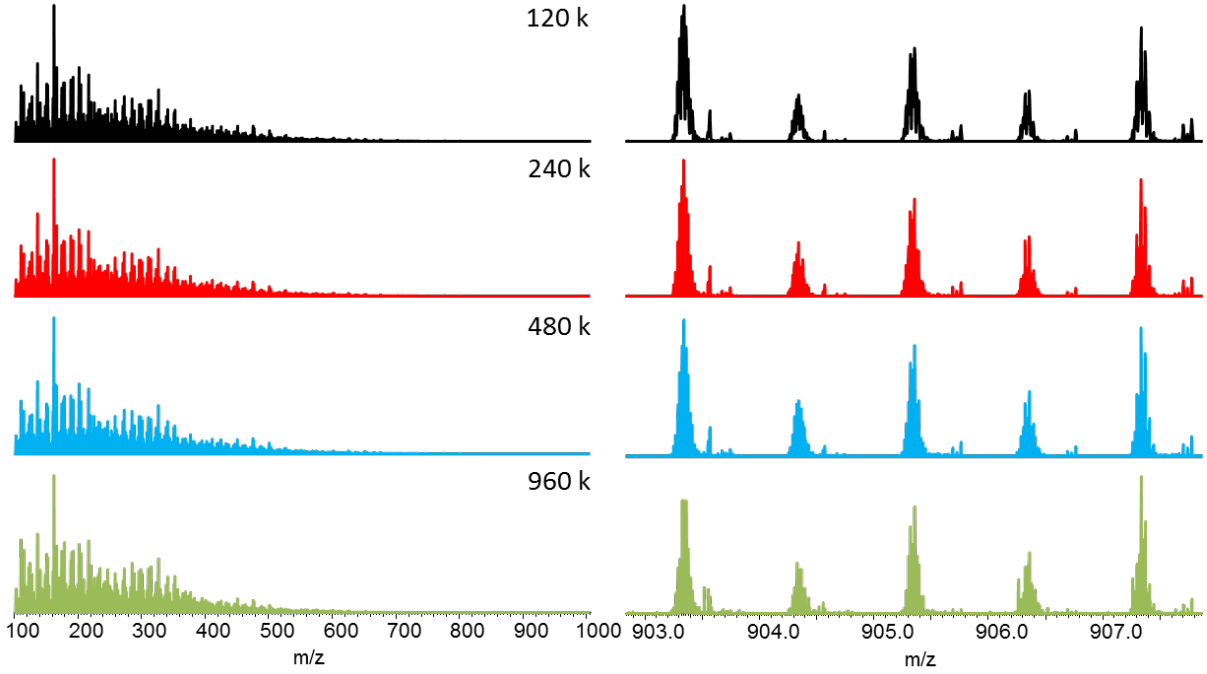

Figure A2-1. Mass spectra comparison using APPI (+) (left graph) and corresponding zoom in mass spectra (right graph) from 903 to 907 Da at resolution 120k, 240k, 480k and 960k (from top to down).

Table A2-1. Detailed classification for detected formulas in the second step of overlap analysis.

	Exclusive				**Dual detection**						**Triple detection**				**Common**	**Total**
APPI(+)	+				+	+	+				+	+	+		+	21703
APCI(+)		+			+			+	+		+	+		+	+	18780
ESI(+)			+			+		+		+	+		+	+	+	25507
ESI(-)				+			+		+	+		+	+	+	+	12315
No.	2582	1303	5748	1209	2916	2665	249	987	129	2916	5956	577	374	528	6384	34523
%	7.5	3.8	16.7	3.5	8.5	7.7	0.7	2.9	0.4	8.5	17.3	1.7	1.1	1.5	18.5	100

Chapter 3 Studying the thermal transformation of lignin into fuels using high solution mass spectrometry

Redrafted from "Xu, Y.; Schrader, W., Studying the thermal transformation of lignin into fuels using high solution mass spectrometry", will be submitted to *Rapid Commun. Mass Spectrom.*

3.1 Abstract

Pyrolysis oils from biomass are a potential alternative substitution for fossil fuels. A significant drawback of pyrolysis biofuels is that high oxygen content resulting in high acidity and instability limits its usage as transport fuel. Much work has been done to improve the quality of pyrolysis oils. One effective way is to use a heterogeneous catalytic approach which helps to remove oxygen and store hydrogen as well to produce petro-like fuel. For a better understanding of the transformation process, high resolution mass spectrometry (HRMS) coupled to APCI (+) was used to study the complex chemical reaction systems including lignin (one big part of biomass) pyrolysis and the catalytic upgrading processes. Based on the HRMS results, lignin and its corresponding pyrolysis based bio-fuel are mainly composed of highly oxygenated compositions. Partial oxygen removal could be observed after pyrolysis, which is mainly because of water elimination and decarboxylation reaction. Further catalytic upgrading helps significantly remove the oxygen content with hydrocarbons showing as main products. To follow these chemical transformations, HRMS plays a vital role.

3.2 Introduction

Nowadays fossil fuels still remain to be the major energy resource around the world to meet the increasing demand of modern industry, which account for 85% share in the world's primary energy consumption in 2018.[1] The burning of fossil fuels creates both short-term (air pollution by releasing toxic chemicals and particles in the air) and long-term (global warming by releasing large amount of CO_2) environmental problems.[2] This great quantity of CO_2 cannot be recycled and absorbed by the limited amount of biomass on the earth in a short time range. Switching from fossil fuels to sustainable and renewable energy resources is a global trend because CO_2 consumption is a global process.[3, 4]

In contrast, while the distribution of fossil fuel which are concentrated to a limited number of countries, renewable energy resources are distributed over wide geographical areas.[5] Solar and wind energy with unlimited amount are the most promising renewable energy resources, which are used to generate electricity. But the storage and long distance transmission of electricity over-production produced by large solar and wind power plant is a challenging process.[6] Also, the solar and wind energy may not always be adequate, especially in darkness or there is less wind. And this means other energy sources such as transport fuel may still be required, which allows to be immediately used for generating energy in this case.[7]

Another renewable energy resource is biomass, including the forms of sugar/starch crops (e.g., sugarcane, wheat), oil plants (e.g., soybean), lignocellulosic biomass (e.g., wood) et al., which can be used to produce bio-fuel. Especially important is biomass waste because it is readily available and does not use crop based resources. One resource of interest is using lignocellulosic biomass for the production of biofuel as it is cheap, reproducible and available for large quantity. Lignin is one of the major components of lignocellulosic biomass, which consists of 16-31 wt% depending on the type of lignocellulosic biomass.[8] And it is always considered to be a waste byproduct in the paper or ethanol production.[9, 10] Lignin is non-linear substituted phenolic polymer built with phenylpropane units, the precursors of which are mainly composed of three monolignols such as p-coumaryl alcohol, coniferyl alcohol and sinapyl alcohol.[11]

There are many options for the conversion of biomass into fuels. These processes include mechanical/chemical process, biological/biochemical and thermochemical processes. The mechanical/chemical process produces biodiesel through the extraction of fatty acid from oil plant by mechanical pressing in combination with transesterification reaction.[12] The

biological/biochemical process contains two conversion approaches, fermentation to convert sugar/starch crops into bio alcohol or anaerobic digestion to convert bio-waste into biogas.[13, 14] Biological/biochemical process is a fairly slow process, taking several days for the transformation. In comparison with these processes, pyrolysis as one well known thermochemical process has no preference for feedstock, which means it can use cheap lignocellulosic biomass or any other kind of carbon-based material for conversion. Moreover, it is a fast process, available to be done in a few seconds or hours.[15, 16] However, it also has its disadvantage. Elemental composition analysis of lignin based pyrolysis biofuel shows that oxygen content of 23-34 wt% generally remained in the pyrolysis oil.[17] A large amount of oxygen content in pyrolysis oil is harmful and restricts its application as an alternative to transport fuel as it shows the physicochemical property of high acidity, corrosiveness, instability, viscosity, low heating value among others.[18, 19] Therefore, the initial pyrolysis biofuel is required to be upgraded, typically using a catalytic hydrotreating approach.[20-22]

Pyrolysis derived biofuel is a complex mixture, with thousands of compositions present inside. In previous research, pyrolysis-GC/MS, GC-MS or GCxGC-MS are commonly used for the characteristic study.[23-26] But the limitation for this analytical method is that only a small fraction of compounds in these complex mixtures were analyzed because of separation efficiency, compounds' volatility, abundance. Fourier transform (FT) based high resolution mass spectrometry (HRMS) coupling with atmospheric pressure ionization (API) techniques allows the determination of the elemental formula with a high mass accuracy, giving a more complete overview of the products in the complex mixtures.[27-29] The right selection of API methods is critical. Electrospray ionization (ESI) is efficient at generating preferable results for polar compounds containing heteroatoms N, O in the structures. To the contrary, atmospheric pressure photo ionization (APPI) and atmospheric pressure chemical ionization (APCI) are more capable to ionize non-polar or less polar compounds. These two ionization methods show similarity with both of them being capable of efficiently ionizing compounds containing aromatic cores. However, one advantage of APCI over APPI is that APCI has a higher tendency to ionize saturated hydrocarbons. Referring to the compounds in lignin and corresponding pyrolysis bio-fuel, commonly two parts exist in the structure: polar parts (a large number of oxygen containing functional groups such as ketone, aldehyde, carboxylic acid, hydroxyl, et al.) and non-polar parts (aromatic cores and aliphatic chains). This indicates all of these ionization techniques can efficiently ionize these compounds in lignin and pyrolysis bio-fuel. However, catalytic upgrading reactions remove oxygen and result in low polar type of hydrocarbons, both aromatic and saturated compounds. ESI and APPI both show

limitations to ionize saturated hydrocarbons. Therefore, APCI shows to be an optimal choice and was applied in this study.

In this work, an analytical method was developed to study different chemical pyrolysis reactions. First, organosolv lignin from poplar wood was used for pyrolysis process to obtain crude biofuel products. And then to reduce oxygen content in initial produced biofuel, catalytic upgrading reaction was performed. All these reactions were studied by using HRMS. While additional studies to optimize the pyrolysis process were done by thermogravimetric analysis.

3.3 Experimental section

3.3.1 Pyrolysis process of organosolv lignin

The procedure to produce organosolv lignin can be found elsewhere.[30] 10 g of organosolv lignin was weighted and then was transferred into quartz glass reactor, which later was installed into the tube furnace (EVA 12/300/E301, Carbolite Gero, Germany). Before starting the pyrolysis reaction, the whole pyrolysis setup was flushed with Argon for 20 min. Then the reactor with organosolv lignin stored was heated from 30 to 600 ^{o}C at a heating rate of 100 ^{o}C min^{-1} and then kept at 600 ^{o}C for 30 min. The volatile products was then cooled down by reflux water, ice/water mixture and dry ice saturated acetone mixture (-78 ^{o}C), respectively. Afterwards, the products were obtained with washing the pipe with methanol and the methanol was removed by vacuum evaporation.

3.3.2 Thermogravimetry

Thermogravimetric analysis was carried out using a Mettler Toledo TGA/DSC 1 Star System with Argon atmosphere at a flow rate of 40 ml min^{-1} and a heating rate of 10 ^{o}C min^{-1} from 35 to 750 ^{o}C.

3.3.3 Mass spectrometry

Organosolv lignin and samples of pyrolysis biofuels were diluted with methanol to a final concentration of 250 µg mL^{-1} and used without further treatment. Biofuels that were obtained from catalytic hydrotreating biofuel, named upgrading biofuel, were diluted with dichloromethane to achieve complete dissolvation. The preparation of upgraded biofuel is described elsewhere.[31] Mass Spectra were obtained from a research-type Orbitrap Elite mass spectrometer (Thermo Fisher Scientific, Bremen, Germany) equipped with commercially available atmospheric pressure chemical ionization (APCI) source. The

spectra were collected in positive mode. For the measurements, each sample was infused with a flow rate of 20 μL min^{-1}, evaporated at 350 ^{o}C with the sheath and auxiliary gas flow of 20 and 10 (arbitrary units), respectively. APCI current was set as 5 kV. Mass spectra were collected with mass window $100 \leq m/z \leq 1000$ using spectral stitching method (windows of 30 Da with 5 Da overlap) and resolving power R= 480,000 (full width half maximum at m/z 400).

3.3.4 Data analysis

Peak assignment was performed using Composer64 (v 1.5.0, Sierra Analytics, Modesto, CA, USA) after internal recalibration according to the following constraints: $C_{0\text{-}200}H_{0\text{-}1000}N_{0\text{-}2}O_{0\text{-}30}S_{0\text{-}2}$, $0 \leq$ DBE ≤ 60 and ±1.0 ppm. DBE number can be calculated based on the formula using the equation: DBE = C - (H/2) + (N/2) + 1, where: C = number of carbon atoms, H = number of hydrogen atoms, and N = number of nitrogen atoms. One DBE is equal to one ring or one double bond.

3.4 Results and discussion

The experimental scheme applied during these studies is shown in Figure 3-1. These steps involve the pyrolysis of lignin into a first product, which then is catalytically transformed into a transport fuel at hydrogen atmosphere condition. After pyrolysis process, dark brown liquid oil was obtained, which exhibited a high viscosity. Further upgrading reaction changed it into yellowish.

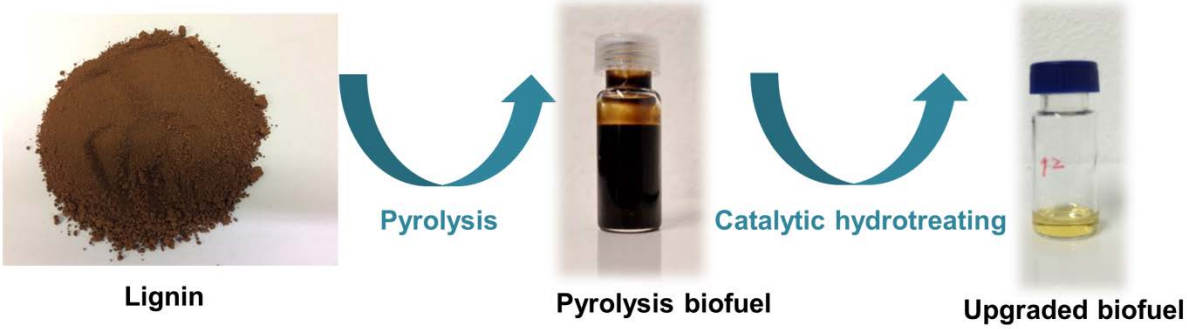

Figure 3-1. Scheme of pyrolysis and catalytic hydrotreating processes.

3.4.1 Pyrolysis process analysis

For a better understanding of the reaction conditions, the thermal decomposition of lignocellulosic material was studied by using thermogravimetric analysis (TG). Previous

reports show that TG degradation temperature of hemicellulose and cellulose was mainly focused on a small temperature range of 220-315°C and 315-400°C while the TG analysis of lignin had a much wider degradation temperature range of 100-900°C.[36] Similar result for TG analysis of lignin was also discovered in our work. Figure 3-2 depicts thermogravimetric and corresponding differential thermogravimetric (DTG) results of lignin. The degradation temperature spanned over a wide temperature range of 200-750 ^{o}C. Lignin degraded fast in the temperature range of 200-450 ^{o}C. After that, it showed a very slow degradation. The peak temperature was located at 369 ^{o}C, corresponding to the maximum degradation rate temperature. A weight loss of 59.7 wt% was observed after the whole heating process. Based on this result, the pyrolysis process was carried out at 600 ^{o}C for 30 min. After the pyrolysis process, it showed around 53.0 wt% of the lignin was transformed into liquid and gaseous products. A slight yield difference, 6.7 wt%, was observed between TG and pyrolysis results. This corresponds well with previous studies, where a slightly higher yield of residue in the reactor after pyrolysis process was observed.[37, 38]

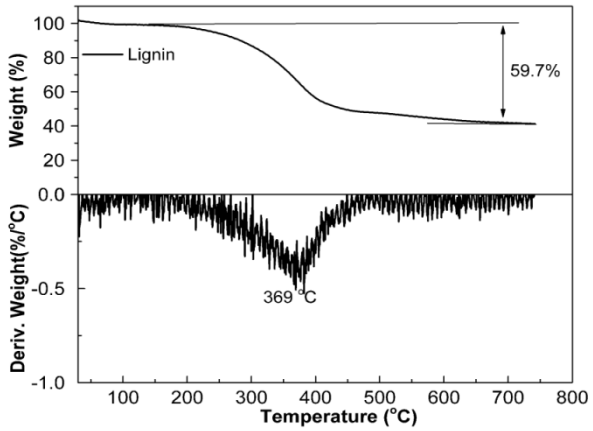

Figure 3-2. TG and DTG curve of organosolv lignin.

3.4.2 APCI Orbitrap mass spectra

Detailed ultrahigh resolution mass spectrometric analysis shows to be an excellent method to understand the detailed conversion reaction of biomass into a fuel. During APCI ionization, both charge and proton transfer reactions happen simultaneously, which yield both radical and protonated cations. A first overview of the positive APCI-MS spectra can be gained from the spectra displayed in Figure 3-3 left column that depicts the different samples. The whole mass spectrum of lignin shows a high intensity in the mass range of 100-700 Da. The top three peaks in lignin mass spectrum at *m/z* 193.0859, 401.1593 and 521.1804 Da were assigned as

protonated molecules with elemental compositions of $[C_{11}H_{12}O_3+H]^+$ (DBE: 6), $[C_{22}H_{14}O_7+H]^+$ (DBE: 11) and $[C_{29}H_{28}O_9+H]^+$ (DBE: 16), respectively. The molecular differences among these compositions are probably corresponding to different types of phenol derivatives which reflect the nature of lignin crosslinked by monolignols. In comparison to lignin, it can be observed that the mass distribution of pyrolysis oil shifted to lower mass range and was primarily placed in the mass range of 100-400 Da. And it showed the top three peaks at *m/z* 155.0703, 169.0859 and 195.1015 Da. These peaks were assigned to protonated composition $[C_8H_{11}O_3+H]^+$, $[C_9H_{12}O_3+H]^+$ and $[C_{11}H_{14}O_3+H]^+$ with DBE calculated as 4, 4 and 5, respectively. These compounds are monolignol derivatives. This means that a formation of small molecules can be derived from the breakdown of big polymer lignin after pyrolysis process. The mass spectrum of the upgraded biofuel shows a high intensity in the mass range of 100-400 Da. The top three peaks was observed at *m/z* 119.0856, 145.1012 and 241.1951 Da, which can be assigned to compositions $[C_9H_{10}+H]^+$, $[C_{11}H_{12}+H]^+$ and $[C_{18}H_{24}+H]^+$ with a DBE value of 5, 6 and 7 correspondingly.

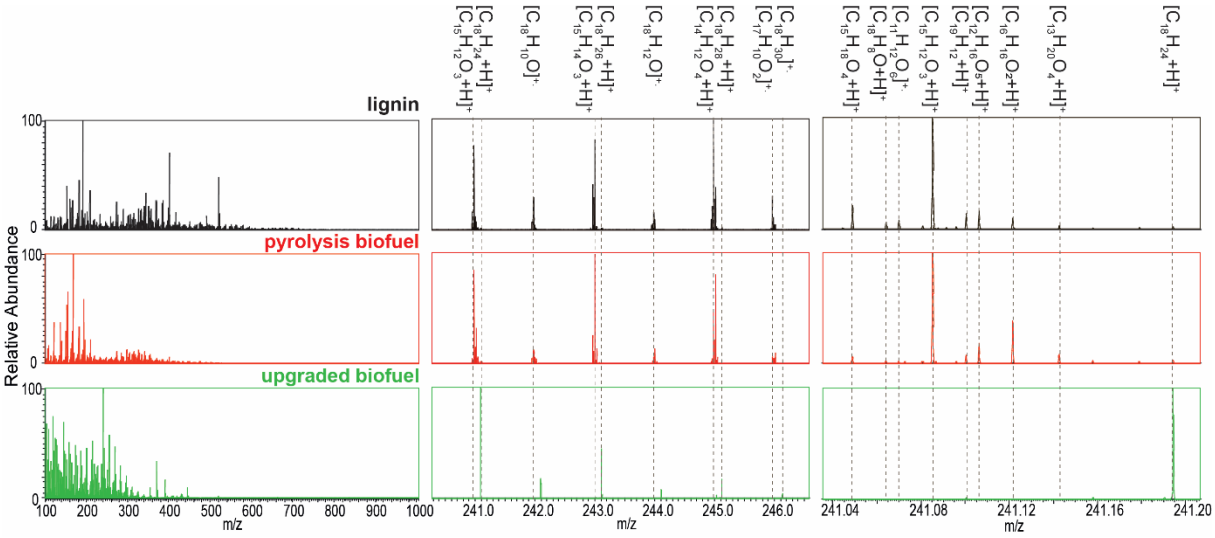

Figure 3-3. Mass spectra comparison of lignin, pyrolysis biofuel and upgrading biofuel in a mass range of 100-1000 Da (left column), 240.0-246.5 Da (middle column) and 241.04-241.20 Da (right column).

Figure 3-3 middle column shows enlarged mass spectra displaying at the mass range of *m/z* 240.0-246.5 Da. The major signals with high intensity were assigned with their elemental compositions. Except those protonated compositions (such as $[C_{15}H_{12}O_3+H]^+$, $[C_{18}H_{24}+H]^+$, $[C_{15}H_{14}O_3+H]^+$, $[C_{18}H_{26}+H]^+$ and $[C_{14}H_{12}O_4+H]^+$), radical compositions such as $[C_{18}H_{10}O]^{+\cdot}$, $[C_{18}H_{12}O]^{+\cdot}$, $[C_{17}H_{10}O_2]^{+\cdot}$ and $[C_{18}H_{30}]^{+\cdot}$ can also be clearly detected in the selected mass range. Further, other magnified mass spectra was selected at *m/z* 241.04-241.20 Da (shown in

Figure 3-3 right column). The mass spectra of lignin and corresponding pyrolysis oil in this region show mainly the oxygenated molecular compositions, with O atoms in the range of 1 to 6 for a single molecule. On the contrary, the intensity of hydrocarbon compositions was relative low in comparison with that of oxygenated compositions. For the upgraded biofuel, this mass range displayed a high intensity for composition $[C_{18}H_{24}+H]^+$.

3.4.3 Class distribution

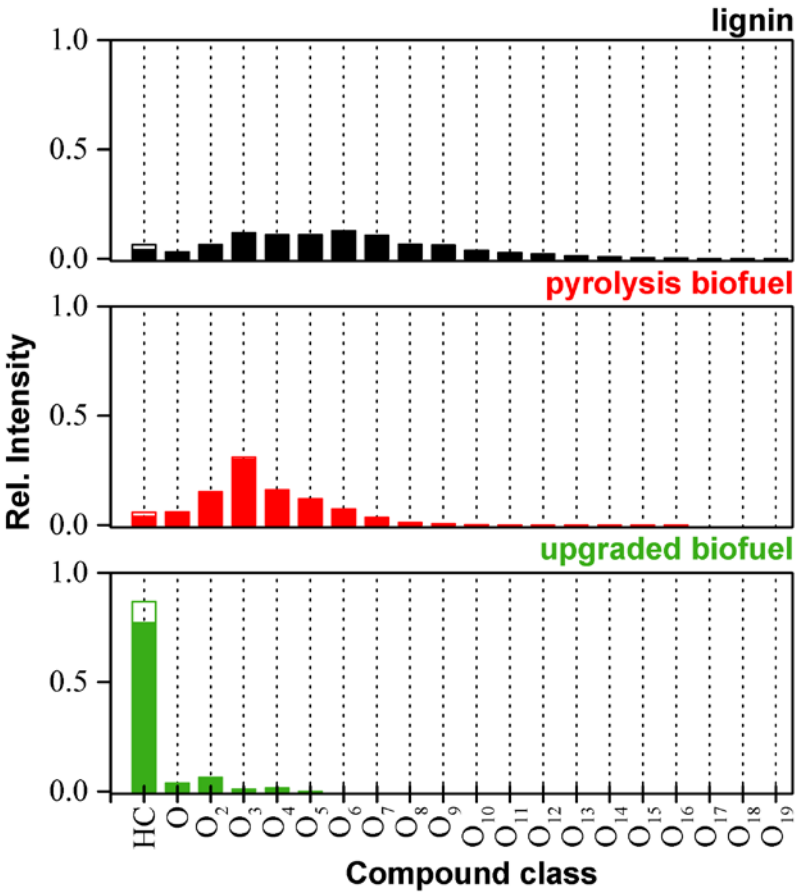

Figure 3-4. Relative intensity distribution of various classes assigned in the positive-ion APCI Orbitrap mass spectra of lignin, pyrolysis biofuel and upgrading biofuel (from top to bottom). The relative intensity is based on the ratio between the intensity of each class and the total intensity calculated by summing all assigned categories in each mass spectra. The solid section of the bars presents protonated cations, $[M+H]^+$ and the empty section represents radical, $M^{+\cdot}$.

The whole mass spectral information of lignin and the corresponding pyrolysis oil is summarized in a relative intensity based distribution plot (shown in Figure 3-4). Both radical and protonated cations are present here together. The intensity ratio of protonated cation to radical cation is 15.3 in lignin, 18.9 in pyrolysis biofuel and 6.5 in upgraded biofuel, respectively. In lignin, a wide range of oxygen atoms for a single molecule was observed with

a maximum oxygen number of 19. The O_6 class was detected with the highest intensity. Pure hydrocarbons only contributed to 6.5 % of the total intensity. After the pyrolysis process, as expected, partial oxygen was removed shifting the oxygen distribution to lower oxygen number classes. Here, the O_3 class was observed with highest intensity in pyrolysis oil and only up to 16 oxygens were detected. Also the intensity of hydrocarbon class did not show an obvious increase with a contribution of 6.0% to the total intensity. For oxygen classes with oxygen number less than or equal to 5, compositions in pyrolysis oil showed a higher relative intensity than that in lignin. Especially for the O_{1-3} classes, the relative intensity of compositions in pyrolysis oil was even two times higher than that in lignin. In comparison, the upgraded biofuel was clearly dominated by the hydrocarbon class, accounting for 77.9% of the total intensity by summing up protonated and radical cations. Only up to 5 oxygen atoms per molecule could be detected. The number of assigned compositions distribution based on compound class shows a similar trend, as shown in Figure A3-1.

3.4.4 DBE vs. carbon count/intensity distribution

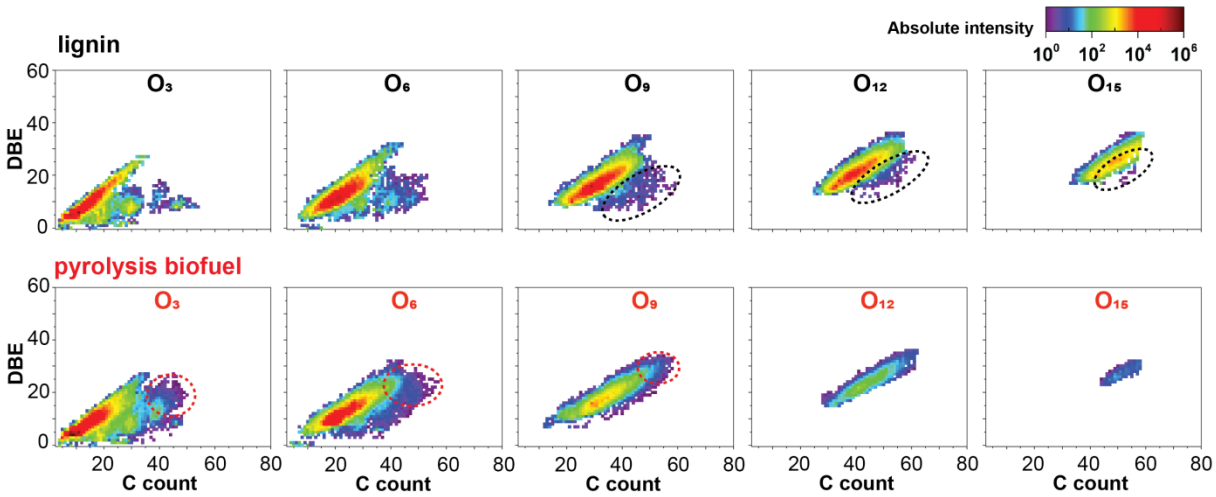

Figure 3-5. Contour plots of DBE versus carbon count for members of the O_3, O_6, O_9, O_{12} and O_{15} classes in the lignin (top) and corresponding pyrolysis biofuel (bottom).

Kendrick plots[39, 40] can provide a meaningful representation about selected properties of the different types of assigned compounds in the complex mixture sample after calculation of each individual signal in mass spectrum. Figure 3-5 and Figure A3-2 depict the Kendrick plots of oxygen classes in lignin, pyrolysis biofuel and upgraded biofuel. In lignin, the O_1 to O_6 classes contain a small amount of compositions with DBE value in the range of 0-3. These compositions could be attributed to lipid extractives, hemicellulose and cellulose derived

sugaric components. The compositions with a DBE value of higher than 4 could be associated with the presence of aromatic ring structure. The O_7 to O_{19} classes only contain compositions with a DBE value of higher than 4. These results indicate that the extracted lignin through organosolv process still contained limited amounts of lipids, hemicellulose and cellulose derived components.

With the increase of the oxygen number in the molecules, the DBE and C count in each composition tends to shift to a higher value. For example, the compositions belonging to low oxygen number class, O_3 class, have C count spanning from 4 to 54 and DBE value ranging from 0 to 27. Among them, only a few compositions contain C count higher than 35. While the compositions belonging to the high oxygen number class, O_{15} class, consist of C count spanning from 33 to 59 and DBE value ranging from 17 to 36. Moreover, Figure 3-6 left column shows the DBE distribution based on normalized relative intensity for several oxygen classes in lignin. The selected classes of O_3, O_6, O_9, O_{12} and O_{15} have a maximum intensity at a DBE value of 6, 11, 16, 21 and 26 accordingly. A DBE difference of 5 between them is more likely to be attributed to the addition of one benzene ring and one double bond (C=C or C=O) in the molecule.

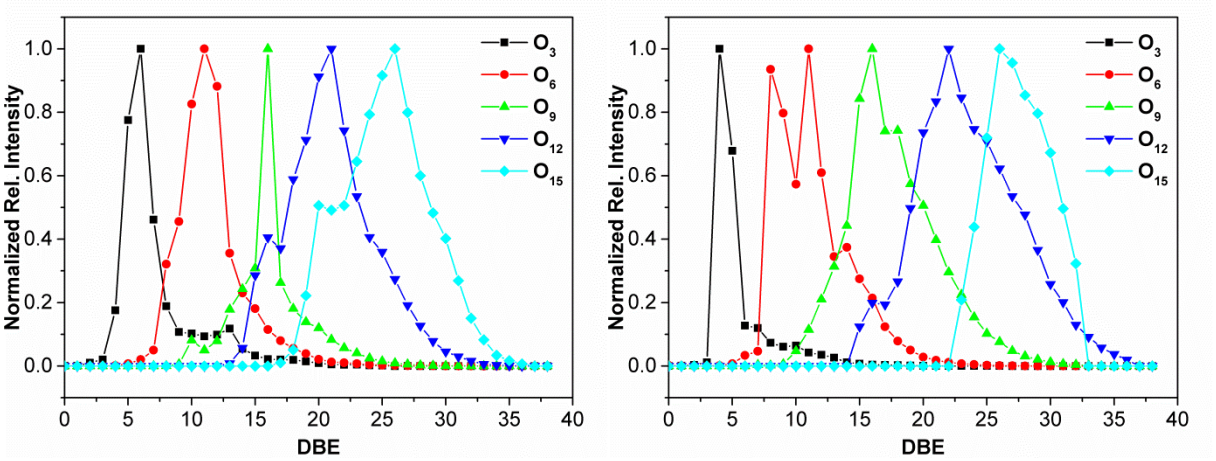

Figure 3-6. DBE versus normalized relative intensity plots for classes O_3, O_6, O_9, O_{12} and O_{15} in lignin (left) and pyrolysis biofuel (right). Normalized relative intensity means the relative intensity for each oxygen class is normalized into the range of 0 to 1.

The similar trend can also be observed in the pyrolysis biofuel derived from lignin. However, still a highly significant difference can be observed for the compositional distribution when comparing between original lignin and corresponding pyrolysis biofuel. Demonstrating the changes can help to gain a better understanding of the pyrolysis transformation of lignin to

pyrolysis biofuel. The big difference was highlighted in the dash cycle between before and after the pyrolysis reaction. At classes with higher oxygen numbers (O_{12} and O_{15} classes), it shows the disappearance of molecular compositions at higher C count with low DBE in lignin. However, at classes with low oxygen numbers (O_3 and O_6 class), it shows appearance of new molecular compositions with relative higher DBE. This information could be explained by the substructure of lignin. The loss of compositions with high oxygen numbers could be associated with the loss of CO_2 from carboxylic acid and water from hydroxyl functional group. And accompanying with loss of water, it also associates with creating double bond to increase DBE. However, the C-O bond dissociation energy of phenol is much higher than those oxygen atoms existing in carboxylic acid, alcohol hydroxyl group, ketone or aldehyde. A short vapor residence time during high temperature pyrolysis process followed by cooling conditions may not be efficient to remove oxygen from phenolic compounds to obtain pure hydrocarbons, and therefore still high oxygen content in pyrolysis oil is left after the pyrolysis process.

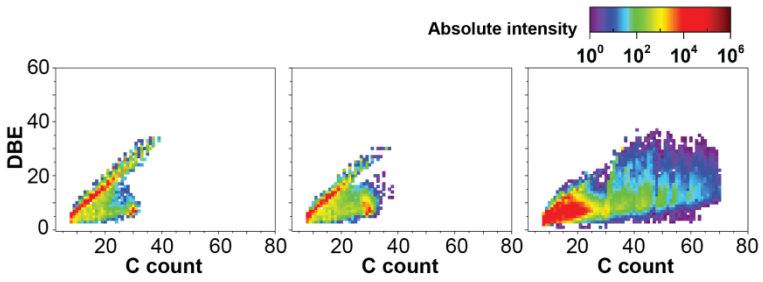

Figure 3-7. Contour plots of DBE versus carbon count for CH class in the lignin (left) and corresponding pyrolysis biofuel (middle) and upgrading biofuel (right).

For an application as a transport fuel, the types and distribution of hydrocarbon compounds are important to gain a better understanding on how the type of compounds change during the different types of transformation. The HC class is displayed in contour plots of lignin, of pyrolysis biofuel and of the upgraded biofuel compared together in Figure 3-7. The compositions of the hydrocarbon class in lignin contained C count from 8 to 39 and DBE value from 3 to 34. The hydrocarbon class in pyrolysis biofuel shows a similar composition distribution with C count from 8 to 38 and DBE value from 3 to 34. In comparison, the hydrocarbon class in the upgraded biofuel has more compositions with C count spanning from 8 to 70 and DBE ranging from 1 to 37. On another side, the increase of assigned compositions number in very low oxygen number class (O_1 and O_2 classes) and the decrease of assigned

compositions number starting from O_3 class can be observed by comparing pyrolysis biofuel and upgraded biofuel (Figure A3-1 and Figure A3-2). Overall, a significant removal of oxygen can be observed after hydrotreating process while the hydrocarbons needed for a quality fuel increase drastically.

3.5 Conclusion

This study provides a new approach for investigation of the complex chemical reaction systems, such as lignin fast pyrolysis process. APCI(+) coupled to HRMS gives compositions at a molecular level with high mass accuracy and sensitivity, which allows us to obtain a detailed understanding of the occurring molecular transformations.

Composition analysis of raw material lignin gave a high amount of oxygen species at a single molecule with a maximum of 19 oxygen number detected. This attributes to the complexity of lignin structure, consisting of multiple oxygen containing functional groups. Partial oxygen removal was observed through the pyrolysis process by analyzing oxygen class distribution and comparing Kendrick plots of low oxygen and high oxygen classes This coordinates with the breakage of big polymer lignin and also loss of oxygen associated functional group requiring low energy, such as H_2O elimination of hydroxyl group attached to the aliphatic chain and decarboxylation of acidic carboxyl group. However, the oxygen removal efficiency is extremely low. Three reasons can be an explanation for this: 1) a short residence time of volatile products at high temperature followed by fast cooling system; 2) a large amount of phenol products produced in the reaction and the removal of phenol hydroxyl group requiring high energy; 3) high amount of H_2 required for removal of oxygen, which cannot be produced during the pyrolysis reaction. Therefore, additional catalytic hydrotreating reaction is essential to remove high oxygen content remained in the crude biofuel. Result show that a significant oxygen removal could be achieved with hydrocarbon class displaying the highest intensity, 77.9%. A maximum of O_5 in a single molecule with low intensity was observed after the upgrading process so this maybe needs more optimization as applied here.

3.6 References

1. Outlook, B. E., *2019 edition*. London, United Kingdom, 2019.
2. Omer, A. M., Energy, environment and sustainable development. *Renew. Sust. Energ. Rev.* **2008,** *12* (9), 2265-2300.
3. Shafiee, S.; Topal, E., When will fossil fuel reserves be diminished? *Energy Policy* **2009,** *37* (1), 181-189.

4. Ellabban, O.; Abu-Rub, H.; Blaabjerg, F., Renewable energy resources: Current status, future prospects and their enabling technology. *Renew. Sust. Energ. Rev.* **2014,** *39*, 748-764.
5. Chow, J.; Kopp, R. J.; Portney, P. R., Energy resources and global development. *Science* **2003,** *302* (5650), 1528-1531.
6. Ueckerdt, F.; Brecha, R.; Luderer, G., Analyzing major challenges of wind and solar variability in power systems. *Renew. Energy* **2015,** *81*, 1-10.
7. de Klerk, A., Transport fuel: Biomass-, coal-, gas-and waste-to-liquids processes. In *Future Energy*, 2020; pp 199-226.
8. Liu, C.; Wang, H.; Karim, A. M.; Sun, J.; Wang, Y., Catalytic fast pyrolysis of lignocellulosic biomass. *Chem. Soc. Rev.* **2014,** *43* (22), 7594-7623.
9. Uğurlu, M.; Gürses, A.; Doğar, Ç.; Yalçın, M., The removal of lignin and phenol from paper mill effluents by electrocoagulation. *J. Environ. Manage.* **2008,** *87* (3), 420-428.
10. Doherty, W. O.; Mousavioun, P.; Fellows, C. M., Value-adding to cellulosic ethanol: Lignin polymers. *Ind. Crops. Prod.* **2011,** *33* (2), 259-276.
11. Bu, Q.; Lei, H.; Zacher, A. H.; Wang, L.; Ren, S.; Liang, J.; Wei, Y.; Liu, Y.; Tang, J.; Zhang, Q.; Ruan, R., A review of catalytic hydrodeoxygenation of lignin-derived phenols from biomass pyrolysis. *Bioresour. Technol.* **2012,** *124*, 470-477.
12. Ma, F.; Hanna, M. A., Biodiesel production: a review1Journal Series #12109, Agricultural Research Division, Institute of Agriculture and Natural Resources, University of Nebraska–Lincoln.1. *Bioresour. Technol.* **1999,** *70* (1), 1-15.
13. Rosales-Calderon, O.; Arantes, V., A review on commercial-scale high-value products that can be produced alongside cellulosic ethanol. *Biotechnol. Biofuels* **2019,** *12* (1), 240.
14. Mata-Alvarez, J.; Macé, S.; Llabres, P., Anaerobic digestion of organic solid wastes. An overview of research achievements and perspectives. *Bioresour. Technol.* **2000,** *74* (1), 3-16.
15. Bridgwater, A.; Peacocke, G., Fast pyrolysis processes for biomass. *Renew. Sustain. Energy Rev.* **2000,** *4* (1), 1-73.
16. Czernik, S.; Bridgwater, A., Overview of applications of biomass fast pyrolysis oil. *Energy Fuels* **2004,** *18* (2), 590-598.
17. Scholze, B.; Meier, D., Characterization of the water-insoluble fraction from pyrolysis oil (pyrolytic lignin). Part I. PY–GC/MS, FTIR, and functional groups. *J. Anal. Appl. Pyrolysis* **2001,** *60* (1), 41-54.
18. Mohan, D.; Pittman Jr, C. U.; Steele, P. H., Pyrolysis of wood/biomass for bio-oil: a critical review. *Energy Fuels* **2006,** *20* (3), 848-889.
19. Bridgwater, A. V., Review of fast pyrolysis of biomass and product upgrading. *Biomass Bioenergy* **2012,** *38*, 68-94.
20. Bridgwater, A., Upgrading biomass fast pyrolysis liquids. *Environ. Prog. Sustain. Energy* **2012,** *31* (2), 261-268.
21. Mu, W.; Ben, H.; Ragauskas, A.; Deng, Y., Lignin pyrolysis components and upgrading—technology review. *Bioenergy Res.* **2013,** *6* (4), 1183-1204.
22. Zhang, S.; Yan, Y.; Li, T.; Ren, Z., Upgrading of liquid fuel from the pyrolysis of biomass. *Bioresour. Technol.* **2005,** *96* (5), 545-550.
23. Zhao, C.; Lercher, J. A., Upgrading pyrolysis oil over Ni/HZSM-5 by cascade reactions. *Angew. Chem. Int. Ed.* **2012,** *51* (24), 5935-5940.
24. Cao, Z.; Engelhardt, J.; Dierks, M.; Clough, M. T.; Wang, G. H.; Heracleous, E.; Lappas, A.; Rinaldi, R.; Schüth, F., Catalysis meets nonthermal separation for the production of (Alkyl) phenols and hydrocarbons from pyrolysis oil. *Angew. Chem. Int. Ed.* **2017,** *56* (9), 2334-2339.

25. Lu, Q.; Zhang, Z.-F.; Dong, C.-Q.; Zhu, X.-F., Catalytic upgrading of biomass fast pyrolysis vapors with nano metal oxides: an analytical Py-GC/MS study. *Energies* **2010,** *3* (11), 1805-1820.
26. Jeon, M.-J.; Jeon, J.-K.; Suh, D. J.; Park, S. H.; Sa, Y. J.; Joo, S. H.; Park, Y.-K., Catalytic pyrolysis of biomass components over mesoporous catalysts using Py-GC/MS. *Catal. Today* **2013,** *204*, 170-178.
27. Vetere, A.; Schrader, W., Mass Spectrometric Coverage of Complex Mixtures: Exploring the Carbon Space of Crude Oil. *ChemistrySelect* **2017,** *2* (3), 849-853.
28. Gaspar, A.; Schrader, W., Expanding the data depth for the analysis of complex crude oil samples by Fourier transform ion cyclotron resonance mass spectrometry using the spectral stitching method. *Rapid Commun. Mass Spectrom.* **2012,** *26* (9), 1047-1052.
29. Kew, W.; Mackay, C. L.; Goodall, I.; Clarke, D. J.; Uhrín, D., Complementary Ionization Techniques for the Analysis of Scotch Whisky by High Resolution Mass Spectrometry. *Anal. Chem.* **2018,** *90* (19), 11265-11272.
30. Wang, X.; Rinaldi, R., Bifunctional Ni catalysts for the one-pot conversion of Organosolv lignin into cycloalkanes. *Catal. Today* **2016,** *269*, 48-55.
31. Cao, Z.; Xu, Y.; Lyu, P.; Dierks, M.; Morales-García, Á.; Schrader, W.; Nachtigall, P.; Schüth, F., Flexibilization of Biorefineries: Tuning Lignin Hydrogenation by Hydrogen Partial Pressure. *ChemSusChem* **2020**.
32. Davin, L. B.; Lewis, N. G., Lignin primary structures and dirigent sites. *Curr. Opin. Biotechnol.* **2005,** *16* (4), 407-415.
33. Furimsky, E., Catalytic hydrodeoxygenation. *Appl. Catal. A Gen.* **2000,** *199* (2), 147-190.
34. Zakzeski, J.; Bruijnincx, P. C.; Jongerius, A. L.; Weckhuysen, B. M., The catalytic valorization of lignin for the production of renewable chemicals. *Chem. Rev.* **2010,** *110* (6), 3552-3599.
35. Hicks, J. C., Advances in C–O bond transformations in lignin-derived compounds for biofuels production. *J. Phys. Chem. Lett.* **2011,** *2* (18), 2280-2287.
36. Yang, H.; Yan, R.; Chen, H.; Lee, D. H.; Zheng, C., Characteristics of hemicellulose, cellulose and lignin pyrolysis. *Fuel* **2007,** *86* (12-13), 1781-1788.
37. Nowakowski, D. J.; Bridgwater, A. V.; Elliott, D. C.; Meier, D.; de Wild, P., Lignin fast pyrolysis: Results from an international collaboration. *J. Anal. Appl. Pyrolysis* **2010,** *88* (1), 53-72.
38. Patwardhan, P. R.; Brown, R. C.; Shanks, B. H., Understanding the fast pyrolysis of lignin. *ChemSusChem* **2011,** *4* (11), 1629-1636.
39. Molnárné Guricza, L.; Schrader, W., Argentation chromatography coupled to ultrahigh-resolution mass spectrometry for the separation of a heavy crude oil. *J. Chromatogr., A* **2017,** *1484*, 41-48.
40. Kendrick, E., A Mass Scale Based on CH2= 14.0000 for High Resolution Mass Spectrometry of Organic Compounds. *Anal. Chem.* **1963,** *35* (13), 2146-2154.

3.7 Appendix

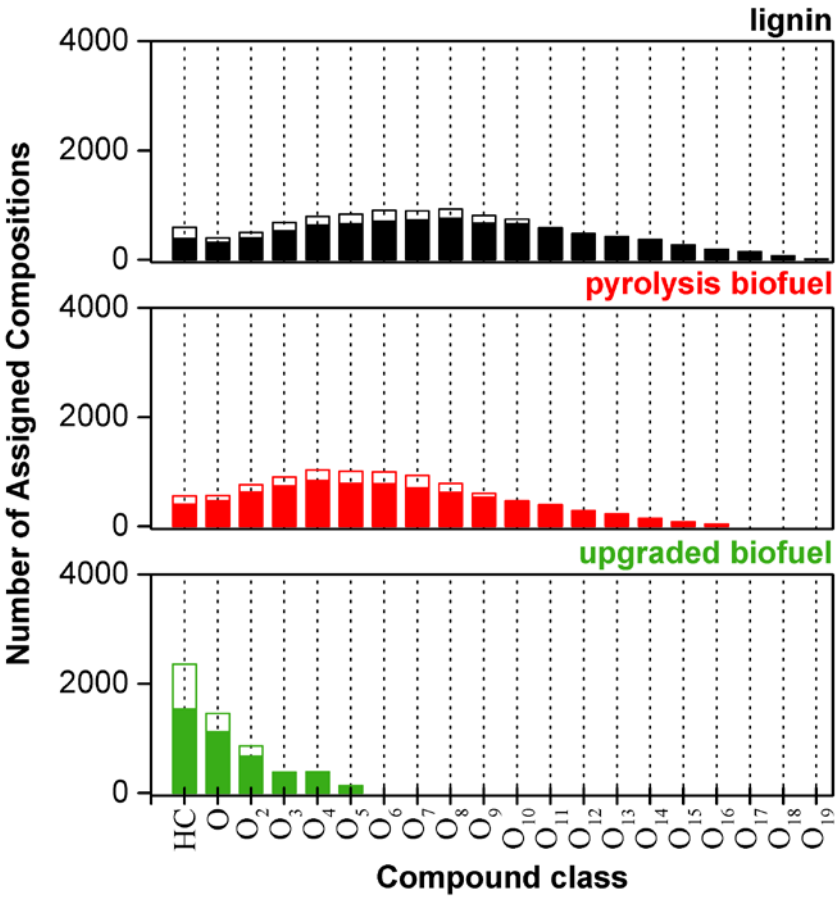

Figure A3-1. Assigned composition distribution of various classes assigned in the positive-ion APCI Orbitrap mass spectra of lignin, pyrolysis biofuel and upgrading biofuel (from top to bottom). The solid section of the bars presents protonated cations, $[M+H]^+$ and the empty section presents radical cations, $M^{+\cdot}$.

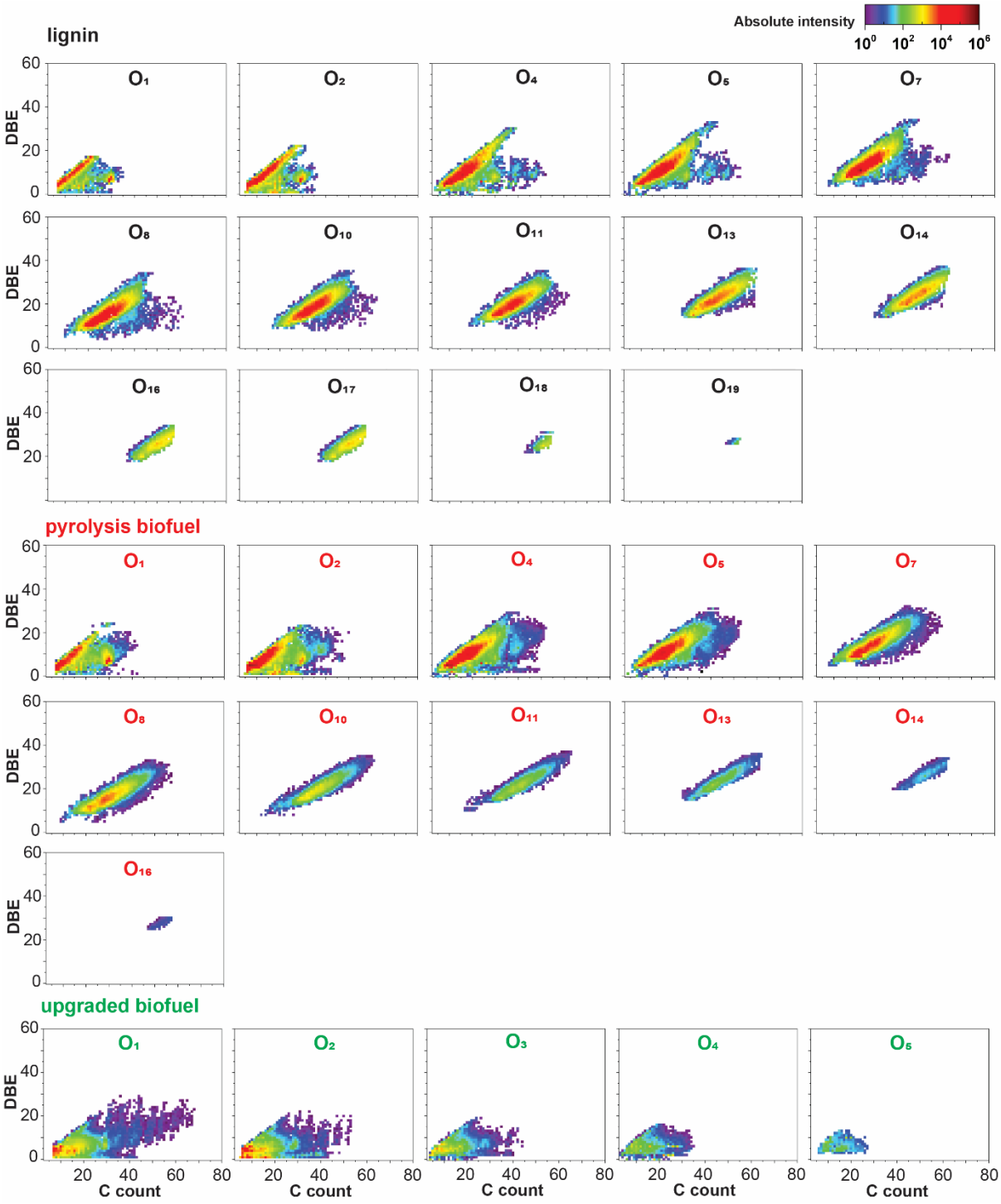

Figure A3-2. Contour plots of DBE versus carbon count for all other oxygen classes in the lignin (top), corresponding pyrolysis biofuel (middle) and upgrading biofuel (bottom).

Chapter 4 Converting municipal plastic waste into useful transport fuels using a pyrolysis process

Redrafted from "Xu, Y.; Schrader, W., Converting municipal plastic waste into useful transport fuels using a pyrolysis process", will be submitted to *ChemSusChem*.

4.1 Abstract

In daily life humankind is producing a significant amount of garbage including household and industrial trash, creating a great environmental concern. On the other side, garbage consists of high amounts of carbon based materials, making it a very useful resource. An easy way to use it is to produce transport fuel obtained through a pyrolysis process. Multiple plastic materials were investigated for this process in this study. TGA studies of single type plastic (polypropylene, polystyrene, low/high density polyethylene and polyvinyl chloride) show that almost complete weight loss could be achieved. A high amount of liquid fuel derived from pyrolysis of polypropylene, polystyrene at 450 ^{o}C and low/high density polyethylene at 500 ^{o}C, more than 70%, was obtained. Using GC-EI-HRMS allows detailed study of pyrolysis liquid fuel products and corresponding mechanism was proposed based on the product distribution. An examination of carbon number distribution reveals the economic potential of plastic liquid fuel, which can be used as alternative to partly substitution of fossil fuel derived gasoline and diesel fuel.

4.2 Introduction

Plastics have a wide impact on human lifestyle, being utilized for producing packages, soft bottles, textiles, toys, electronic devices and numerous other important or less important products. This is attributed to general plastic properties that they are light, durable, resistant to corrosion by most chemicals, easy to be processed and low production cost on a large scale level.[1, 2] Since the beginning of commercial plastic production, plastic production has surged from 1.5 million tons in 1950 to 348 million tons in 2018.[3, 4] The most commonly used plastics in our daily life are polyethylene terephthalate (PET), high density polyethylene (HDPE), polyvinyl chloride (PVC), low density polyethylene (LDPE), polypropylene (PP) and polystyrene (PS) with plastic identification code from 1 to 6, respectively, accounting for around 81 % of the total European plastic demand in 2016.[5, 6]

The major problem behind using plastics is that most of them are not easily degradable, taking decades to hundreds of years for nature degradation.[7-9] Homogenous plastic is a valuable resource, thus, it is of tremendous importance to recycle and transform them back into custom products. The plastic recycling process can be categorized into two major pathways: 1) mechanical recycling, where plastic is sorted, cleaned and regenerated; 2) chemical recycling, where plastic is degraded into basic components.[10-12] Nowadays plastic recycling is still at a low extent. Roland Geyer, et al. reported that an estimated 79% of the global plastic waste was discarded into dumpsites, 12% was incinerated and only 9% was reused from recycling in 2015. Discarded plastic either goes into landfilling or dumps into the ocean, which subsequently forms microplastic and has a negative impact on environment, wildlife and human health.[13-18] On the other hand, even when plastics are properly recycled, however, each recycling cycle shortens the lifespan of the plastics due to additional heating and alternation of the polymer chain. After several rounds of recycling, plastic quality significantly decreases, leaving the material useless for reproduction anymore. This means that the final end-use of the material is important where still high amounts of the plastic waste go into landfilling or ends up trash in the oceans.[19]

Aside from the recycling and microplastic issues, the conflict between uprising energy demand and depletion of conventional fossil energy sources raises a big concern and keeps crude oil prices high. Nowadays 85% of the total world energy consumption is attributed to consumption of fossil fuel.[20] The depletion of fossil fuel, especially for the reservation of natural gas and oil, happens in a foreseeable future, and therefore, measures has to be taken

before it becomes a reality.[21, 22] Using renewable energy resources (e.g., solar, wind, hydro power) is a solution, but is still in a developing stage and requires a massive infrastructure input.[23-25] A compensate strategy is to use plastic waste, especially at current situation of insufficient waste management. Plastic waste derived from fossil fuel has a comparable calorific value to that of hydrocarbon fuel, thus, providing a better opportunity as an alternative to dumpsites.[26, 27]

Therefore, energy recovery is a necessary step for those recycled low quality plastics or improper treated plastic waste. This process can also be viewed as a thermochemical recycling process. Conventional incineration of plastic waste is a simple, but disputable process to generate heat and electricity, raising a great environmental issue of producing dioxin and heavy metal in the smoke.[28-30] One way to thermally crack polymer materials is by using pyrolysis. This is not without drawbacks since pyrolysis needs a high input of energies, which is conducted at a high temperature under an inert condition. Although a large pyrolysis reactor is available in the industry, increasing pyrolysis capacity of plastic waste is still a challenging process because of extreme sample complexity it has to deal with.[10, 31, 32]

Since this is an easy way to crack polymers into fuels we used pyrolysis as a tool in this *trash-to-fuel* setup. In this study, general plastic types such as PET, HDPE, PVC, LDPE, PP and PS, are used to investigate the pyrolysis process. The objective of this study is to transform plastic waste into valuable fuels and to achieve a good understanding of the conversion process. The pyrolysis products were studied by using GC-EI-HRMS (high resolution mass spectrometry) to examine the detailed compounds' information.

4.3 Experimental section

4.3.1 Materials

Six different polymer materials were used in this study. Household plastic waste was collected for plastic PET (from drink bottles), HDPE (from shower gel bottles), PVC (from water tubing), PP (from shampoo bottles) and PS (from coffee cups). Labels for household plastic waste were removed, which were later washed with clean water, dried and shredded into small pieces. For plastic LDPE, commercially available plastic pellets were used.

4.3.2 Thermogravimetry

TG measurements were performed using a Mettler Toledo TGA/DSC 1 Star System connected to data acquisition station. For each measurement, around 2 mg of sample were placed in the TGA cell at an inert gas (argon) flow rate of 40 mL min^{-1}. Each sample (plastic PP, PET, LDPE, HDPE, PS and PVC, individually) was heated from 35 to 750 ^{o}C at a heating rate of 10 ^{o}C min^{-1}. For plastic PP, additional experiments were carried out by heating the sample from 35 to 400 or 450 ^{o}C and kept at this temperature for further 1 h reaction.

4.3.3 Development of a pyrolysis setup

A lab scale pyrolysis system was developed here. As described in Figure A4-1, the whole pyrolysis setup contains several parts: a 1480 W tube furnace (EVA 12/300 B, Carbolite Gero, Germany), a quartz glass reactor (H x W: 300 mm x 50 mm) with continuous argon supply, a cooling trap system and a waste gas cleaning part. The cooling trap system consists of a cooling water bridge that is followed by two different cooling steps. The first step consists of two consecutive ice water baths (4 ^{o}C) and the second step is a single dry ice saturated acetone bath (-78 ^{o}C). The waste gas cleaning container was filled with KOH saturated solution.

4.3.4 Pyrolysis process

Pyrolysis of each plastic was carried out individually in a quartz glass reactor, which was installed into and externally heated by a tube furnace. Around 20 g material each time was weighted and added into the reactor. Before starting pyrolysis reaction, the reactor was located and fluidized with argon continuously for roughly 20 min to remove air and humidity out of the system. For the reaction, the furnace was heated at a maximum heating rate of 100 ^{o}C min^{-1} until reaching to the desired temperature, followed by an isothermal step of 1 h. The reactor was continuously fluidized with an argon flow of 0.2 mbar during the transfer reaction process. After exiting the reactor, the pyrolysis volatiles passed through the cooling trap system. Inorganic gaseous halogens were removed by bubbling pyrolysis gas through KOH saturated solution. The products were collected from each cooling trap and weighted. Products on the surface of cooling water column were washed out with dichloromethane, dried under vacuum evaporation and weighted as well. The amount of residue left in the pyrolysis reactor was determined.

4.3.5 GC-EI-Orbitrap

GC/MS measurements were performed with a Q Exactive GC (Thermo Fisher, Bremen, Germany), consisting of a AI/AS 1310 autosampler equipped TRACE 1300 series GC coupled to a Q Exactive Orbitrap MS. The injection volume of an individual sample was 0.2 µL and dichloromethane was used as injector cleaning solvent. The sample injector was operated at 300 ^{o}C and split mode was selected with a split flow of 80 mL min^{-1}, and a purge flow of 5 mL min^{-1}. High purity helium (N5.0) was used as a carrier gas at a constant flow rate of 1.2 mL min^{-1}. The GC separation was carried out on a RTX$^{@}$-1ms capillary column (30 m x 0.25 mm ID, 0.25 um). The temperature program was performed with a starting temperature of 35 ^{o}C, which was increased to a final temperature of 320 ^{o}C at a heating rate of 10 ^{o}C min^{-1} and then held at 320 ^{o}C for additional 5 min. Transfer line temperature was set to 320 ^{o}C. The eluted compounds from GC were ionized by EI at an electron energy of 70 eV. The mass spectra were recorded in full scan mode with a mass range of 30-600 Da at a mass resolution of 120,000 (FWHM at *m/z* 200). Collected GC-MS data were imported and characterized against NIST library by MassLib (MSP Kofel, Zollikofen, Switzerland).

4.4 Results and discussion

4.4.1 TG analysis

For a better understanding of the thermal degradation of polymers, initial studies were carried out using thermogravimetric analysis to determine the optimum reaction parameters. The graphs are summarized in Figure 4-1 .Of the six different polymer materials only one shows a different course. The results show that PVC has two major degradation steps while all other curves only show a single degradation step. The $T_{p'}$ of first degradation stage occurs at 299 ^{o}C with a loss of 72.5 wt% (Table 4-1). The second degradation $T_{p''}$ is located at 457 ^{o}C with a degradation loss of 14.7 wt%. In comparison, other types of polymers such as PET, PP, PS, LDPE and HDPE only show a single degradation step, mainly observed at a high temperature range from 350 to 500 ^{o}C. The TG curve of HDPE, LDPE, PP and PS presents a high weight loss with less than 5 wt% residue in the TG sample plates whereas there is still a high amount of residue (22.1 wt%) for degradation curve of PET. A high weight loss during degradation process indicates it has the high potential to obtain an efficient transforming of plastic waste into fuels when pyrolysis process is applied. Among the hydrocarbon plastics, thermal degradation temperature follows the order of PS < PP < HDPE ≈ LDPE. The difference could be attributed to the stability of radical intermediates formed during heating process. Direct

single point C-C cleavage of plastic PE, PP and PS (Scheme 4-2) at a high temperature leads to the formation of single radical —·,  and  , respectively, which show a decreasing order of radical stability.

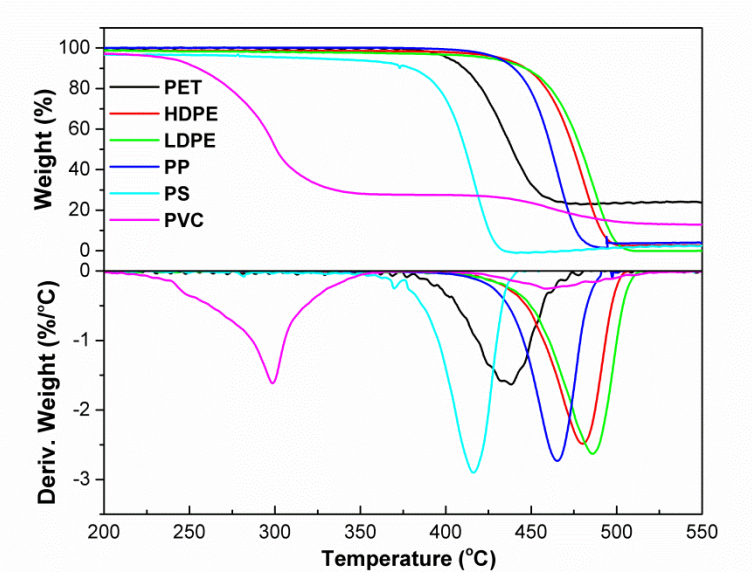

Figure 4-1. Zoom in TG and DTG profiles of individual plastics in a temperature range from 200 to 550 °C.

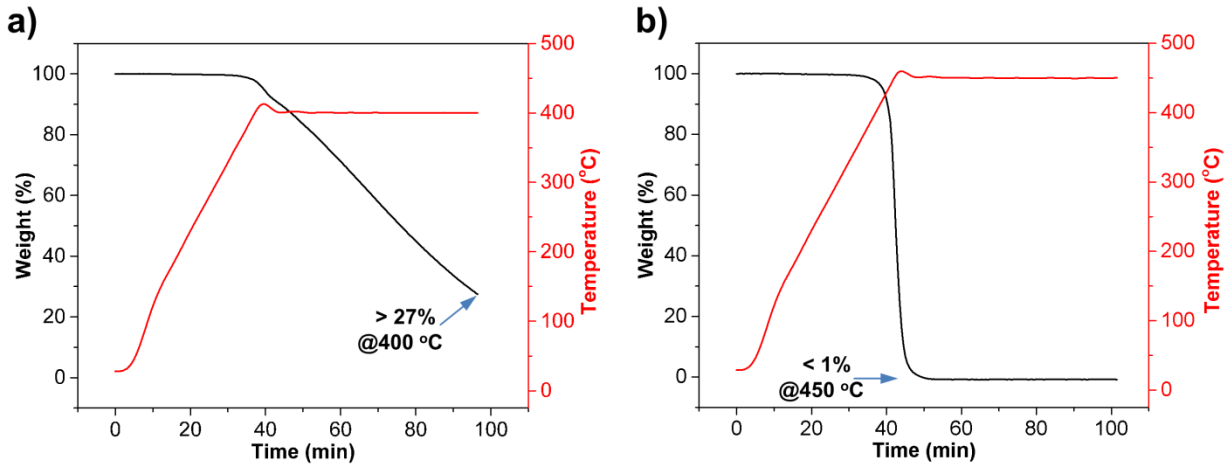

Figure 4-2. TG curve of PP at a heating rate of 10 °C min^{-1} up to 400 (a) or 450 °C (b) and then hold at this max temperature for 1 h.

This thermogravimetric experiments for different types of plastic waste provides insights into the temperature dependency and indicate that a temperature higher than 400 °C is required for an efficient pyrolysis process. But it still does not give any indication about the reaction time that is needed for complete degradation. Therefore, TG analysis was further carried out for

plastic PP by increasing the temperature to a certain temperature of either 400 or 450 ^{o}C followed by maintaining at this constant temperature for 1 h reaction time. As shown in Figure 4-2, there is still 27 wt% residue left in the sample plate after 1 h further degradation at 400 ^{o}C. However, when increasing temperature to 450 ^{o}C, the degradation efficiency was significantly improved. There is only less than 1 wt% residue left after 10 min degradation time at 450 ^{o}C.

Table 4-1. Summary of decomposition temperatures (e.g., onset temperature To, peak temperature Tp and end point temperature Te) and weight losses of individual plastic.

Plastic	**T_o/^{o}C**	**T_p/^{o}C**	**T_e/^{o}C**	**Loss/wt%**	
PET	413	438	454	77.9	
HDPE	446	481	498	97.3	
LDPE	448	485	505	>99	
PP	436	465	482	95.9	
PS	396	416	428	97.2	
PVC	237	299	351	72.5	87.2
	414	457	509	14.7	

4.4.2 Pyrolysis of PP

Generally, the pyrolysis process converts materials into three major components, char, gas and a pyrolysis oil. Liquid fuel is easier to be stored whereas gas is more efficient to be used for producing energy. The distribution of pyrolysis products is highly dependent on the reaction conditions. In this study, different reaction conditions such as temperature, reaction time were investigated. First, the pyrolysis process was carried out for plastic PP at individual temperature, 400, 450, 500 and 550 ^{o}C, respectively. All the experiments were performed on a mass of 20 g and each reaction condition was performed by altering the temperature. Yields of liquid fuel and pyrolysis residue were determined on a mass basis and the remaining part was calculated as gas. It shows only a small part of PP, around 20 wt%, is transformed into oil and gas at 400 ^{o}C (Figure 4-3 a). A significant increase of gas and oil yields (> 99 wt%) was observed by increasing the pyrolysis temperature to 450 ^{o}C, while there is almost no difference of product yield distribution when increasing the temperature to 500 ^{o}C. Further increasing the temperature from 500 to 550 ^{o}C, the yield of gas increases from 21.4 wt% to

31.8 wt% whereas the yield of oil decreases from 78.1 wt% to 67.6 wt%. The oil to gas ratio is shown in Figure 4-3 d. A slight increase of oil to gas ratio from 3.0 to 3.7 was observed when increasing temperature from 400 to 450 ^{o}C and it then stays flat between 450 and 500 ^{o}C. Later it significantly drops from 3.7 to 2.2.

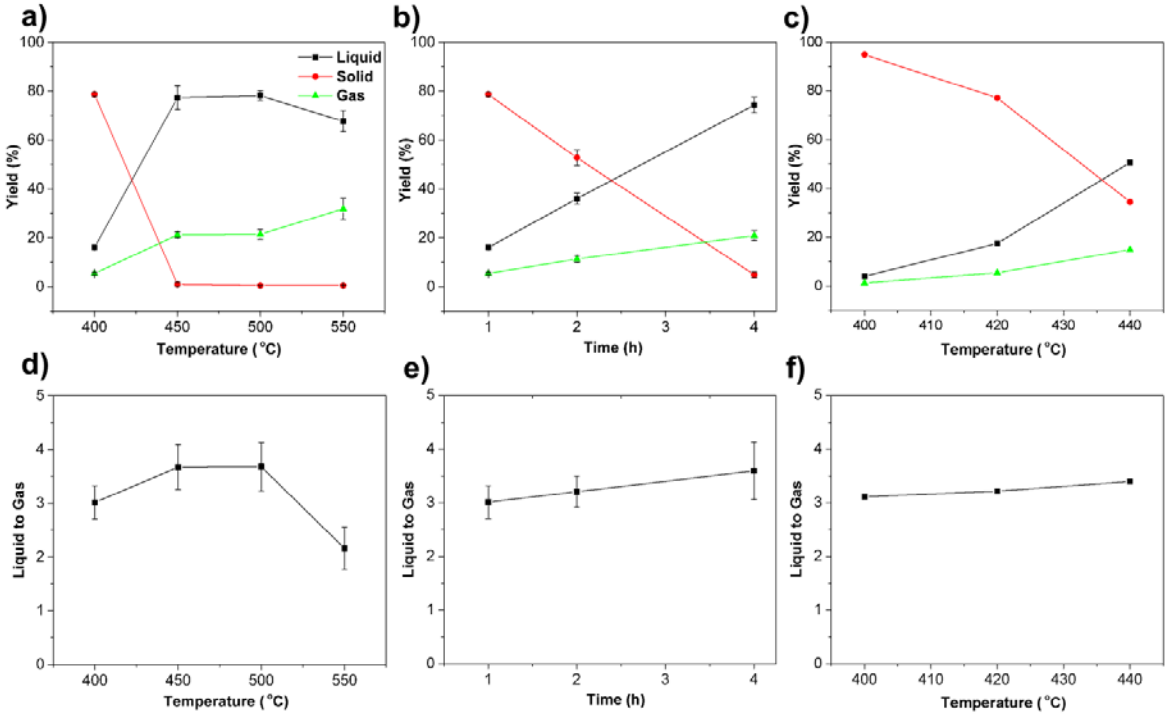

Figure 4-3. Plots of temperature versus the pyrolysis products yield (a) or liquid to gas ratio (d) for plastic PP. Plots of reaction time at temperature 400 ^{o}C versus the pyrolysis products yield (b) or liquid to gas ratio (e). Plots of temperature versus the products yield (c) or liquid to gas ratio (f).

As low transformation efficiency happens at a low temperature of 400 ^{o}C with 1 h pyrolysis, the effect of reaction time was examined for products yield, shown in Figure 4-3 b and e. It can be observed that a linear increase of liquid and gas yields accompanies with the increase of reaction time. Compared to product yield with a reaction time of 1 h, the residue inside the reactor almost disappears after 4 h pyrolysis process. The liquid yield increases from 16.0 wt% to 74.3 wt% and the gas yield increases from 5.3 wt% to 20.9 wt%. The gas to liquid ratio is also calculated and no significant change is observed among different reaction times.

A third reaction condition was investigated. The pyrolysis was carried out at 400 ^{o}C with a reaction time of 20 min, followed by a step by step temperature increasing procedure. At each temperature, the products were collected, weighted and the residue in the reactor was acting as a starting material for next temperature pyrolysis procedure. The results are shown in Figure 4-3 c and f. Increasing temperature from 400 to 420 ^{o}C, the degradation rate is relative

slow with liquid yield increasing from 3.9 wt% to 17.5 wt% and gas yield increasing from 1.3 wt% to 5.4 wt%, respectively. In comparison, the degradation rate is more than two times higher when increasing the temperature from 420 to 440 ^{o}C. For the liquid to gas ratio, there is almost no change.

4.4.3 Pyrolysis of individual plastics

The pyrolysis process was further extended to other plastic material, such as PET, PS, PVC, LDPE and HDPE and the product distribution is shown in Figure 4-4. Based on TG and DTG analysis information, a temperature higher than 450 ^{o}C is required to shorten the reaction time and to achieve an efficient transformation. After the pyrolysis process at 450 ^{o}C for 1 h, a minor difference (2.3 wt%, 2.0 wt%, 4.7 wt% and 2.7 wt% for PET, PP, PS and PVC, respectively) between pyrolysis residue and TG residue was observed. However, still a big part of LDPE and HDPE (51.7 wt% and 36.9 wt%, respectively) was not transformed at 450 ^{o}C. This result correlates well with TG weight loss analysis as the TG curve shows that complete degradation of LDPE and HDPE occurs at a higher temperature. Increasing the pyrolysis temperature from 450 to 500 ^{o}C leads to complete degradation as well (1.5 wt% and 1.1 wt% residue, respectively).

The pyrolysis volatiles were cooled down by using cooling steps with two steps ice water baths (4 ^{o}C), following by one step dry ice saturated acetone bath (-78 ^{o}C). Different fractions were collected. The heavy fraction with heavy compounds can be obtained from ice/water bath and the light fraction with light compounds can be collected from dry ice saturated acetone bath. Condensed products of PET and HDPE appear to be solid and wax-like, respectively, whereas pyrolysis of other plastics obtained more liquid fuels. The pyrolysis process of PP leads to the highest amount of light oil fraction with a yield of 19.3 wt%.

In respect of gas distribution, the pyrolysis of PET and PVC containing a high quantity of heteroatoms (O and Cl) obtained a higher amount of non-condensable gas in comparison with hydrocarbon plastics. This might be attributed to loss of CO, CO_2 and HCl which does not happen in hydrocarbon plastics during pyrolysis at non-oxygen atmosphere condition. Theoretically, 58.7 wt% HCl would form during PVC decomposition if the dehydrochlorination was complete. Rosa Miranda et al.[33] discovered 58 wt% gas loss was assigned to HCl and only less than 0.5 wt% gas loss was attributed to other gases after the complete decomposition of plastics. In comparison, theoretically a 40.6-58.3 wt% loss for PET decomposition can be calculated at the basis of weight loss of CO and CO_2. Chika

Muhammad et al.[34] found that nearly 35 wt% gas loss was observed and more than 30 wt% gas was assigned to the release of CO and CO_2. Similarly, in our study, a high amount of gas loss for PVC (44.4 wt%) and PET (35.3 wt%) was observed during pyrolysis. Among hydrocarbon plastics, PS has the least quantity of non-condensable gas formed after pyrolysis.

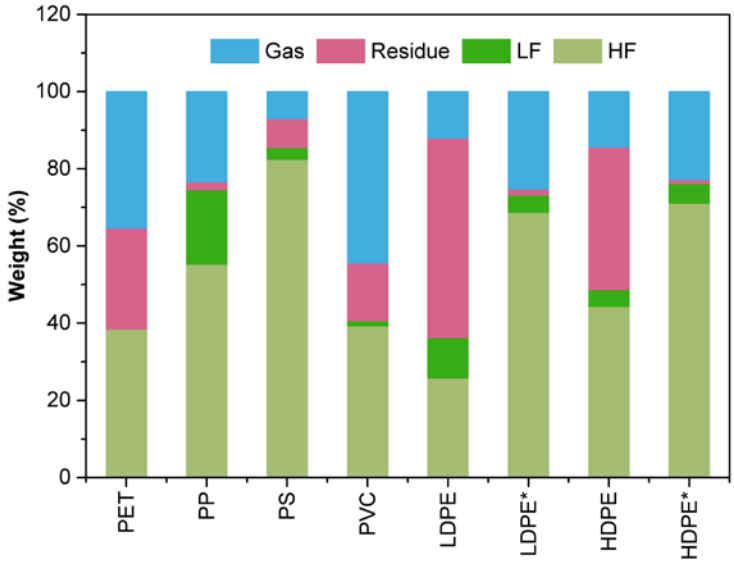

Figure 4-4. Pyrolysis products yield at 450 ^{o}C for individual plastics and 500 ^{o}C only for LDPE, HDPE shown with superscript star.

4.4.4 Structure characterization and mechanistic study

Pyrolysis oils including light and heavy fractions derived from plastic waste materials were analyzed by using GC-EI-Orbitrap. The data of four different materials are shown in Figure 4-5. The structural characterization was elucidated by searching MassLib (Table 4-2, Table A4-1, Table A4-2 and Table A4-3, Scheme 4-1, Scheme A4-1, Scheme A4-2 and Scheme A4-3). There is a slight shift of dead volume time for GC chromatogram measured at different date because of slight cutting at the end of GC column. Pyrolysis of PP produces a lot propylene dimer and trimer derivatives. These derivatives not only contain linear alkenes (e.g., 2-methylpentene, 4-methyl-2-pentene) and dienes (e.g., 4-mehtyl-1,3-pentadiene), but also cyclic alkanes (e.g., 1,3,5-trimethylcyclohexane) and alkene (e.g., 3,5-dimethylcyclopentene). Similar compounds can be detected from the pyrolysis oil obtained from LDPE with an emphasis on compounds derived from multiple ethylene units. A small amount of aromatics (e.g., toluene, m-xylene) can also be characterized. One significant difference is that a series of adjacent characteristic peaks can be observed, which has also been revealed before, but only with evidence of low resolution mass spectra data.[35-37] Serious

attention should be taken into consideration for the identification of these heavier compounds. An alkane molecule with 12 carbon number can produce at least 355 isomers and many of them cannot be found in mass spectral library, which makes the characterization of even heavier compounds extremely difficult. But by using high resolution Orbitrap mass spectrometry, we can detect these molecular ions and their characteristic fragment ions with high mass accuracy. Therefore, the results presented in the table only give an indication of the types of high molecular weight compounds present in the pyrolysis oils. These characteristic signals are assigned to alkane and alkenes with the difference of one carbon unit.

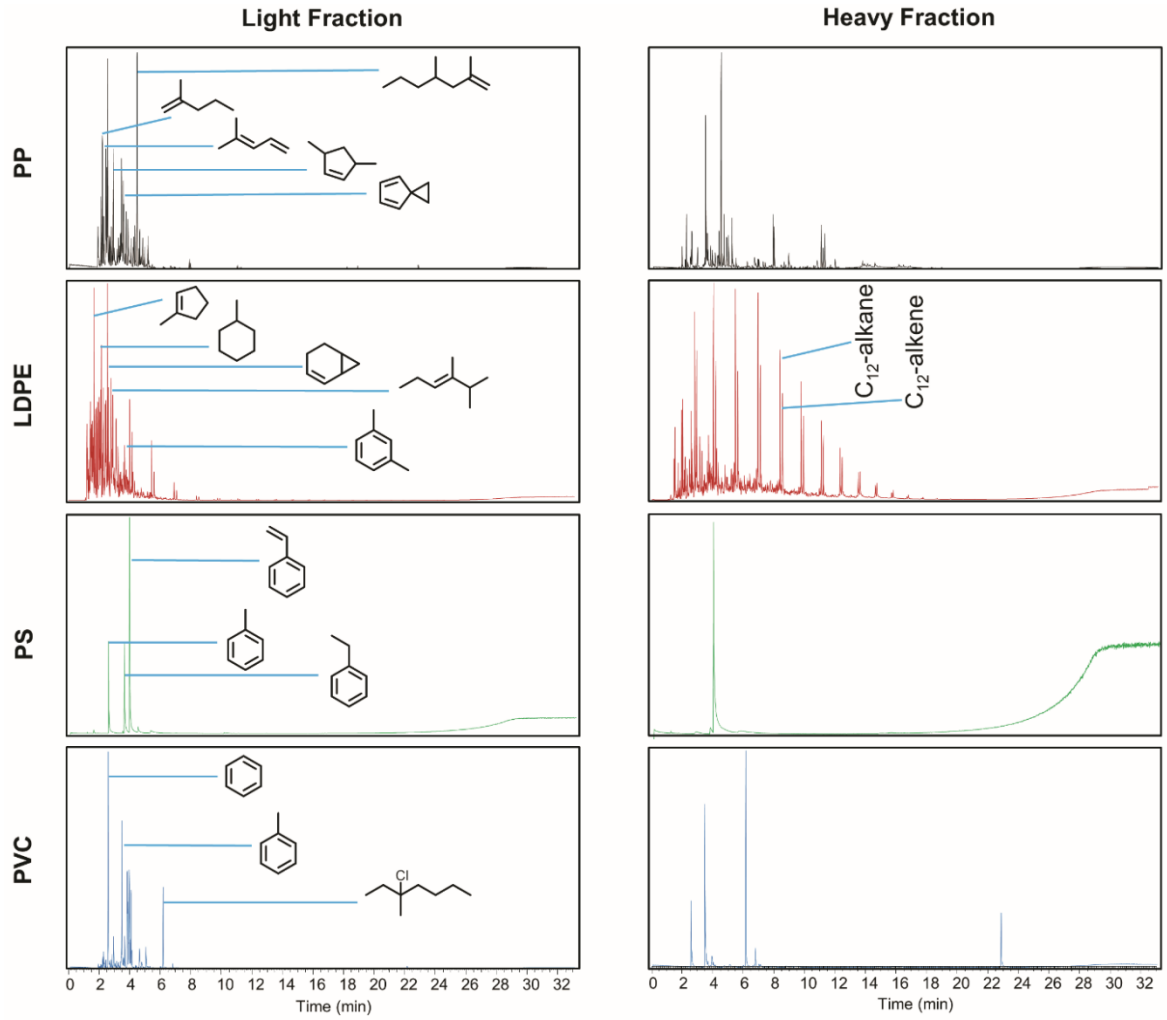

Figure 4-5. TIC signal of light (left) and heavy (right) fractions of plastics PP, LDPE, PS and PVC pyrolysis oils obtained at 450 ^{o}C.

Table 4-2. Composition of the oil resulting from pyrolysis of LDPE.

Peak No.	RT (min)	NIST ID	SI (%)	Name	Formula	Error a/b (ppm)*	Area (%)*	Error a/b (ppm)#	Area (%)#
1	1.3	NJ291890	76	1,3-pentadiene	C_5H_8	0.9/0.4	0.13	X/X	X
2	1.35	NJ19032	80	cyclopentene	C_5H_8	-0.6/-0.33	1.12	X/X	X
3	1.44	NJ118192	73	4-methyl-2-pentene	C_6H_{12}	1.4/0.8	2.82	1.5/0.7	0.72
4	1.48	NJ152055	70	1,1,2-trimethylcyclopropane	C_6H_{12}	1.3/0.6	1.4	X/X	X
5	1.52	NJ139415	69	3-methylcyclopentene	C_6H_{10}	1/0.3	0.35	X/X	X
6	1.69	NJ231297	81	1-methylcyclopentene	C_6H_{10}	1.5/0.7	5.71	1.3/0.3	0.73
7	1.78	NJ210237	55	1-methylenecyclopentene	C_6H_8	0.1/0.8	3.6	0.5/1.1	0.23
8	1.85	NJ231296	67	2,4-hexadiene	C_6H_{10}	1.7/0.7	2.6	1.4/0.5	0.33
9	1.93	NJ114027	59	1,2-dimethylcyclopentane	C_7H_{14}	1.6/1.6	4.97	1/0.2	2.42
10	2	NJ113117	50	3-heptene	C_7H_{14}	1.7/1.8	3.89	1.3/1.1	1.9
11	2.08	NJ113640	60	3,5-dimethylcyclopentene	C_7H_{12}	1.5/0.9	1.01	1.5/1.2	0.18
12	2.12	NJ150272	67	propan-2-ylidenecyclobutane	C_7H_{12}	1.8/1.7	2.33	1/0.8	0.55
13	2.16	NJ61214	69	methylcyclohexane	C_7H_{14}	2.2/1.3	3.56	1.7/0.9	0.97
14	2.28	NJ62523	68	1-methyl-2-methylenecyclopentane	C_7H_{12}	1.5/1.3	5.45	1.4/1.1	0.82
15	2.35	NJ113662	71	1-methyl-1.4-hexadiene	C_7H_{10}	1.8/0.8	0.42	X/X	X
16	2.43	NJ114407	70	1-ehtylcyclopentene	C_7H_{12}	1/0.6	2.56	1.4/1.1	0.97
17	2.46	NJ61211	72	toluene	C_7H_8	2.1/0.8	1.82	0.4/0.5	0.32
18	2.55	NJ152427	67	bicyclo[4.1.0]-2-heptene	C_7H_{10}	0.4/-0.1	5.78	2/1.3	2.15
19	2.61	NJ237922	64	1,3-cycloheptadiene	C_7H_{10}	1.8/1.3	2.72	1.4/0.7	1.06
20	2.8	NJ149380	78	2,3-dimethyl-3-hexene	C_8H_{16}	1.7/1.8	6.87	0.9/1.4	5.46
21	2.92	NJ160212	78	3-ethyl-3-methylpentane	C_8H_{18}	1.2/X	2.74	1.1/1.3	2.96
22	3.12	NJ113437	70	1-methyl-2-methylenecyclohexane	C_8H_{14}	1.5/0.7	4.18	1.6/0.7	2.27
23	3.26	NJ113476	76	ethylcyclohexane	C_8H_{16}	0.3/0.1	1.41	1.2/1	1.02
24	3.6	NJ291455	54	m-xylene	C_8H_{10}	2/1.7	1.47	1.6/0.8	1.15
25	3.7	NJ139463	68	1-ehtylcyclohexene	C_8H_{14}	1.8/1	1.18	1.5/0.7	0.85
26	4.01	X	X	C_9-alkene	C_9H_{18}	1/0.9	0.55	0.9/0.9	5.7
27	4.16	X	X	C_9-alkane	C_9H_{20}	0.9/-0.1	3.57	0.5/-1	3.44
28	5.44	X	X	C_{10}-alkene	$C_{10}H_{20}$	1.2/2.1	1.98	1.7/X	6.52
29	5.6	X	X	C_{10}-alkane	$C_{10}H_{22}$	0.3/0.7	0.78	-0.4/0.5	4.65
30	6.91	X	X	C_{11}-alkene	$C_{11}H_{22}$	0.6/1.4	0.6	0.3/0.7	6.1
31	7.08	X	X	C_{11}-alkane	$C_{11}H_{24}$	0.6/0.3	0.29	1.4/0.9	4.33
32	8.36	X	X	C_{12}-alkene	$C_{12}H_{24}$	0.1/1.8	0.17	0.3/0	4.7
33	8.51	X	X	C_{12}-alkane	$C_{12}H_{26}$	0.6/X	0.13	0.5/X	3.53
34	9.75	X	X	C_{13}-alkene	$C_{13}H_{26}$	-0.4/0.4	0.09	-0.1/-0.7	3.62
35	9.88	X	X	C_{13}-alkane	$C_{13}H_{28}$	0.2/-0.3	0.08	0.1/-0.5	2.66
36	11.05	X	X	C_{14}-alkene	$C_{14}H_{28}$	-1/X	0.09	-0.2/-0.5	2.75
37	11.19	X	X	C_{14}-alkane	$C_{14}H_{30}$	-0.8/X	0.07	-0.1/X	2.16
38	12.29	X	X	C_{15}-alkene	$C_{15}H_{30}$	0.2/-1.9	0.06	1/0.3	1.56
39	12.41	X	X	C_{15}-alkane	$C_{15}H_{32}$	0.2/0	0.06	-0.2/X	1.54
40	13.47	X	X	C_{16}-alkene	$C_{16}H_{32}$	-1.6/0.7	0.04	-0.2/X	0.9
41	13.58	X	X	C_{16}-alkane	$C_{16}H_{34}$	-0.5/X	0.07	0.2/0	0.9

42	14.58	X	X	C_{17}-alkene	$C_{17}H_{34}$	-1/-0.3	0.03	0.6/-1	0.42
43	14.68	X	X	C_{17}-alkane	$C_{17}H_{36}$	-1.1/X	0.05	0.6/X	0.59
44	15.63	X	X	C_{18}-alkene	$C_{18}H_{36}$	-1/X	0.03	0.1/1.8	0.2
45	15.74	X	X	C_{18}-alkane	$C_{18}H_{38}$	0.9/0.4	0.04	-0.5/X	0.33
46	16.65	X	X	C_{19}-alkene	$C_{19}H_{38}$	0.2/X	0.02	-0.7/X	0.08
47	16.74	X	X	C_{19}-alkane	$C_{19}H_{40}$	0.3/X	0.03	0.7/X	0.15
48	17.61	X	X	C_{20}-alkene	$C_{20}H_{40}$	-1.3/X	0.02	0.1/X	0.04
49	17.7	X	X	C_{20}-alkane	$C_{20}H_{42}$	-0.1/X	0.03	X/X	0.07
50	18.53	X	X	C_{21}-alkene	$C_{21}H_{42}$	0.4/X	0.01	1/X	0.02
51	18.61	X	X	C_{21}-alkane	$C_{21}H_{44}$	0.2/X	0.02	X/X	0.04
52	19.4	X	X	C_{22}-alkene	$C_{22}H_{44}$	-1.4/X	0.01	X/X	0.01
53	19.48	X	X	C_{22}-alkane	$C_{22}H_{46}$	-1.1/X	0.01	X/X	0.02
54	20.25	X	X	C_{23}-alkene	$C_{23}H_{46}$	-1/X	0.01	X/X	0
55	20.32	X	X	C_{23}-alkane	$C_{23}H_{48}$	X/X	0.01	X/X	0.01
56	21.06	X	X	C_{24}-alkene	$C_{24}H_{48}$	X/X	0.01	X/X	0
57	21.13	X	X	C_{24}-alkane	$C_{24}H_{50}$	X/X	0.01	X/X	0.01
total							79.06		84.11

Note: * and # stand for light and heavy fraction, respectively. Error a and b stand for the error of the molecular composition and its corresponding ^{13}C composition, respectively. The capital letter X represents the corresponding result cannot be found.

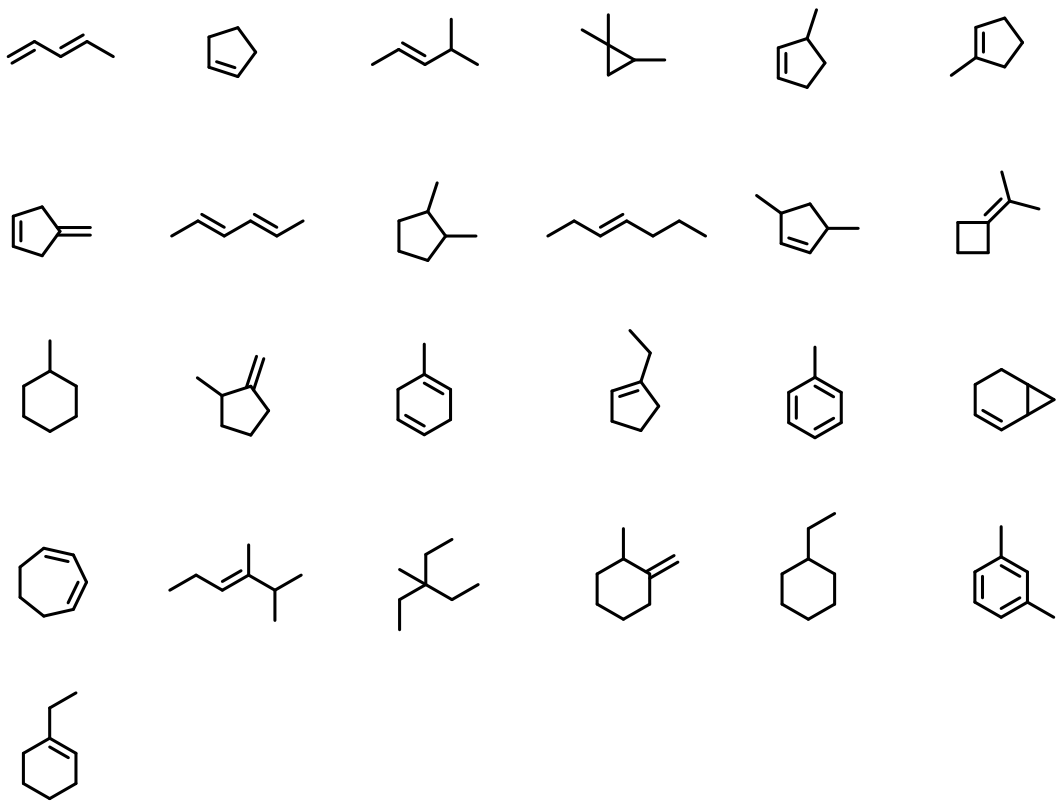

Scheme 4-1. The identified compound structure accordingly resulting from pyrolysis of LDPE.

The results for the other materials are a bit different. The data for the PS pyrolysis products only reveal monomer derivatives with the major components including toluene, ethylbenzene and styrene. The pyrolysis products for PVC mostly consist of non-chlorinated hydrocarbons.

Based on comparison with data from different databases, the spectra can be assigned to a number of different compounds which allows propose a corresponding mechanism, depicted in Scheme 4-2. Based on this data we can suggest that pyrolysis of olefinic polymers proceeds through a free radical mechanism, which corresponds well with data that have been reported about the thermal behavior of crude oil.[38] Initially, random C-C bond cleavage along the polymer chain forms single radical species, followed by hydrogen re-arrangement to generate single radical isomers. Once these single radicals are formed, they can be consumed immediately by β-scission to produce smaller single radicals and alkenes or by β-H abstraction to generate alkenes. Produced alkene compound can further undergo another random C-C bond cleavage to produce diene. A big polymer can also break at both sides to produce bi-radicals, followed by radical re-arrangements and cyclization reactions to produce different cyclic rings. A diene and alkene can form a cyclohexene through a Diels–Alder reaction, followed by removal of hydrogen or dealkylation to produce aromatic compounds. Two radicals can combine with each other to produce hydrocarbons with side chains of different length.

In comparison to pure hydrocarbon polymers, halogenated polymer like PVC degrades through a different mechanism. The first step in PVC pyrolysis is dehydrochlorination, which results in the release of large amount of HCl. This is caused by the cleavage of the weakest C–Cl bond to release Cl radicals from the PVC backbone, which then abstracts hydrogen to form HCl. Chlorine in the plastic backbone for PVC promotes the formation of aromatic compounds, which constitutes to 40.6 % of the total TIC.

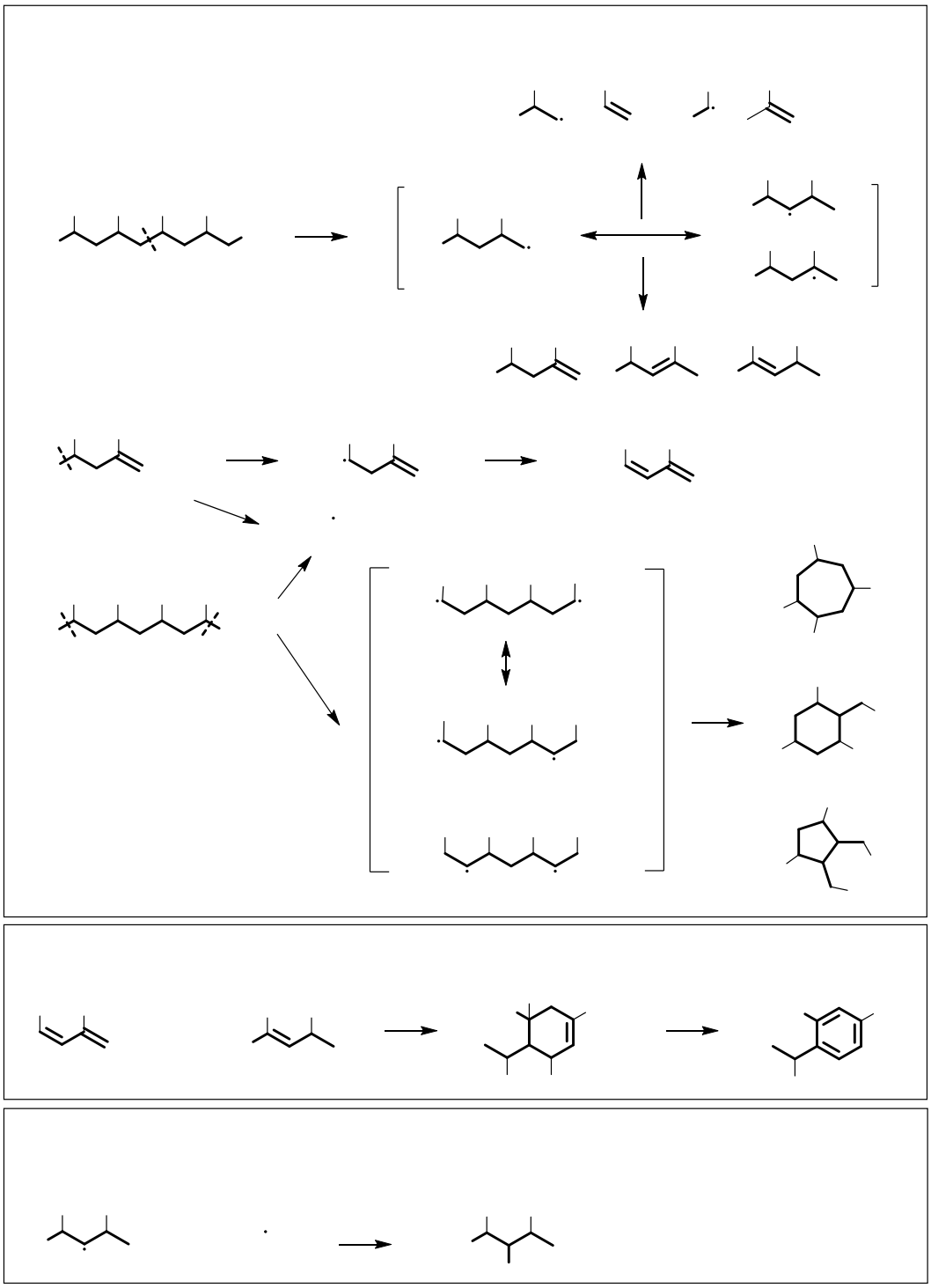

Scheme 4-2. Mechanism proposal for pyrolysis of LDPE (X= H), PP (X= methyl group) and PS (X= phenyl group).

4.4.5 Fuel application

Gasoline and diesel are the most commonly used transport fuel, which are mainly produced by fractional distillation from petroleum oil. Gasoline generally consists of low molecular

weight compounds with C_{5-11} and diesel fuel is composed of molecules with C_{12-20}. This criterion can be used for evaluating the potential application of plastic fuel.

Comparison of the chromatograms obtained from light and heavy fraction of LDPE pyrolysis fuel shows that a good separation was achieved. The chromatogram of light fraction show compounds with a short retention time, eluting mainly first 7 min. After 7 min, the chromatogram contains a few heavier compounds (C_{12-20}) in very low intensity, which only contributes to 1.1% of the TIC (Figure 4-6). In comparison, the heavy fraction chromatogram shows signals with high intensity in the retention time range1-17 min. Heavy compounds with $C_{>20}$ can be detected. Semi-quantification of this fraction shows that light compounds with $C_{\leqslant 11}$ (73.7%) have a higher amount than heavy compounds with C_{12-20} (26.2%).

For other plastic fuel light and heavy fractions, a slight (PP) or almost no clear (PS and PVC) separation was observed. The heavy fraction from PP also contains only a slight amount of heavy compounds (C_{12-20}) with 16.6%. Both light and heavy fractions of PS and PVC pyrolysis fuels display a low retention time in GC chromatography. Based on these analyses, the separation process using different cooling traps did not go well in our current experimental setup, but it shows a potential to be used as alternative to fossil fuel derived gasoline and diesel range fuel since both heavy and light fractions contains mainly compounds with $C_{\leqslant 20}$. To further improve the quality of trash fuels, a clean-up step is required. One way to obtain a better defined fuel could be through a distillation process of the pyrolysis oils.

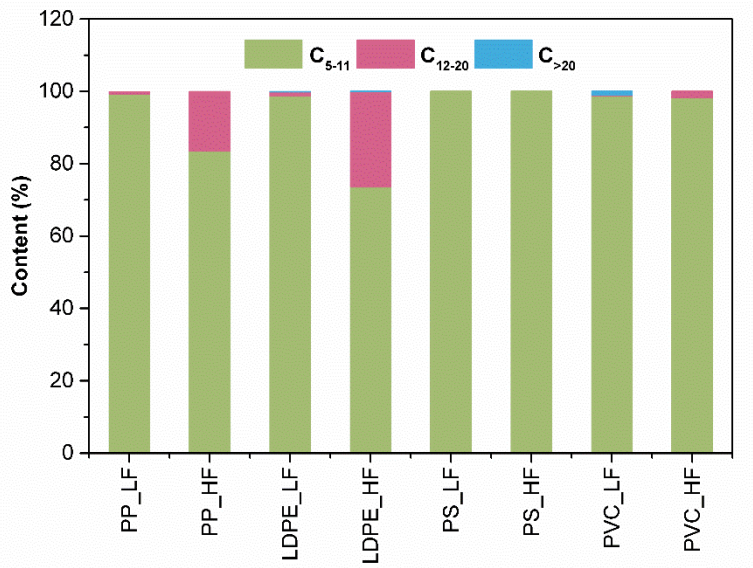

Figure 4-6. Semi-quantification of light and heavy fraction from pyrolysis derived plastic (PP, LDPE, PS and PVC, respectively) fuels.

4.5 Conclusion

In this work, plastics PET, HDPE, PVC, LDPE, PP and PS were investigated for their behavior during pyrolysis degradation. Thermogravimetric analysis for individual polymers was conducted to study the potential degradation behavior and to optimize the reaction conditions. Thermogravimetric analysis of PVC shows two degradation steps whereas thermogravimetric analysis for other plastics gives a single degradation step with a degradation temperature order of PS < PET < PP < HDPE ≈ LDPE. For the pyrolysis process, temperature and reaction time are two important pyrolysis parameters. A high temperature can significantly decrease the reaction time required for the pyrolysis process. The type of material also has a significant impact on the pyrolysis products distribution. The pyrolysis of PVC and PET produce a high amount of gaseous compounds while the pyrolysis of PS produces the least amount of gas. Instead, the pyrolysis of PS produces the highest liquid yield. The pyrolysis liquid fuels derived from different plastic types were further studied by high resolution GC-EI-Orbitrap, revealing the structural information about different fuels. A free radical mechanism was suggested, involving a series of reactions such as chain scission, beta-scission, beta-H-abstraction, cyclization, Diels–Alder reaction, radical recombination. The fuel quality was simply evaluated for potential application of gasoline and diesel range fuels based on GC retention time. Overall, this study successfully demonstrated that pyrolysis is an efficient way to convert plastic wastes to fuels. A better understanding of the pyrolysis of plastic materials was also achieved through the systematic study of different types plastic.

4.6 References

1. Andrady, A. L.; Rajapakse, N., Additives and chemicals in plastics. In *Hazardous Chemicals Associated with Plastics in the Marine Environment*, Springer: 2016; pp 1-17.
2. Ibeh, C. C., *Thermoplastic materials: properties, manufacturing methods, and applications*. CRC Press: 2011.
3. Bellas, J.; Gil, I., Polyethylene microplastics increase the toxicity of chlorpyrifos to the marine copepod Acartia tonsa. *Environ. Pollut.* **2020,** *260*, 114059.
4. Zhang, F.; Yao, C.; Xu, J.; Zhu, L.; Peng, G.; Li, D., Composition, spatial distribution and sources of plastic litter on the East China Sea floor. *Sci. Total Environ.* **2020,** *742*, 140525.
5. Yu, J.; Sun, L.; Ma, C.; Qiao, Y.; Yao, H., Thermal degradation of PVC: A review. *Waste Manage.* **2016,** *48*, 300-314.
6. Strungaru, S.-A.; Jijie, R.; Nicoara, M.; Plavan, G.; Faggio, C., Micro-(nano) plastics in freshwater ecosystems: abundance, toxicological impact and quantification methodology. *Trends Anal. Chem.* **2019,** *110*, 116-128.
7. Shah, A. A.; Hasan, F.; Hameed, A.; Ahmed, S., Biological degradation of plastics: a comprehensive review. *Biotechnol. Adv.* **2008,** *26* (3), 246-265.

8. Hoàng, E. M.; Lowe, D., Lifetime prediction of a blue PE100 water pipe. *Polym. Degrad. Stab.* **2008,** *93* (8), 1496-1503.
9. Barnes, D.; Milner, P., Drifting plastic and its consequences for sessile organism dispersal in the Atlantic Ocean. *Mar. Biol.* **2005,** *146* (4), 815-825.
10. Garcia-Nunez, J.; Pelaez-Samaniego, M.; Garcia-Perez, M.; Fonts, I.; Abrego, J.; Westerhof, R.; Garcia-Perez, M., Historical developments of pyrolysis reactors: a review. *Energy Fuels* **2017,** *31* (6), 5751-5775.
11. Ragaert, K.; Delva, L.; Van Geem, K., Mechanical and chemical recycling of solid plastic waste. *Waste Manag.* **2017,** *69*, 24-58.
12. Rozenstein, O.; Puckrin, E.; Adamowski, J., Development of a new approach based on midwave infrared spectroscopy for post-consumer black plastic waste sorting in the recycling industry. *Waste Manag.* **2017,** *68*, 38-44.
13. Andrady, A. L., The plastic in microplastics: A review. *Mar. Pollut. Bull.* **2017,** *119* (1), 12-22.
14. Thompson, R. C.; Moore, C. J.; Vom Saal, F. S.; Swan, S. H., Plastics, the environment and human health: current consensus and future trends. *Philos. Trans. R. Soc. Lond., B, Biol. Sci.* **2009,** *364* (1526), 2153-2166.
15. Corcoran, P. L.; Biesinger, M. C.; Grifi, M., Plastics and beaches: a degrading relationship. *Mar. Pollut. Bull.* **2009,** *58* (1), 80-84.
16. Halden, R. U., Plastics and health risks. *Annu. Rev. Public Health* **2010,** *31*, 179-194.
17. Teuten, E. L.; Saquing, J. M.; Knappe, D. R.; Barlaz, M. A.; Jonsson, S.; Björn, A.; Rowland, S. J.; Thompson, R. C.; Galloway, T. S.; Yamashita, R., Transport and release of chemicals from plastics to the environment and to wildlife. *Philos. Trans. R. Soc. Lond., B, Biol. Sci.* **2009,** *364* (1526), 2027-2045.
18. Rochman, C. M.; Browne, M. A.; Halpern, B. S.; Hentschel, B. T.; Hoh, E.; Karapanagioti, H. K.; Rios-Mendoza, L. M.; Takada, H.; Teh, S.; Thompson, R. C., Classify plastic waste as hazardous. *Nature* **2013,** *494* (7436), 169-171.
19. Geyer, R.; Jambeck, J. R.; Law, K. L., Production, use, and fate of all plastics ever made. *Sci Adv* **2017,** *3* (7), e1700782.
20. Coady, D.; Parry, I.; Le, N.-P.; Shang, B., Global fossil fuel subsidies remain large: An update based on country-level estimates. *IMF Working Papers* **2019,** *19* (89), 39.
21. Shafiee, S.; Topal, E., When will fossil fuel reserves be diminished? *Energy Policy* **2009,** *37* (1), 181-189.
22. Bardi, U., Peak oil, 20 years later: failed prediction or useful insight? *Energy Res. Soc. Sci.* **2019,** *48*, 257-261.
23. Jacobson, M. Z.; Delucchi, M. A., Providing all global energy with wind, water, and solar power, Part I: Technologies, energy resources, quantities and areas of infrastructure, and materials. *Energy Policy* **2011,** *39* (3), 1154-1169.
24. Eleftheriadis, I. M.; Anagnostopoulou, E. G., Identifying barriers in the diffusion of renewable energy sources. *Energy Policy* **2015,** *80*, 153-164.
25. Pickard, W. F.; Shen, A. Q.; Hansing, N. J., Parking the power: Strategies and physical limitations for bulk energy storage in supply–demand matching on a grid whose input power is provided by intermittent sources. *Renew. Sust. Energ. Rev.* **2009,** *13* (8), 1934-1945.
26. Wong, S.; Ngadi, N.; Abdullah, T. A. T.; Inuwa, I. M., Current state and future prospects of plastic waste as source of fuel: A review. *Renew. Sust. Energ. Rev.* **2015,** *50*, 1167-1180.
27. Panda, A. K.; Singh, R. K.; Mishra, D., Thermolysis of waste plastics to liquid fuel: A suitable method for plastic waste management and manufacture of value added products—A world prospective. *Renew. Sust. Energ. Rev.* **2010,** *14* (1), 233-248.

28. Wang, K.-S.; Chiang, K.-Y.; Lin, S.-M.; Tsai, C.-C.; Sun, C.-J., Effects of chlorides on emissions of toxic compounds in waste incineration: study on partitioning characteristics of heavy metal. *Chemosphere* **1999,** *38* (8), 1833-1849.
29. Verma, R.; Vinoda, K.; Papireddy, M.; Gowda, A., Toxic pollutants from plastic waste-a review. *Procedia Environ. Sci.* **2016,** *35*, 701-708.
30. Abad, E.; Adrados, M.; Caixach, J.; Fabrellas, B.; Rivera, J., Dioxin mass balance in a municipal waste incinerator. *Chemosphere* **2000,** *40* (9-11), 1143-1147.
31. Venderbosch, R.; Prins, W., Fast pyrolysis technology development. *Biofuel. Bioprod. Bior.* **2010,** *4* (2), 178-208.
32. Butler, E.; Devlin, G.; McDonnell, K., Waste polyolefins to liquid fuels via pyrolysis: review of commercial state-of-the-art and recent laboratory research. *Waste Biomass Valori.* **2011,** *2* (3), 227-255.
33. Miranda, R.; Pakdel, H.; Roy, C.; Darmstadt, H.; Vasile, C., Vacuum pyrolysis of PVCII: Product analysis. *Polym. Degrad. Stab.* **1999,** *66* (1), 107-125.
34. Muhammad, C.; Onwudili, J. A.; Williams, P. T., Thermal Degradation of Real-World Waste Plastics and Simulated Mixed Plastics in a Two-Stage Pyrolysis–Catalysis Reactor for Fuel Production. *Energy Fuels* **2015,** *29* (4), 2601-2609.
35. Sharma, B. K.; Moser, B. R.; Vermillion, K. E.; Doll, K. M.; Rajagopalan, N., Production, characterization and fuel properties of alternative diesel fuel from pyrolysis of waste plastic grocery bags. *Fuel Process. Technol.* **2014,** *122*, 79-90.
36. González-Pérez, J. A.; Jiménez-Morillo, N.; de La Rosa, J.; Almendros, G.; González-Vila, F. J., Pyrolysis-gas chromatography–isotope ratio mass spectrometry of polyethylene. *J. Chromatogr. A* **2015,** *1388*, 236-243.
37. Kumar, S.; Singh, R., Recovery of hydrocarbon liquid from waste high density polyethylene by thermal pyrolysis. *Braz. J. Chem. Eng.* **2011,** *28* (4), 659-667.
38. Kondyli, A.; Schrader, W., Understanding “fouling” in extremely complex petroleum mixtures. *ACS Appl. Energy Mater.* **2020,** *3* (8), 7251-7256.

4.7 Appendix

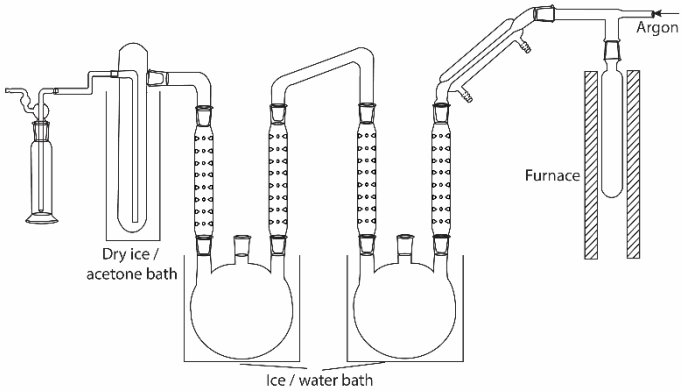

Figure A4-1. Schematic diagram of designed pyrolysis setup.

Table A4-1. Composition of the oil resulting from pyrolysis of PP.

Peak No.	RT (min)	NIST ID	SI (%)	Name	Formula	Error a/b (ppm)*	Area (%)*	Error a/b (ppm)#	Area (%)#
1	2.22	NJ19326	78	2-methylpentene	C_6H_{12}	1.3/0.6	6.86	1.3/0.2	3.66
2	2.31	NJ19318	75	4-methyl-2-pentene	C_6H_{12}	1.7/0.9	3.530	1.5/0.6	0.54
3	2.45	NJ149696	78	4-mehtyl-1,3-pentadiene	C_6H_{10}	1.8/1	5.76	1.3/0.3	0.95
4	2.53	NJ114239	66	1,3-dimethylcyclopentane	C_7H_{14}	1.6/1.2	2.510	0.9/1	0.78
5	2.82	NJ114027	75	1,2-dimethylcyclopentane	C_7H_{14}	1.1/1.2	2.29	X/X	X
6	2.94	NJ113640	59	3,5-dimethylcyclopentene	C_7H_{12}	1.8/1.5	7.830	1.1/0.7	2.11
7	3	NJ150272	60	propan-2-ylidenecyclobutane	C_7H_{12}	1.1/0.9	0.35	X/X	X
8	3.19	NJ113453	65	5,5-dimethyl-1.3-hexadiene	C_8H_{14}	1.7/1	0.79	X/X	X
9	3.27	NJ62523	58	1-methyl-2-methylenecyclopentane	C_7H_{12}	1.3/1	1.4	X/X	X
10	3.48	NJ152867	59	spiro[2.4]-4.6-heptadiene	C_7H_8	1.2/1.1	5.23	0.9/-0.8	12.5
11	3.62	NJ113436	66	3,5-dimethylcyclohexene	C_8H_{14}	0.9/0.6	6.160	1/0.1	0.47
12	3.78	NJ1605	65	1,1,2-trimethylcyclopentane	C_8H_{16}	0.9/0.5	2.860	0.8/0.3	1.66
13	3.9	NJ113461	90	1,2,3-trimethylcyclopentene	C_8H_{14}	1.3/0.4	2.840	1.6/0.6	1.67
14	4.28	NJ113442	70	1,6-dimethylcyclohexene	C_8H_{14}	1.4/0.4	2.59	1.6/0.8	1.72
15	4.36	NJ114126	68	1,3,5-trimethylcyclohexane	C_9H_{18}	0.5/-0.1	1.86	1.4/0.6	2.87
16	4.5	NJ113516	76	2,4-dimethylheptene	C_9H_{18}	1.1/1.1	16.140	1.2/1.3	21.22
17	4.85	NJ114765	64	3,3,5-trimethylcyclohexene	C_9H_{16}	0.5/-0.4	1.51	1.4/0.2	2.63
18	4.98	NJ113515	80	1,2,4,4-tetramethylcyclopentene	C_9H_{16}	1.6/0.5	1.210	2.7/1.5	2.45
total							71.72		55.23

Note: * and # stand for light and heavy fraction, respectively. Error a and b stand for the error of the molecular composition and its corresponding ^{13}C compositon, respectively. The capital letter X represents the corresponding result cannot be found.

Table A4-2. Composition of the oil resulting from pyrolysis of PS.

Peak No.	RT (min)	NIST ID	SI (%)	Name	Formula	Error a/b (ppm)*	Area (%)*	Error a/b (ppm)#	Area (%)#
1	1.55	NJ228005	60	chloroform	$CHCl_3$	X/X	1.01	X/X	X
2	2.51	NJ61211	92	toluene	C_7H_8	-1.2/-1	18.59	X/X	X
3	3.54	NJ228326	86	ethylbenzene	C_8H_{10}	1.4/0.8	23.64	X/X	X
4	3.88	NJ229644	90	styrene	C_8H_8	-0.7/-0.8	49.79	0.9/0.7	96.49
5	4.42	NJ114201	80	cumene	C_9H_{12}	1.1/0.1	2.99	X/X	X
6	5.27	NJ617890	58	alpha-methylstyrene	C_9H_{10}	0.5/-0.1	3.35	X/X	X
total							99.37		96.49

Table A4-3. Composition of the oil resulting from pyrolysis of PVC.

Peak No.	RT (min)	NIST ID	SI (%)	Name	Formula	Error a/b (ppm)*	Area (%)*	Error a/b (ppm)#	Area (%)#
1	2.23	NJ289588	75	2,3-dimethyl-2-butene	C_6H_{12}	1.7/0.8	0.82	X/X	X
2	2.57	NJ228009	87	benzene	C_6H_6	1.2/-0.4	23.53	-2.8/-4.5	14.57
3	2.75	NJ231296	69	2,4-hexadiene	C_6H_{10}	1.5/0.6	0.64	X/X	X
4	2.83	NJ114027	71	1,2-dimethylcyclopentane	C_7H_{14}	0.9/0.2	1.14	X/X	X
5	3.48	NJ61211	91	toluene	C_7H_8	-0.1/0.1	11.67	0.8/0.9	34.01
6	3.83	NJ100813	66	1-butyl-2-methylcyclopropane	C_8H_{16}	0.9/0.6	3.87	X/X	X
7	3.86	NJ113457	80	3-ethyl-3-hexene	C_8H_{16}	1.5/0.5	2.47	X/X	X
8	3.95	NJ113485	71	3-methyl-3-heptene	C_8H_{16}	1.1/0.1	16.74	1.8/0.9	3.48
9	4.02	NJ149380	72	2,3-dimethyl-3-hexene	C_8H_{16}	1.3/0.3	1.57	X/X	X
10	4.06	NJ114011	69	2-ethyl-1-hexene	C_8H_{16}	1.5/0.5	7.51	X/X	X
11	4.12	NJ114273	68	1-ethyl-2-methylcyclopentane	C_8H_{16}	1.3/0.6	1.54	X/X	X
12	4.62	NJ228326	73	ethylbenzene	C_8H_{10}	1.2/0.3	2.58	X/X	X
13	5.04	NJ228063	70	m-xylene	C_8H_{10}	1.5/0.8	2.81	X/X	X
14	6.17	NJ114670	67	3-chloro-3-methylheptane	$C_8H_{17}Cl$	X/X	9.78	X/X	39.13
15	6.78	NJ4500	67	3-(chloromethyl)heptane	$C_8H_{17}Cl$			X/X	3.54
total							86.67		94.73

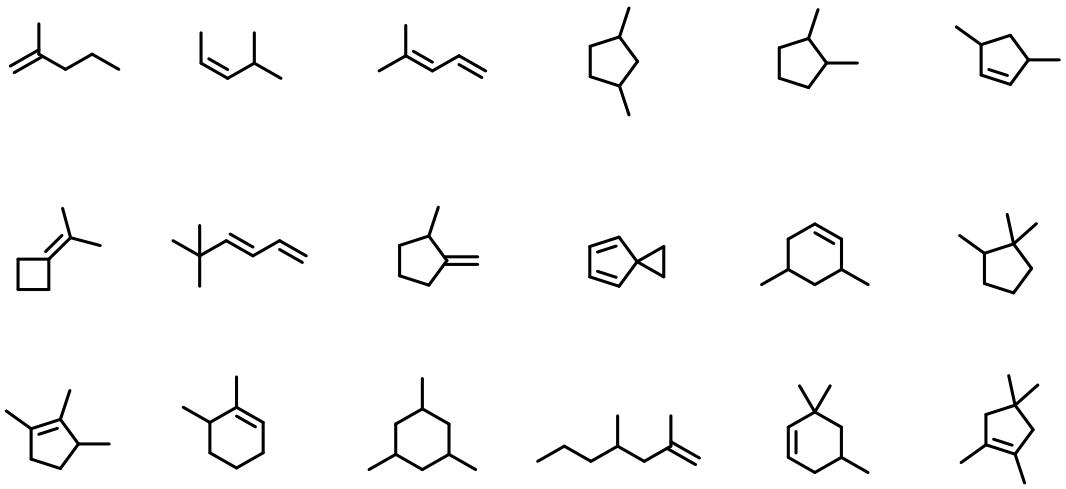

Scheme A4-1. The identified compound structure accordingly resulting from pyrolysis of PP.

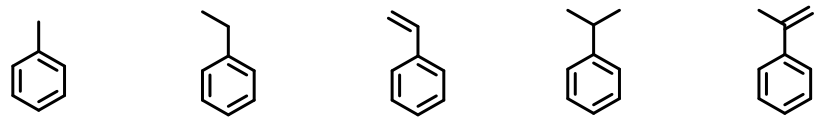

Scheme A4-2. The identified compound structure accordingly resulting from pyrolysis of PS.

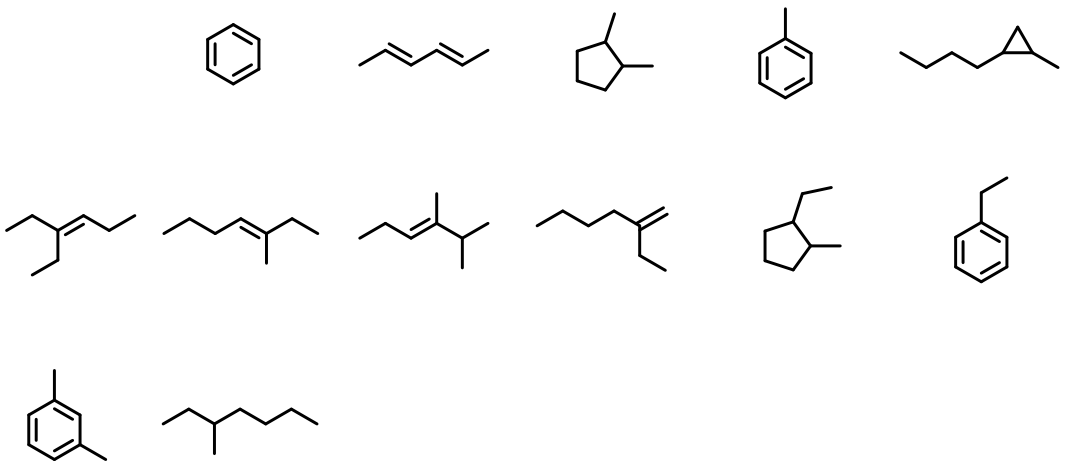

Scheme A4-3. The identified compound structure accordingly resulting from pyrolysis of PVC.

Chapter 5 *Waste-to-Fuel*: Producing gasoline and diesel type fuels derived from low value polymers by successive pyrolysis and distillation

Redrafted from "Xu, Y.; Schrader, W., *Waste-to-Fuel*: Producing gasoline and diesel type fuels derived from low value polymers by successive pyrolysis and distillation", will be submitted to *ACS Applied Energy Materials*.

5.1 Abstract

Plastics have been widely applied for usage in our daily life, such as packages, textiles, electric devices and many other applications. In return, the usage of plastic productions also generates a large amount of household and industrial plastic wastes. Plastic *waste-to-fuel* can be a final solution for waste management and can additionally serve as alterative partial substitution of fossil fuel. A study of using a successive pyrolysis and distillation to obtain high quality fuels (gasoline and diesel type fuels) from plastics is presented. The results show that a highly efficient transformation of plastic *waste-to-fuel* can be achieved through a pyrolysis process. The analysis of initial pyrolysis fuel by using GC-high resolution mass spectrometry (HRMS) shows a wide range of compounds (gasoline, diesel and wax range) coexisting in the pyrolysis oil, presenting a low quality fuel. After distillation, the separation of plastic fuel into gasoline and diesel type fuels can be confirmed by analytical data.

5.2 Introduction

The plastic industry has developed considerably fast over the last century since the invention of synthetic polymer derived from the petrochemical resources. Polymers have tremendous benefits over other types of materials (e.g., metal, glass, wood) attributed to its intrinsic properties of light weight, cheap price, durability among others.[1] Polymers can be easily shaped into almost anything with the aid of an injection molding machine, and thus, it provides endless possibility of applications in our daily life.[2] It has been widely manufactured into products such as packages, textiles, electric devices and many other applications. Owing to modernization, urbanization, rapidly growing population et al., the consumption of plastic products has increased dramatically from 0.35 to 348 million tons from 1950 to 2018 to satisfy the commercial demands.[3]

Accompanying with the widespread of plastic products, using plastics also create tremendous problems when they come to the end of their use phase. The natural degradation process of plastics (by exposing them into heat, UV light, microorganism et al.) could last from several decades to some centuries.[4-6] A good waste management is essential by creating a plastic lifecycle (closed loop of plastic) to reuse it.[7] If we as a human race do not find a way force full usage cycle of plastic materials, they will all end up on waste dumping in the environment, creating problems such as the microplastic that is now showing up. One typical recycling process is called mechanical recycling, which associates with process of plastics waste collecting, cleaning, sorting and regeneration. However, in reality, it raises a big concern whether the sorted plastics can be reused for the process of new production.[8] First, the addition of various additives in plastics including functional additives, colorants, fillers, and reinforcements helps to form a defined color, shape and texture in the final plastic products.[9] Second, plastic recycling and new production processes require additional heat cycles which decrease the lifespan of plastic and thus limit the number of times for recycling. Therefore, even the plastic with the same resin identification code (RIC) cannot be simply combined to directly make new products. Currently, the plastic recovery rate is still at a low level. According to a report published in 2015, only 20% of the total plastic waste was recycled globally.[10] The rest of them ends up in landfills, is dumped into oceans or burned in incinerators, which poses a severe risk towards global environment (e.g., soil, water and air pollution), health (e.g., human and wildlife health) and economy (e.g., costal tourism, fisheries).[11-14]

These inherent issues in the process of plastics waste management motivate us to seek alternative technologies leading to better use of the plastics waste. Polymers are carbonaceous materials and have a comparable heating value to fossil fuels.[15-17] Energy recovery of recycling residue or low quality plastics through simple pyrolysis process is promising and receives intensive interest with the purpose of obtaining valuable fuels. The pyrolysis processes of plastics were widely investigated, the compounds resulted from which is always a mixture of gasoline, diesel and even wax type hydrocarbons.[18-20] To improve the fuel quality, catalytic pyrolysis processes of plastics needs to be applied. And this process generally results in a slightly higher amount of gasoline range compounds, however, it is still unavoidable to introduce part of diesel range and also sometimes wax range compounds.[21-24] Therefore, a distillation process is a necessary step to separate pyrolysis plastic fuel into different type fuel to meet the fuel specification.

One of the most common analytic techniques, GC-MS, generally using quadrupole as mass detector, has been widely applied for the study of plastic to fuel.[25-27] The complexity of plastic fuel and the lack of standards typically result in an unconfident identification of compounds. Improvement can be gained by adding better analytical methods and technology. High resolution mass spectrometry by using Orbitrap or FT-ICR shows the advantage of giving more accurate compositional assignments.[28-30] Here, we first time report to use commercial available GC-EI-Orbitrap to investigate the pyrolysis of plastic materials and the distillation of the obtained pyrolysis oils to improve the plastic fuel quality. Moreover, previous studies of plastic *waste-to-fuel* generally present a simple study of either using several types of single plastic or just plastic mixtures.[31-33] Here, we conduct a more elaborate study by investigating both of them to check whether developed method of plastic *waste-to-fuel* in this study can be generally transferred from single plastic to complex plastic samples.

5.3 Experimental section

5.3.1 Materials

Polypropylene (PP), low density polyethylene (LDPE) and high density polyethylene (HDPE) pellets were purchased from Sinopec Shanghai Petrochemical Company Limited. Polystyrene (PS) pellets were purchased from Jiangsu Citic Guoan New Material Company Limited. Alkane standard solution C_{8-20} (~40 mg L^{-1} each dissolved in hexane) was purchased from Sigma Aldrich.

5.3.2 Thermogravimetric analysis (TGA)

TG measurements were performed using a Mettler Toledo TGA/DSC 1 Star System connected to data acquisition station. For each measurement, 2-3 mg of sample was placed in the TGA cell at an inert gas (argon) flow rate of 40 mL min^{-1}. LDPE was heated from 35 to 400 or 450 or 500 ^{o}C at a heating rate of 10 ^{o}C min^{-1} and then held at this temperature for further 1 h reaction.

5.3.3 Pyrolysis process

A variety of plastic samples, including single plastic (LDPE, PP and PS) and plastic mixture (PP/LDPE, PP/PS, LDPE/PS, LDPE/PP/PS and LDPE/HDPE/PP/PS) with each type of them having the equal weight ratio, were used for pyrolysis process. Each pyrolysis process was carried out at 500 ^{o}C in a quartz glass reactor with a dimension of H x W: 300 mm x 50 mm, which was installed into and externally heated by a 1480 W tube furnace EVA 12/300 B (Carbolite Gero, Germany). Around 20 g material in total each time was weighted and placed into the reactor. Before starting pyrolysis reaction, the reactor was swept with argon continuously for roughly 20 min to push the air out of the reactor. The system was heated at a maximum heating rate of 100 ^{o}C min^{-1} until reaching to the desired temperature, followed by an isothermal step of 1 h. The volatiles were swept away by an argon flow at a pressure of 0.2 mbar during the whole heating process. After exiting the reactor, the pyrolysis volatiles passed through a cooling water column and then two different cooling systems were applied, as shown in Figure 5-2. Setup A contains two ice water baths (4 ^{o}C) and one cooling trap with dry ice saturated acetone bath (-78 ^{o}C). A second optimized Setup B has two ice water baths (4 ^{o}C), two cooling traps with dry ice saturated acetone bath (-78 ^{o}C). The products were collected from each cooling trap and weighted. Products on the surface of cooling water column was washed out with dichloromethane, dried under vacuum evaporation overnight and weighted as well. The residue in the pyrolysis reactor was weighted.

5.3.4 Distillation of the pyrolysis fuels

A fractional distillation process was carried out with the distillation setup shown in Figure A5-1. Briefly, 10 g of plastic fuel was added into a distillation flask, which was stirred and heated on a magnetic stirrer with a hot plate and a thermocouple. In a step by step distillation procedure, fractions at various temperature cuts 130, 155, 180, 205, 230, 270, 300, 330 and 360 ^{o}C were collected. The separation of gasoline, diesel and wax type fuels from pyrolysis plastic fuels was conducted at a temperature of 270 ^{o}C and 430 ^{o}C. The distillation

process with a temperature lower than 300 °C was conducted at atmospheric pressure. Otherwise it was performed as a vacuum distillation with 1 mbar achieved by using an oil pump Duo 10 M (Pferffer Vacuum, Germany). The vacuum distillation temperature can be calculated through an open tool by inputting recorded vacuum value and the desired atmospheric pressure target temperature.[34] Before the vacuum distillation process, the temperature was first cooled down to room temperature, then a vacuum was applied, after that the temperature was increased to the calculated vacuum distillation temperature to operate a vacuum distillation process.

5.3.5 GC-EI-Orbitrap

High resolution GC/MS measurements were performed on a Q Exactive GC (Thermo Fisher, Bremen, Germany), consisting of a AI/AS 1310 autosampler equipped TRACE 1300 series GC coupled to a Q Exactive Orbitrap MS. The injection volume of individual sample was 0.2 µL and toluene was used as injector cleaning solvent. The sample injector was held at 300 °C and split mode was selected with a split flow of 80 mL min^{-1}, and a purge flow of 5 mL min^{-1}. High purity helium (N5.0) was used as a carrier gas at a constant flow rate of 1.2 mL min^{-1}. The GC separation was carried out on a RTX-1 ms capillary column (30 m x 0.25 mm ID, 0.25 um). The temperature program was performed with an initial temperature of 35 °C, which was increased to a final temperature of 320 °C at a heating rate of 10 °C min^{-1} and then held at 320 °C for additional 5 min. Transfer line temperature was set to 320 °C. The eluted compounds from GC were ionized by EI at an electron energy of 70 eV. The mass spectra were recorded in full scan mode with a mass range of 30-600 Da at a mass resolution of 120k (FWHM at *m/z* 200). Collected GC-MS data was imported and identified against NIST library by using MassLib (MSP Kofel, Zollikofen, Switzerland).

5.4 Results and discussion

5.4.1 TG analysis

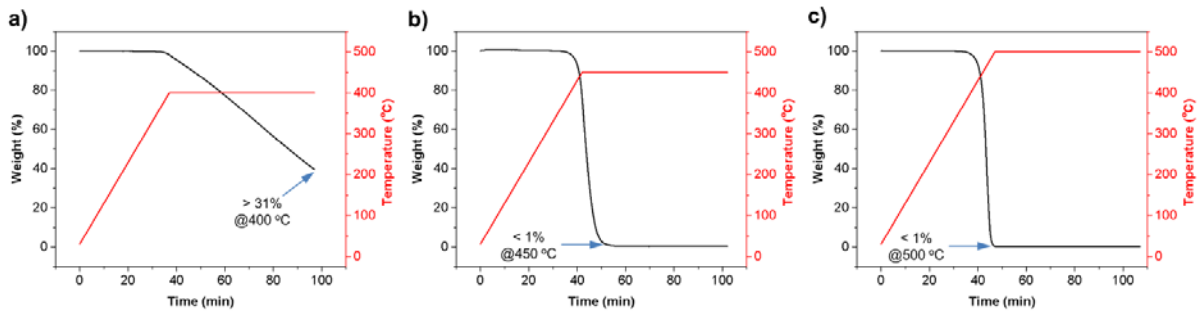

Figure 5-1. TG curve of LDPE from 30 ^{o}C up to 400 (a) or 450 (b) or 500 ^{o}C (c) at a heating rate of 10 ^{o}C min^{-1} and then hold at this max temperature for 1 h.

TG analysis was conducted for LDPE by increasing the temperature to a certain temperature of 400, 450 or 500 ^{o}C followed by maintaining at this constant temperature for further 1 h reaction time. As shown in Figure 5-1, the graph displays a steady weight loss at 400 ^{o}C and there is still 31 wt% residue left in the sample plate after 1 h. However, when increasing the temperature to 450 ^{o}C, the degradation efficiency was significantly improved by showing a steep slope. After the reaction, there is only less than 1 wt% of solid residue. The degrading time can be further shortened within 5 min when keeping the reaction temperature at 500 ^{o}C. These studies indicate that a temperature of higher than 400 ^{o}C is required for LDPE degradation and a temperature of higher than 450 ^{o}C can significantly decrease the reaction time.

5.4.2 Pyrolysis using initial designed setup

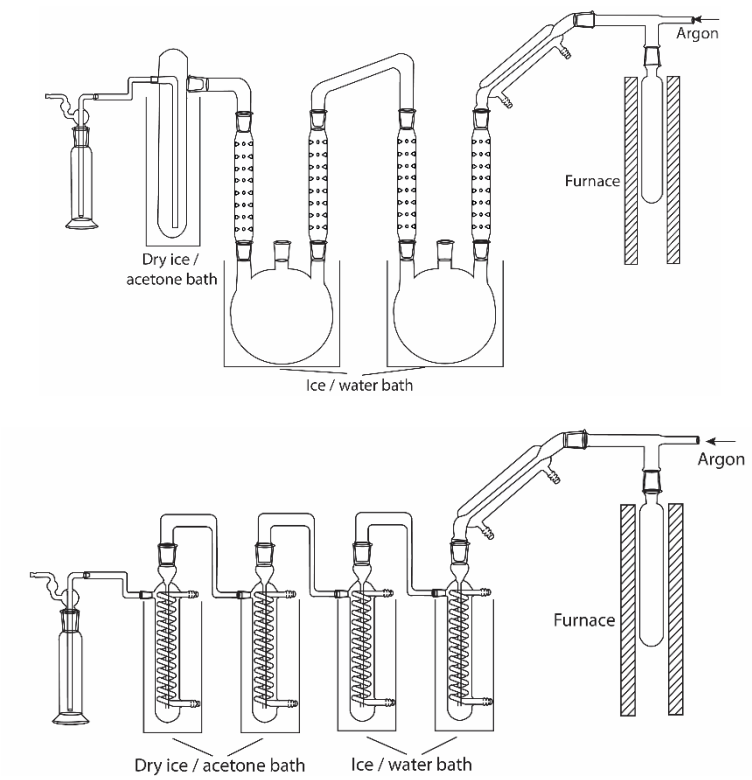

Figure 5-2. Schematic diagram of pyrolysis setup A (up) and B (down).

After the TG studies, the conditions of the pyrolysis was transferred to the pyrolysis reactor. An initial study was conducted using an initial designed pyrolysis setup, Setup A, shown in

Figure 5-2. This setup uses two three necked flasks (ice water baths) and a column (dry ice saturated acetone bath). Generally, pyrolysis converts materials into three major components, residue, gas and condensed products. In this process, the yields of pyrolysis residue and condensed products (light and heavy fractions) were weighted on a mass basis and the remaining part was calculated as gas. For a detailed study, LDPE was used at different temperatures, 450 and 500 ^{o}C. Figure 5-3 compares the pyrolysis product distribution. The result shows that pyrolysis of LDPE at 450 ^{o}C is an incomplete process, displaying a high amount of residue (51.7 wt%) while pyrolysis at 500 ^{o}C has almost complete transformation of LDPE to condensed product and gas.

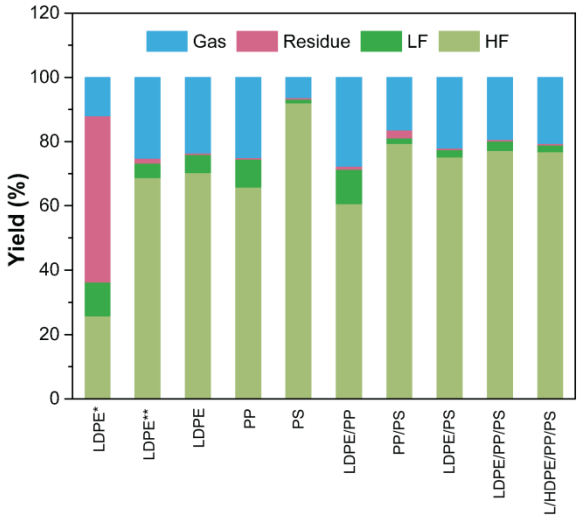

Figure 5-3. The first two columns are corresponding to pyrolysis products distribution at 450 (noted with the star) and 500 ^{o}C (noted with two stars) from plastic pellets LDPE using pyrolysis setup A. Columns from 3 to 10 (from left to right) are corresponding to pyrolysis products distribution at 500 ^{o}C from plastic pellets LDPE, PP, PS, PP/LDPE(1:1), PP/PS(1:1), LDPE/PS (1:1), LDPE/PP/PS (1:1:1) and LDPE/HDPE/PP/PS (1:1:1:1) using optimized pyrolysis setup B.

The pyrolysis process is a combination of degradation and evaporation process at a certain temperature. Once a compound with proper molecular size is generated, it evaporated out from pyrolysis reactor and was directly cooled down by cooling traps. Figure 5-4 compares the light and heavy fraction total ion current (TIC) signal obtained at different pyrolysis conditions. A separation can be observed between the light and heavy fractions. The heavy fraction derived from a high pyrolysis temperature at 500 ^{o}C shows a higher retention time than that achieved at 450 ^{o}C, indicating that it contains heavier compounds. Both the light fractions contain slight amount of heavy compounds.

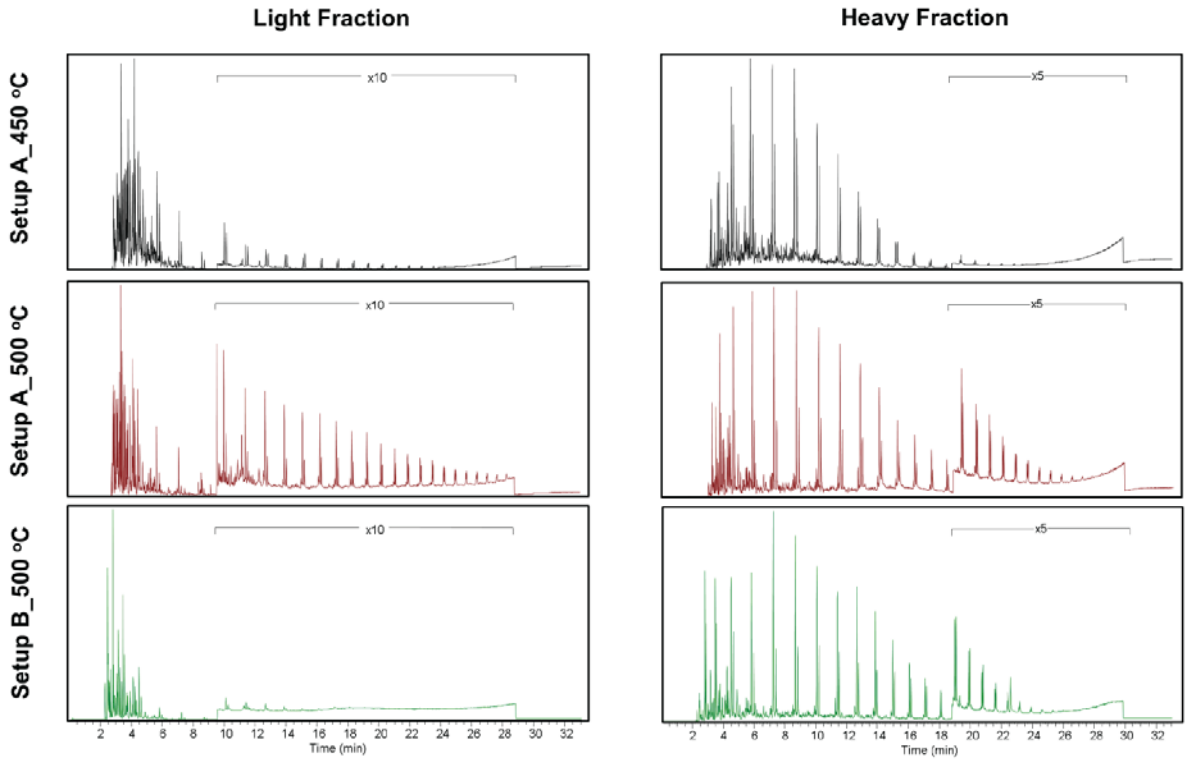

Figure 5-4. The TIC signal comparison between light and heavy fraction of pyrolysis LDPE fuels obtained at 450, 500 ^{o}C using setup A and 500 ^{o}C using setup B.

5.4.3 Pyrolysis using an optimized setup

While the studies described above have been obtained by using Setup A, it was problematic in regard to the type of mixtures that were trapped. Therefore an optimization of the cryotrapping had to be made. In comparison with the pyrolysis setup A, setup B has an optimized cooling system by using four times coil columns as oil collectors instead of using two three necked flask (ice water baths) and an column (dry ice saturated acetone bath), which provides a bigger surface area to volume ratio and therefore gives a better cooing for pyrolysis volatiles. It does not show any big difference of pyrolysis products distribution by using different setup. As expected, the light fraction using optimized pyrolysis setup B has a much lower amount of heavy compounds than that using pyrolysis setup A.

5.4.4 Pyrolysis of complex plastic samples

A variety of plastic samples, including other single plastics (PP and PS) and plastic mixtures (PP/LDPE, PP/PS, LDPE/PS, LDPE/PP/PS and LDPE/HDPE/PP/PS with each type of them having the equal weight ratio), were studied for this process by using the optimized pyrolysis setup. As can be seen in Figure 5-3, the pyrolysis at 500 ^{o}C also works well for other single

plastics and even for more complex plastic mixtures. All these processes achieve almost complete *waste-to-fuel* transformation, with residue yield in the range of 0.5-2.5 wt%. In all cases of this study, the light fraction has a small weight contribution (less than 11.0 wt%).The pyrolysis results of single plastic show that the pyrolysis of PS gives the lowest gas yield (6.3 wt%) and the highest liquid yield (93.1 wt% calculated by weight combination of light and heavy fractions). Pyrolysis of LDPE produces comparable gas and liquid yield as that of PP pyrolysis (26.7 wt% versus 25.0 wt% for liquid yield and 71.8 wt% versus 74.5 wt% for gas yield, respectively). Among the yield distribution obtained by pyrolysis of plastic mixtures, the pyrolysis of LDPE/PP mixture has the highest gas yield (27.7 wt%) and lowest liquid yield (71.3 wt%) whereas the pyrolysis of PP/PS mixture generates the lowest gas yield (16.4 wt%) and highest liquid yield (81.1 wt%).

5.4.5 Analysis of LDPE pyrolysis fuel

The pyrolysis of LDPE produces an oils that shows a characteristic GC-chromatogram, revealing a periodic set of three peaks that appear along the retention time, can be assigned to a series of dienes, alkenes and alkanes (Figure 5-5a) and present in periodicals of different chain length. For example, the molecular ion composition and corresponding ^{13}C composition of major peaks in the retention time of 9.5-10.5 min can be detected for C_{12}-diene, C_{12}-alkene and C_{12}-alkane with a low ppm error (below 1 ppm) Figure 5-5b). Molecular ion ($M^{+\cdot}$) peaks can be preceded by $[M-2]^{+\cdot}$, $[M-4]^{+\cdot}$, et al. resulting from the loss of H_2. These molecular ion composition assignments can also be further confirmed by major characteristic fragment ions, having a DBE value of 2.5 for C_{12}-diene, 1.5 for C_{12}-alkene and 0.5 for C_{12}-alkane, respectively, which can be interpreted by the loss of an alkane radical. The alkane series in the pyrolysis LDPE fuel can also be confirmed by the measurement of a standard mixture made up of n-alkane compounds from C_8 to C_{20} (Figure A5-3), showing a good agreement of the retention times between them for the same alkane composition. A simple mechanism is suggested for this characteristic pattern. As shown in Figure 5-5c, the formation of alkene and alkane associates with the breakage of LDPE at a pyrolysis temperature, followed by the addition of hydrogen radical to form a short molecular alkane, the combination of another alkane radical to reform a relative long alkane and the disassociation of hydrogen radical to form alkene. Similar process can also happen to alkene to generate a diene and different alkenes.

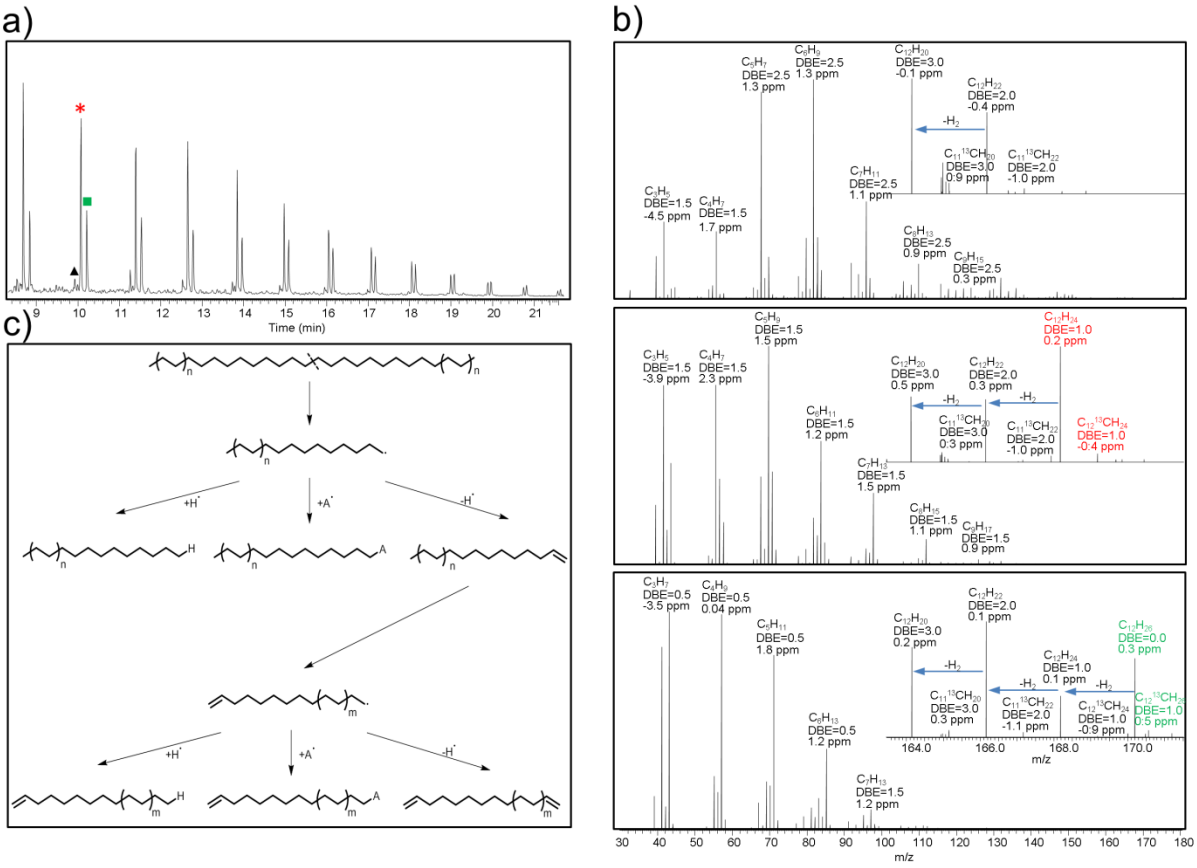

Figure 5-5. a) The zoom in TIC signal in the range of 8-22 min for heavy fraction of LDPE plastic fuels obtained at and 500 ^{o}C using setup A. The three adjacent peaks are highlighted. b) EI MS spectra for the highlighted peaks in the graph a. c) A mechanism proposal for LDPE pyrolysis. The letter of n, m represents a number and m is less than n. A$^{\cdot}$ is corresponding to a hydrocarbon radical.

Based on the compositional analysis, a wide range of compounds with carbon atoms from 5 up to 24, 31 and 29 coexist in the pyrolysis oil obtained at 450, 500 ^{o}C using pyrolysis setup A and 500 ^{o}C using pyrolysis setup B, respectively. It is in well agreement with previous research that the discovered heavy compounds have carbon atoms more than 15, even up to 40 for PE pyrolysis fuel by using GC-MS or GC-FID.[21, 35, 36] As a transport fuel, gasoline and diesel are the mostly used energy sources. Gasoline has a final boiling point of 210 ^{o}C with the standards European Norm 228 (EN228) and 195 ^{o}C with the standards created by European Automobile Manufacturers' Association (ACEA), respectively, whereas diesel has a final boiling point of 360 ^{o}C (EN590) and 350 ^{o}C (ACEA), respectively.[36, 37] The defined final boiling points for gasoline and diesel fuel allow the separation of compounds with carbon atoms 5-11 and 12-20, respectively. According to this, the initially produced pyrolysis oil from LDPE is a general low quality type of fuel, which is a complex mixture of gasoline, diesel and even wax range compounds. Therefore, it needs to be upgraded for the purpose of different usage, such as gasoline or diesel type fuel.

5.4.6 Distillation separation into gasoline and diesel type fuels

Distillation fractions of LDPE pyrolysis oil at various cutting temperatures were collected and analyzed using GC-EI-Orbitrap. As can be seen in Figure 5-6, a continuous separation is observed through step by step distillation procedure using an increased temperature. The compounds' peaks are mainly located in the retention time of 2.6-3.7 min at a temperature cut 130 ^{o}C. The signal at a temperature cut 230 ^{o}C has a retention time of 3.6-8.8 min. The signal at an even higher temperature cut 360 ^{o}C displays a higher retention time of 10.6-16.3 min.

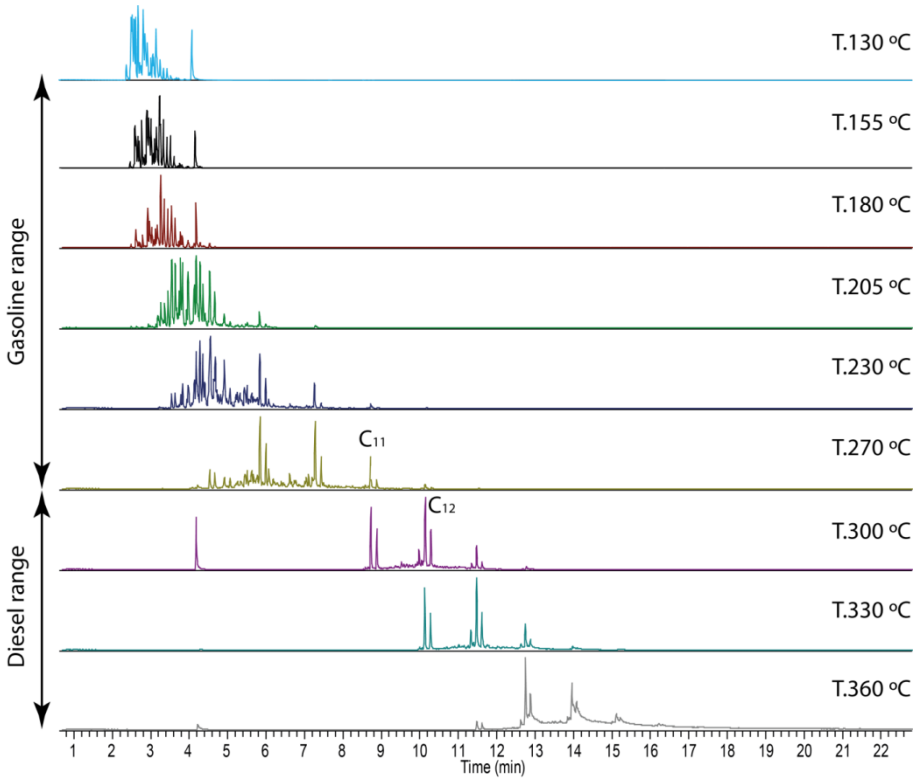

Figure 5-6. The TIC comparison of fractions obtained at individual temperature cuts from LDPE pyrolysis oil. The peak at retention time 4.14 min is assigned to toluene, which is used for cleaning autosampler.

Evaluating the separation temperature between gasoline and diesel range fuels is based on compositional analysis in this study. Typically, identical compounds appear in a wide temperature range when conducting a distillation process of a complex mixture. In our study, the peak of the compositions with carbon atoms 11 mainly appear in two fractions obtained at temperature cuts 270 and 300 ^{o}C. The TIC signal of the fraction at temperature cut 270 ^{o}C is almost completely made up of gasoline type compounds from C_5 to C_{11} while the TIC signal of the fraction at temperature cut 300 ^{o}C has a high amount of diesel range compounds from C_{12} to C_{20}. A similar distillation separation for PP pyrolysis fuel is also achieved, shown in Figure A5-2.

Further distillation of each fuel from all plastic samples into gasoline and diesel type fuels were conducted in a temperature range of 25-270 and 270-430 ^{o}C, respectively. The gasoline, diesel and wax (the residue after the distillation) were weighted and the yield distribution is shown in Figure 5-7. A recovery of more than 90 wt% is achieved for different plastic materials. A yield of more than 50 wt% is obtained as gasoline type fuel. The highest yield of gasoline, diesel and wax type product is obtained from distillation of PS (60.1 wt%), LDPE (35.5 wt%) and LDPE/HDPE/PP/PS pyrolysis oils (31.9 wt%), respectively. The lowest yield of gasoline, diesel and wax product is received from distillation of LDPE/HDPE/PP/PS (48.3 wt%), PS (12.8 wt%) and LDPE pyrolysis oils (12.1 wt%), respectively.

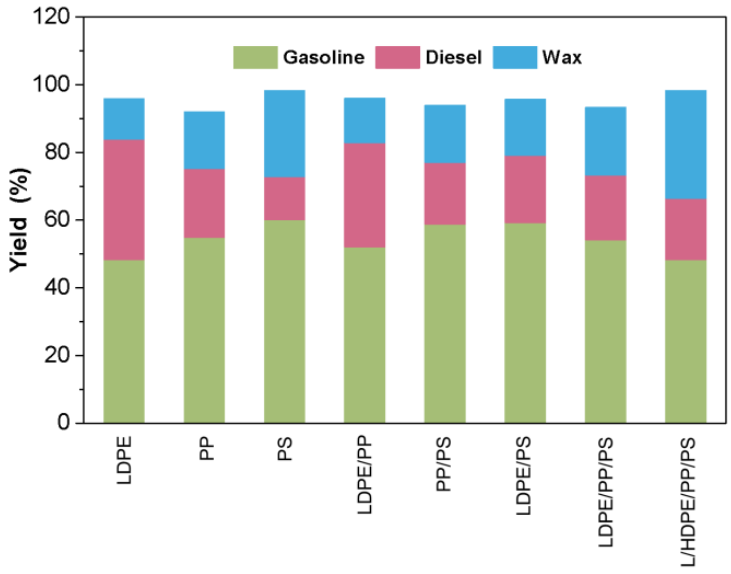

Figure 5-7. Distillation products distribution of pyrolysis plastic fuels.

All the gasoline and diesel type fuel fractions derived from pyrolysis of plastic waste were collected and studied in detail by using GC-EI-Orbitrap. As shown in Figure 5-8, clear separations between gasoline and diesel type fuels are achieved as expected. The distillation of the different pyrolysis fuels also allows a detailed view of the products. The gasoline and diesel type fuel derived from distillation of LDPE fuel has a retention time range of 2-11 and 8-18 min, respectively. Similar characteristic patterns (a series of alkane, alkene and diene peaks) as discussed before can be observed. The gasoline and diesel type fuel derived from distillation of LDPE fuel has a retention time range of 2-9 and 8-22 min, respectively. In our previous study, the heavy compounds in the diesel type fuel are less likely to be observed in

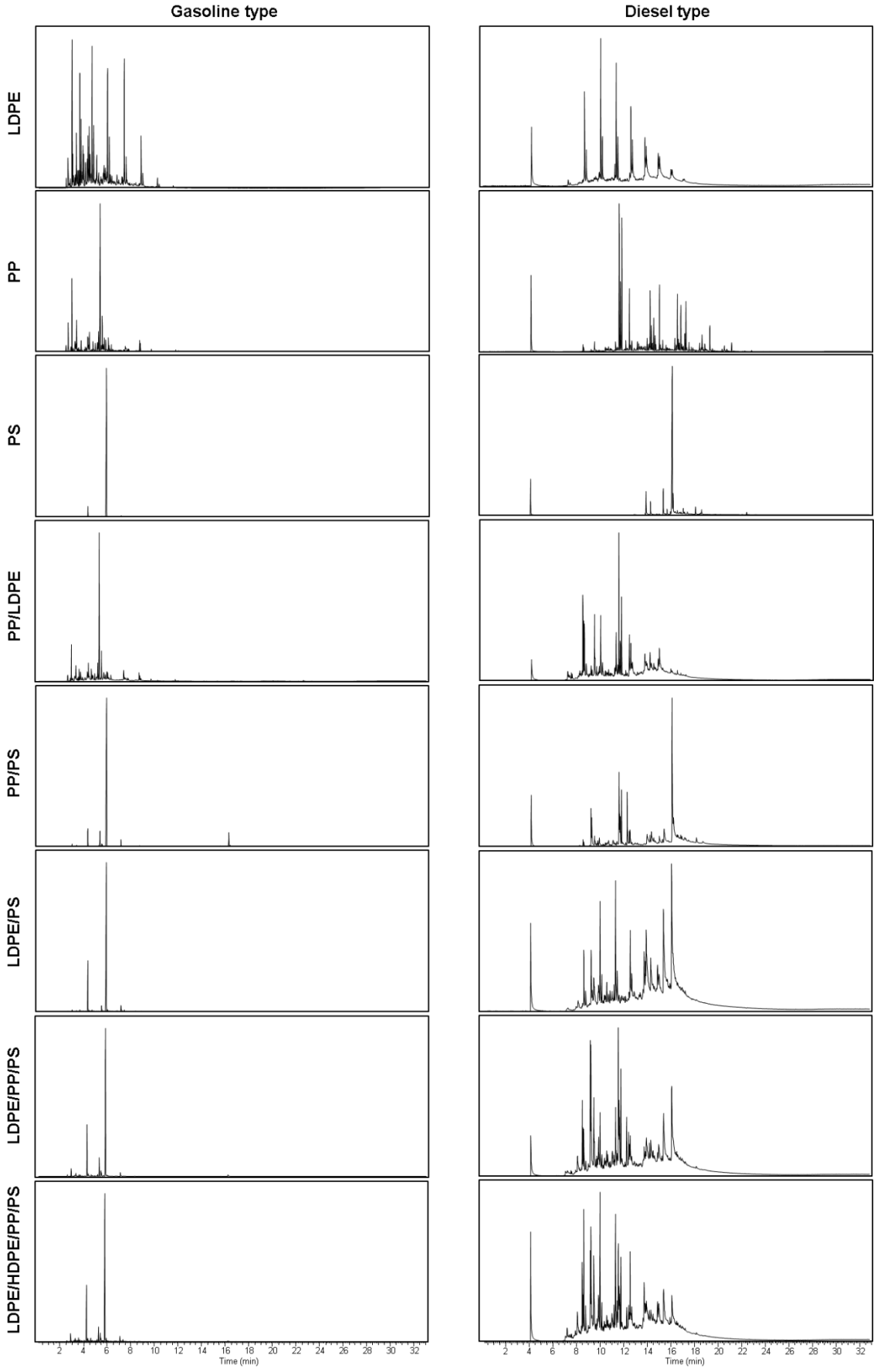

Figure 5-8. The TIC signal of gasoline and diesel type fuel obtained from distillation of pyrolysis plastic fuels.

the TIC signal of the initial PP fuel due to a dominating peak at the retention time 5.3 min. These heavy compounds with somehow repetitive pattern proposed by E. Duemichen[38] are probably assigned to propylene tetramer, pentamer, hexamer and heptamer derivatives. However, the characterization of these compounds' EI-MS spectra against NIST library cannot get a reasonable hit due to the lack of standards spectra in the library. In comparison, a bigger retention time gap is observed between gasoline (5-6 min) and diesel (14-19 min) type fuel derived from distillation of the PS fuel because the degradation of PS into monomer, dimer et al. leads to a significant difference of the number of carbon atoms. The gasoline type fuel contributed to 60.1 wt% of the total pyrolysis PS fuel, is almost completely made up of styrene. The diesel type fuel consists of styrene dimer derivatives such as [1,1'-bi(cycloheptane)]-2,2',4,4',6,6'-hexaene, 1,2-diphenylpropane, 1,3-diphenylpropane, 1,3-diphenyl-1-butene and 1-phenyl-1,2,3,4-tetrahydronaphthalene (Table A5-1 and Scheme A5-1) which is hardly revealed due to dominating presence of styrene in the initial pyrolysis PS fuel in our previous study. The gasoline type fuel derived from pyrolysis PS containing mixture fuel shows a less complex TIC signal due to dominating presence of styrene whereas the diesel type fuel resembles a complex TIC signal by removal of styrene.

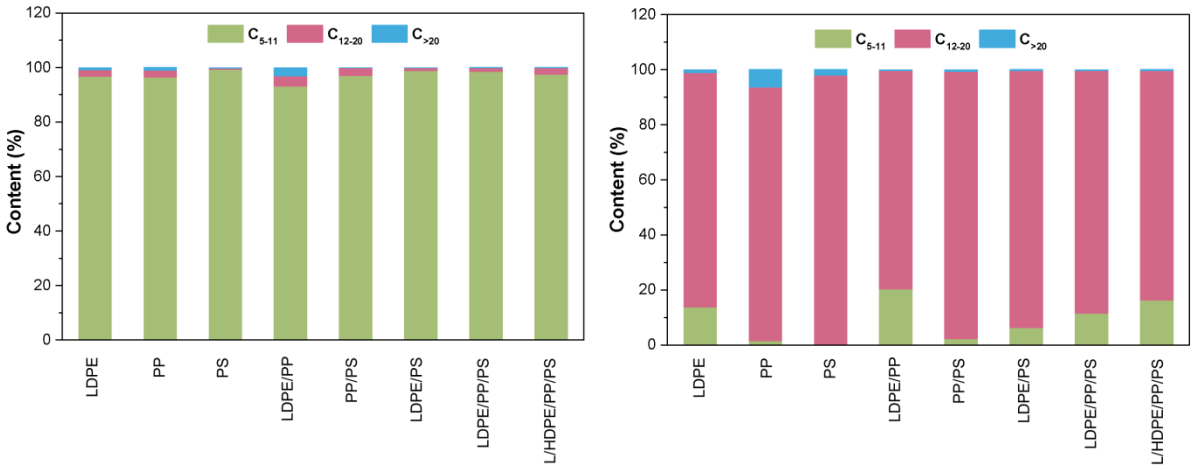

Figure 5-9. Carbon atoms distribution of gasoline (left graph) and diesel type fuels (right graph) derived from pyrolysis plastic fuels.

According to the TIC signal of n-alkane mixture shown in Figure A5-3, the alkane with C_{11} and C_{20} are corresponding to the retention time of 8.9 and 19.0 min, respectively. Based on this, the TIC signal of a sample measured at the same condition can be separated into gasoline range region (0–8.9 min), diesel range region (8.9–19.0 min), and wax range region (19.0–33.0 min). Semi-quantification of gasoline and diesel type fuel is conducted based on

the retention time and the peak area. Gasoline type fuels derived from distillation show a high content of light compounds with carbon atoms ranging from 5-11 (C_{5-11}) which make up more than 90% (Figure 5-9). In comparison, diesel type fuels show a high content of heavy compounds with carbon atoms ranging from 12-20 (C_{12-20}), around or more than 80%. In some diesel type fuels obtained from LDPE, LDPE/PP, LDPE/PP/PS and LDPE/HDPE/PP/PS, they also contain relative high content of C_{5-11} (10-20%) and this is because the composition of C_{11} distributes in both gasoline and diesel type fuels as we discussed before. This analysis in turn proves that the separation of initial pyrolysis plastic fuels into gasoline and diesel type fuels is successfully achieved by a simple distillation process.

5.5 Conclusion

This study successfully demonstrated pyrolysis is an efficient method for the transformation of *waste-to- fuel*. In this work, the pyrolysis of different plastic materials were individually and in combination optimized in regard to producing better liquid pyrolysis oils. The different conditions include optimized temperatures for the different types of plastic materials and especially an optimized cryocondensation setup for the oils. The liquid fractions were collected as light and heavy fractions depending on their cooling traps and then studied by high resolution GC-EI-Orbitrap. The optimized setup gave a better separation and a temperature of 500 ^{o}C resulted in a complete *waste-to-fuel* transformation. The optimized pyrolysis conditions were transferred from individual compounds to complex plastic mixtures, giving a highly efficient transformation of *waste-to-fuel*.

Further GC-EI-Orbitrap compositional analysis show that initial pyrolysis LDPE fuels consist of a mixture of gasoline, diesel and wax range compounds, which underlines the importance of using a distillation approach to achieve a high quality fuel by separating them into different types of fuels. An optimized distillation procedure was then demonstrated for this fuels conducted at various temperature cuts to determine separation temperature between gasoline and diesel type fuels based on the compositional analysis. Finally, an optimized distillation temperature was successfully applied for the separation of gasoline, diesel and wax type fuels from various plastic fuels obtained in this study. The limitation of this study here is that comprehensive fuel properties characterization (e.g., fuel density, kinematic viscosity, calorific value, octane number and cetane number) were not studied for further evaluation of resulted fuel quality.

Overall, this work presents a successful case of using successive pyrolysis and distillation processes to obtain high quality gasoline and diesel type fuels from both single plastic and complex plastic waste samples.

5.6 References

1. Andrady, A. L.; Neal, M. A., Applications and societal benefits of plastics. *Philos. Trans. R. Soc. B* **2009,** *364* (1526), 1977-1984.
2. Donovan, R., The plasticating process in injection molding. *Polym. Eng. Sci* **1974,** *14* (2), 101-111.
3. Birch, Q. T.; Potter, P. M.; Pinto, P. X.; Dionysiou, D. D.; Al-Abed, S. R., Sources, transport, measurement and impact of nano and microplastics in urban watersheds. *Rev. Environ. Sci. Biotechnol.* **2020**, 1-62.
4. Shah, A. A.; Hasan, F.; Hameed, A.; Ahmed, S., Biological degradation of plastics: a comprehensive review. *Biotechnol. Adv.* **2008,** *26* (3), 246-265.
5. Barnes, D.; Milner, P., Drifting plastic and its consequences for sessile organism dispersal in the Atlantic Ocean. *Mar. Biol.* **2005,** *146* (4), 815-825.
6. Kyrikou, I.; Briassoulis, D.; Environment, t., Biodegradation of agricultural plastic films: a critical review. *J. Polym.* **2007,** *15* (2), 125-150.
7. Hopewell, J.; Dvorak, R.; Kosior, E., Plastics recycling: challenges and opportunities. *Philos. Trans. R. Soc. B* **2009,** *364* (1526), 2115-2126.
8. Vilaplana, F.; Karlsson, S., Quality concepts for the improved use of recycled polymeric materials: a review. *Macromol. Mater. Eng.* **2008,** *293* (4), 274-297.
9. Hahladakis, J. N.; Velis, C. A.; Weber, R.; Iacovidou, E.; Purnell, P., An overview of chemical additives present in plastics: migration, release, fate and environmental impact during their use, disposal and recycling. *J. Hazard. Mater.* **2018,** *344*, 179-199.
10. Ritchie, H.; Roser, M. Plastic Pollution. https://ourworldindata.org/plastic-pollution (Accessed Sep. 2018).
11. Thompson, R. C.; Swan, S. H.; Moore, C. J.; Vom Saal, F. S., Our plastic age. *Phil. Trans. R. Soc. B* **2009,** *364*, 1973-1976.
12. da Costa, J. P.; Santos, P. S.; Duarte, A. C.; Rocha-Santos, T., (Nano) plastics in the environment–sources, fates and effects. *Sci. Total Environ.* **2016,** *566*, 15-26.
13. Hermabessiere, L.; Dehaut, A.; Paul-Pont, I.; Lacroix, C.; Jezequel, R.; Soudant, P.; Duflos, G., Occurrence and effects of plastic additives on marine environments and organisms: A review. *Chemosphere* **2017,** *182*, 781-793.
14. Assamoi, B.; Lawryshyn, Y., The environmental comparison of landfilling vs. incineration of MSW accounting for waste diversion. *Waste Manage.* **2012,** *32* (5), 1019-1030.
15. Wasilewski, R.; Siudyga, T., Energy recovery from waste plastics. *Chemik* **2013,** *67* (5), 435-445.
16. Miskolczi, N.; Angyal, A.; Bartha, L.; Valkai, I., Fuels by pyrolysis of waste plastics from agricultural and packaging sectors in a pilot scale reactor. *Fuel Process. Technol.* **2009,** *90* (7), 1032-1040.
17. Miandad, R.; Barakat, M. A.; Rehan, M.; Aburiazaiza, A. S.; Ismail, I. M. I.; Nizami, A. S., Plastic waste to liquid oil through catalytic pyrolysis using natural and synthetic zeolite catalysts. *Waste Manage.* **2017,** *69*, 66-78.
18. Sharma, B. K.; Moser, B. R.; Vermillion, K. E.; Doll, K. M.; Rajagopalan, N., Production, characterization and fuel properties of alternative diesel fuel from pyrolysis of waste plastic grocery bags. *Fuel Process. Technol.* **2014,** *122*, 79-90.

19. Kumar, S.; Singh, R., Recovery of hydrocarbon liquid from waste high density polyethylene by thermal pyrolysis. *Braz. J. Chem. Eng.* **2011,** *28* (4), 659-667.
20. Kiran Ciliz, N.; Ekinci, E.; Snape, C. E., Pyrolysis of virgin and waste polypropylene and its mixtures with waste polyethylene and polystyrene. *Waste Manage.* **2004,** *24* (2), 173-181.
21. Muhammad, C.; Onwudili, J. A.; Williams, P. T., Thermal Degradation of Real-World Waste Plastics and Simulated Mixed Plastics in a Two-Stage Pyrolysis–Catalysis Reactor for Fuel Production. *Energy Fuels* **2015,** *29* (4), 2601-2609.
22. López, A.; de Marco, I.; Caballero, B. M.; Laresgoiti, M. F.; Adrados, A.; Aranzabal, A., Catalytic pyrolysis of plastic wastes with two different types of catalysts: ZSM-5 zeolite and Red Mud. *Appl. Catal., B* **2011,** *104* (3), 211-219.
23. Marcilla, A.; Beltrán, M. I.; Navarro, R., Thermal and catalytic pyrolysis of polyethylene over HZSM5 and HUSY zeolites in a batch reactor under dynamic conditions. *Appl. Catal., B* **2009,** *86* (1), 78-86.
24. Ratnasari, D. K.; Nahil, M. A.; Williams, P. T. J. J. o. a.; pyrolysis, a., Catalytic pyrolysis of waste plastics using staged catalysis for production of gasoline range hydrocarbon oils. *J. Anal. Appl. Pyrolysis* **2017,** *124*, 631-637.
25. Yousef, S.; Eimontas, J.; Striūgas, N.; Zakarauskas, K.; Praspaliauskas, M.; Abdelnaby, M. A. J. F., Pyrolysis kinetic behavior and TG-FTIR-GC–MS analysis of metallised food packaging plastics. **2020,** *282*, 118737.
26. Qin, L.; Han, J.; Zhao, B.; Wang, Y.; Chen, W.; Xing, F. J. J. o. A.; Pyrolysis, A., Thermal degradation of medical plastic waste by in-situ FTIR, TG-MS and TG-GC/MS coupled analyses. **2018,** *136*, 132-145.
27. Xu, F.; Wang, B.; Yang, D.; Ming, X.; Jiang, Y.; Hao, J.; Qiao, Y.; Tian, Y. J. E. C.; Management, TG-FTIR and Py-GC/MS study on pyrolysis mechanism and products distribution of waste bicycle tire. **2018,** *175*, 288-297.
28. Vetere, A.; Schrader, W., Mass Spectrometric Coverage of Complex Mixtures: Exploring the Carbon Space of Crude Oil. *Chemistry Select* **2017,** *2* (3), 849-853.
29. Panda, S. K.; Andersson, J. T.; Schrader, W., Characterization of supercomplex crude oil mixtures: what is really in there? *Angew Chem Int Ed Engl* **2009,** *48* (10), 1788-91.
30. Gaspar, A.; Schrader, W., Expanding the data depth for the analysis of complex crude oil samples by Fourier transform ion cyclotron resonance mass spectrometry using the spectral stitching method. *Rapid Communications in Mass Spectrometry* **2012,** *26* (9), 1047-1052.
31. Hall, W. J.; Williams, P. T., Analysis of products from the pyrolysis of plastics recovered from the commercial scale recycling of waste electrical and electronic equipment. *Journal of Analytical and Applied Pyrolysis* **2007,** *79* (1), 375-386.
32. Mangesh, V.; Padmanabhan, S.; Tamizhdurai, P.; Ramesh, A. J. J. o. C. P., Experimental investigation to identify the type of waste plastic pyrolysis oil suitable for conversion to diesel engine fuel. **2020,** *246*, 119066.
33. Undri, A.; Frediani, M.; Rosi, L.; Frediani, P. J. J. o. a.; pyrolysis, a., Reverse polymerization of waste polystyrene through microwave assisted pyrolysis. **2014,** *105*, 35-42.
34. Aldrich, S. Pressure-Temperature Nomograph Interactive Tool. https://www.sigmaaldrich.com/chemistry/solvents/learning-center/nomograph.html.
35. Ratnasari, D. K.; Nahil, M. A.; Williams, P. T., Catalytic pyrolysis of waste plastics using staged catalysis for production of gasoline range hydrocarbon oils. *J. Anal. Appl. Pyrolysis* **2017,** *124*, 631-637.
36. Kassargy, C.; Awad, S.; Burnens, G.; Kahine, K.; Tazerout, M., Gasoline and diesel-like fuel production by continuous catalytic pyrolysis of waste polyethylene and polypropylene mixtures over USY zeolite. *Fuel* **2018,** *224*, 764-773.

37. ACEA, A., EMA, JAMA, *Worldwide Fuel Charter*. 2006; p 1-68.
38. Duemichen, E.; Eisentraut, P.; Celina, M.; Braun, U., Automated thermal extraction-desorption gas chromatography mass spectrometry: A multifunctional tool for comprehensive characterization of polymers and their degradation products. *J. Chromatogr., A* **2019,** *1592*, 133-142.

5.7 Appendix

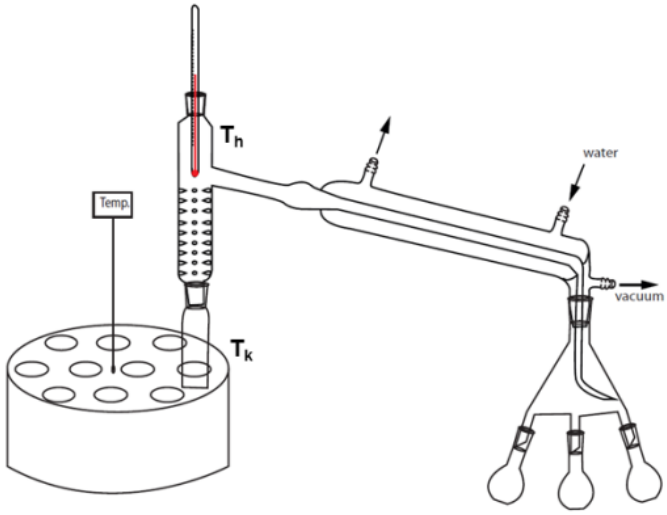

Figure A5-1. Schematic diagram of distillation setup.

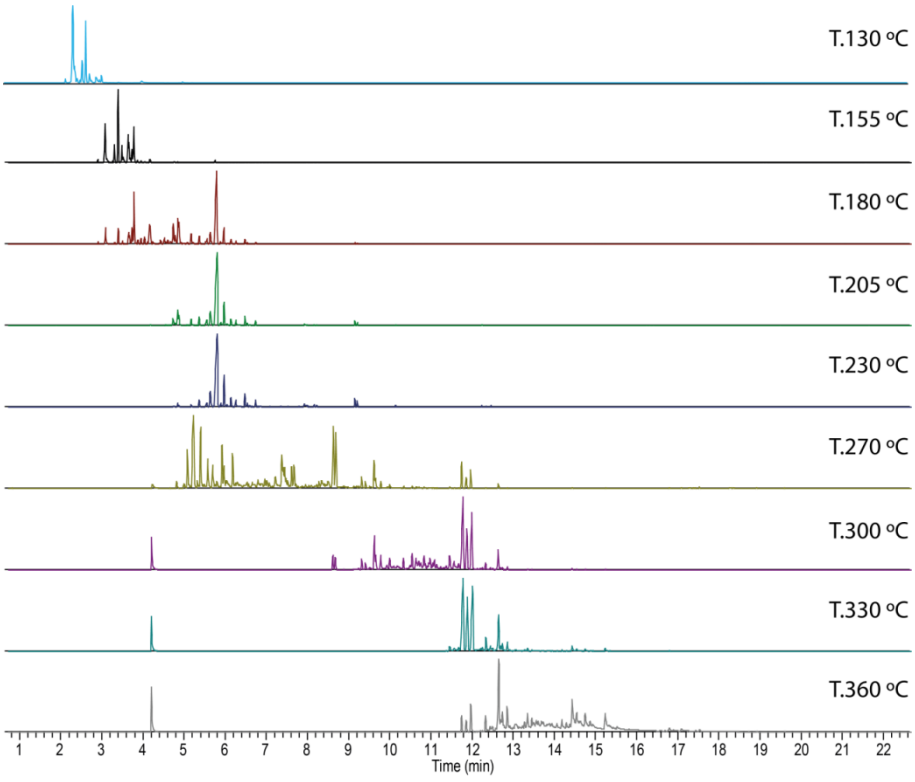

Figure A5-2. The TIC comparison of fractions obtained at individual temperature cuts from PP pyrolysis fuel.

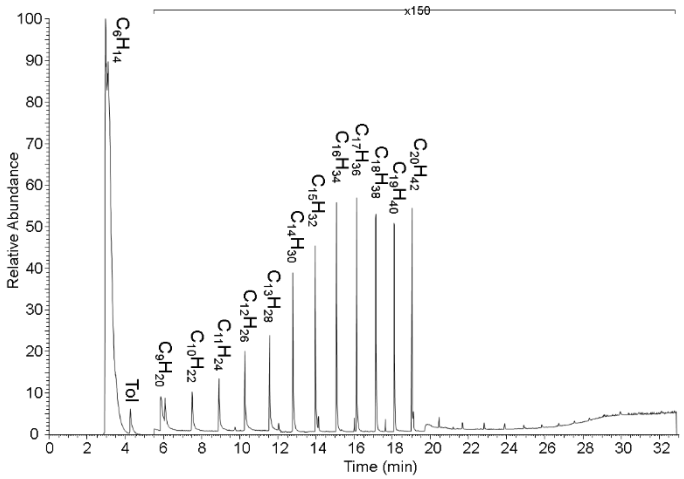

Figure A5-3. Total ion current of a mixture of n-alkane compounds ($C_{8\text{-}20}$).

Table A5-1. Composition of the diesel type fuel resulting from pyrolysis PS.

Peak No.	RT (min)	ID	SI (%)	Name	Formula	Error a/b (ppm)	Area (%)
1	13.98	NJ7578	80	[1,1'-bi(cycloheptane)]-2,2',4,4',6,6'-hexaene	$C_{14}H_{14}$	0.73/-0.03	6.38
2	14.35	NJ34633	57	1,2-diphenylpropane	$C_{15}H_{16}$	1.07/X	3.85
3	15.45	NJ133399	60	1,3-diphenylpropane	$C_{15}H_{16}$	0.14/0.38	6.67
4	16.22	NJ9505	56	1,3-diphenyl-1-butene	$C_{16}H_{16}$	0.79/0.65	66.44
5	16.65	NJ9509	50	1-phenyl-1,2,3,4-tetrahydronaphthalene	$C_{16}H_{16}$	0.06/-0.15	0.64
Total							83.98

Note: Error a and b stand for the error of the molecular composition and its corresponding ^{13}C compositon, respectively. The capital letter X represents the corresponding result cannot be found.

Scheme A5-1. The identified compound structure accordingly resulting from PS diesel type fuel.

Chapter 6 Comprehensive characterization of pyrolysis PS fuel by using GC-EI-Orbitrap and DI-APCI Orbitrap

Redrafted from "Xu, Y.; Schrader, W., Comprehensive characterization of pyrolysis PS fuel by using GC-EI-Orbitrap and DI-APCI Orbitrap", will be submitted to *Fuel*.

6.1 Abstract

In this study, we are trying to understand the complexity of pyrolysis fuel obtained from polystyrene (PS), which has been rarely studied. Two different types Fourier Transform based Orbitrap mass spectrometer, GC-EI-Orbitrap and DI-APCI Orbitrap, were used as analytical tools for this study. GC-EI-Orbitrap is capable of studying volatile and thermally stable compounds. Styrene monomer and its derivatives were found in the original pyrolysis fuel, in a light fraction (LF) and also in a heavy fraction (HF) obtained at different condensation temperatures in the cooling trap of the pyrolysis system. In addition to these compounds, several styrene dimer derivatives were detected by GC-EI-Orbitrap analysis of distillation fractions. In comparison, DI-APCI Orbitrap mass spectrometry can discover a broader range of chemical compositions from volatile (styrene monomer derivatives) to non-volatile compounds (styrene octamer derivatives). Three isomers for non-volatile styrene tetramer derivative composition with an elemental composition $C_{32}H_{30}$ were successfully discovered by collision induced dissociation studies, which allows proposing a corresponding mechanism based on these data.

6.2 Introduction

The pyrolysis process receives a wide interest from researchers and industry as it is an easy but very promising technique for the production of fuels on a large scale level. One example for pyrolysis presented in our previous study is using biomass as feedstock.[1-3] However, initial produced pyrolysis biofuel is generally a low quality type of fuel, containing a high content of oxygen, 28-40 wt%.[4] This type of biofuel shows general physicochemical properties of low pH, low heating value, instability, corrosiveness, high viscosity et al. Therefore a typical hydrotreating process is required to upgrade the fuel quality by removing oxygen inside the fuel.[5-7]

In comparison with biomass, plastic, a carbon-rich material, has a higher calorific value (CV), and thus it can be served as a better feedstock for producing high quality pyrolysis fuel.[8-10] The wide application of plastic in our daily life results in a significant amount of plastic into waste. After usage, recycling is applied to reuse plastic waste, however, it still remains at a low extent.[11, 12] The major challenge here is that plastic waste mainly composed of hydrocarbons is hardly degraded environmentally.[13-15] Discarded plastic waste, either goes into landfilling or oceans, has a tremendous negative effect on environment, human and wildlife health.[16-19] Therefore, production of fuels from plastic waste through pyrolysis process can also provide a solution to tackle this challenging issue. While linear polymers lead mainly to smaller aliphatic-type of fuels, a more aromatic precursor polymer should lead to a more aromatic-type of fuel. Here, the mixture of different polymer materials can lead to a fuel that follows the regulations in regard to the octane rating to get a fuel with high anti-knock properties. This is a necessity if a fuel is being used as transport fuel.

Pyrolysis is a very process that typically forms very complex mixtures. It has been shown, that pyrolysis biofuel contains thousands of chemical compositions.[20-22] However, the complexity of pyrolysis plastic fuel is still unknown. To understand such complex mixture, sophisticated analytical methods are required to achieve the comprehensive and complementary characterization of the mixture. One or two dimensional GC-MS are methods generally used for characterization of such volatile compounds for over decades.[23-27] It is capable of studying volatile and low molecular weight substances. In addition, high resolution mass spectrometry by utilizing a Fourier Transform based analyzers (Orbitrap and ICR) is extremely powerful for the characterization of complex mixture.[28-31] The high mass accuracy and sensitivity of this method allows to determine the exact molecular formula, which can provide a more complete overview of pyrolysis products. To the best of our knowledge, this is

the first study to apply such sophisticated analytical methodologies for the study of pyrolysis plastic fuels, which is important to gain a deep understanding of the chemical reactions during pyrolysis.

In this work, we mainly focus on developing a method to study the complexity of pyrolysis fuel and understand the chemical reactions during pyrolysis process using plastic polystyrene (PS) as feedstock. To achieve this goal, two different types of FT based Orbitrap mass spectrometers, GC-EI-Orbitrap and DI-APCI Orbitrap, were used for this study. The initial pyrolysis PS fuel was fractionated into various fractions through distillation. The obtained pyrolysis fuels and distillation fuels were characterized by both analytical methods.

6.3 Experimental section

6.3.1 Pyrolysis process

Pyrolysis process was carried out at 500 ^{o}C in a quartz glass reactor with a dimension of (H x W: 300 mm x 50 mm), which was installed into and externally heated by a 1480 W tube furnace EVA 12/300 B (Carbolite Gero, Germany). Around 20 g polystyrene pellets (Jiangsu Citic Guoan New Material Company Limited, China) was weighted and added into the reactor. Before starting the pyrolysis reaction, the reactor was swept with argon continuously for roughly 20 min to push the air and humidity out of the reactor. The system was heated at a maximum heating rate of 100^{o}C min^{-1} until reaching to the desired temperature, followed by an isothermal step of 1 h. The volatiles were swept away by argon at a pressure of 0.2 mbar during the whole heating process. After exiting the reactor, the pyrolysis volatiles passed through a cooling water column, then two times ice/ water bath (4 ^{o}C) and two times dry ice saturated acetone bath (-78 ^{o}C). The products were collected from each cooling trap and weighted. Products on the surface of cooling water column was washed out with dichloromethane, dried under vacuum evaporation overnight and weighted as well. The residue in the pyrolysis reactor was weighted.

6.3.2 Distillation process

A simple lab scale fractional distillation was performed. Distillation was carried out with 10 g of pyrolysis oil. Fractions, F1 and F2, were obtained at a heating temperature range of 25-270^{o}C and 270-430^{o}C, respectively. The distillation residue was treated as F3 fraction. The distillation process with a temperature of lower than 300^{o}C was conducted at atmospheric pressure. In addition, a vacuum distillation at 1 mbar was carried out by utilizing an oil pump

Duo 10 M (Pferffer vacuum, Germany). The vacuum distillation temperature can be calculated accordingly through pressure-temperature nomograph interactive tool.[32] Before the vacuum distillation process, the temperature was first cooled down to room temperature, then a vacuum was applied, after that the temperature was increased to the calculated vacuum distillation temperature to operate a vacuum distillation process.

6.3.3 GC-EI-Orbitrap

GC-MS measurements were performed on a Q Exactive GC (Thermo Fisher, Bremen, Germany), consisting of a AI/AS 1310 autosampler equipped TRACE 1300 series GC coupled to a Q Exactive Orbitrap MS. The injection volume was 0.2 µL and toluene was used as injector cleaning solvent. Sample injector was held at 300^{o}C in split mode with a split flow of 80 mL min^{-1} and a purge flow of 5 mL min^{-1}. High purity helium (N5.0) was used as a carrier gas at a constant flow rate of 1.2 mL min^{-1}. The GC separation was carried out on a RTX$^{@}$-1ms capillary column (30 m x 0.25 mm ID, 0.25 um). The temperature program was performed with an initial temperature of 35^{o}C, which was increased to a final temperature of 320^{o}C at a heating rate of 10^{o}C min^{-1} and then held at 320 ^{o}C for additional 5 min. Transfer line temperature was set to 320^{o}C. The eluted compounds from GC were ionized by EI at an electron energy of 70 eV. The mass spectra were recorded in full scan mode with a mass range of 30-600 Da at a mass resolution of 120, 000 (FWHM at *m/z* 200). Collected GC-MS data were imported and characterized against NIST library by MassLib (MSP Kofel, Zollikofen, Switzerland).

6.3.4 DI (Direct injection)-APCI Orbitrap

Each individual sample (pyrolysis PS fuels, distillation fuels) was diluted with dichloromethane to a final concentration of 250 µg ml^{-1} and used without further treatment. Mass Spectra were recorded on a research-type Orbitrap Elite mass spectrometer (Thermo Fisher Scientific, Bremen, Germany) equipped with commercially available atmospheric pressure chemical ionization (APCI) source. The spectra were collected in positive mode. For the measurements, each sample was infused with a flow rate of 20 µl min^{-1}, evaporated at 350 ^{o}C with the sheath and auxiliary gas flow of 20 and 10 (arbitrary units), respectively. APCI current was set as 5 kV. Mass spectra were collected with a mass window 100 $\leq$ *m/z* $\leq$ 1000 using spectral stitching method (windows of 30 Da with 5 Da overlap) and resolving power *R*= 480,000 (full width half maximum at *m/z* 400).

6.3.5 Data analysis

Peak assignment was performed using Composer64 (v 1.5.0, Sierra Analytics, Modesto, CA, USA) after internal recalibration according to the following constraints: $C_{0-200}H_{0-1000}N_{0-2}O_{0-30}S_{0-2}$, $0 \leq DBE \leq 60$ and ±1.0 ppm. DBE number can be calculated based on the formula using the equation: DBE = C - (H/2) + (N/2) + 1, where: C = number of carbon atoms, H = number of hydrogen atoms, and N = number of nitrogen atoms. One DBE is equal to one ring or one double bond.

6.4 Results and discussion

6.4.1 GC-EI-Orbitrap analysis of pyrolysis fuel

Pyrolysis process of PS was conducted at a temperature of 500 ^{o}C. Generally, pyrolysis converts starting materials into three major components, condensed product, gas and residue. In this study, the condensed product was separated into two fractions, light fraction (LF) obtained from dry ice saturated acetone bath and heavy fraction (HF) obtained from ice/ water bath. In this process, the yield of pyrolysis residue, LF and HF was weighted on a mass basis and the remaining part was calculated as gas. The LF, HF, gas and residue had a product yield of 1.1%, 92%, 6.3% and 0.5%, respectively. This means a very efficient plastic PS to fuel transformation was achieved at a pyrolysis temperature of 500^{o}C.

The two fractions, LF and HF obtained at different condensation temperatures, were analyzed by GI-EI-Orbitrap. It is assumed that HF contains heavier compounds due to the condensation temperature than that LF fraction, which means a higher retention time should be observed. However, the expected result was not achieved as no clear separation was observed between LF and HF. The results of EI mass spectra against NIST library were summarized in Table 6-1 and the compounds' structures were depicted in Scheme 6-1. Only three major peaks can be observed in the GC chromatograph. These peaks are corresponding to volatile and low molecular weight compounds, such as ethylbenzene at 5.1 min, styrene at 5.5 min and 2-phenyl-1-propene at 6.7 min. The compound styrene had the dominated peak with a TIC signal contribution of more than 90%.

Due to the high concentration of styrene in both LF and HF fractions, the compounds with a higher retention time cannot be observed. To address this issue, a distillation process was used later to separate the pyrolysis oil into several fractions. This can help increase the concentration of low abundant compounds to make them being observed.

Table 6-1. Identification results of pyrolysis fractions (LF and HF) and distillation fractions (F1 and F2).

Peak No.	RT (min)	ID	SI	Compound	Formula	LF		HF		F1		F2	
						Area（%）	Error a/b (ppm)	Area（%）	Error a/b (ppm)	Area（%）	Error a/b (ppm)	Area（%）	Error a/b (ppm)
1	5.1	NJ228326	54	ethylbenzene	C_8H_{10}	3.2	1.1/0.3	0.6	1.2/0.5	0.9	1.2/0.2	X	X/X
2	5.5	NJ229644	89	styrene	C_8H_8	93.5	0.1/-0.2	96.8	0.6/0.3	98.1	0.3/-0.1	X	X/X
3	6.7	N2024	39	prop-1-en-2-ylbenzene	C_9H_{10}	3.3	0.9/0.6	2.6	0.6/0.4	1.0	0.4/0.2	X	X/X
4	14.0	NJ7578	80	[1,1'-bi(cycloheptane)]-2,2',4,4',6,6'-hexaene	$C_{14}H_{14}$	X	X/X	X	X/X	X	X/X	5.8	0.7/-0.0
5	14.4	NJ34633	57	1,2-diphenylpropane	$C_{15}H_{16}$	X	X/X	X	X/X	X	X/X	3.8	1.1/X
6	15.5	NJ133399	60	1,3-diphenylpropane	$C_{15}H_{16}$	X	X/X	X	X/X	X	X/X	7.5	0.1/0.4
7	16.2	NJ9505	56	1,3-diphenyl-1-butene	$C_{16}H_{16}$	X	X/X	X	X/X	X	X/X	67.9	0.8/0.7
8	16.7	NJ9509	50	1-phenyl-1,2,3,4-tetrahydronaphthalene	$C_{16}H_{16}$	X	X/X	X	X/X	X	X/X	0.8	0.1/-0.2
Total						100		100		100		85.8	

Note: Error a and b stand for the error of the molecular composition and its corresponding ^{13}C composition, respectively. The capital letter X represents the corresponding result cannot be found.

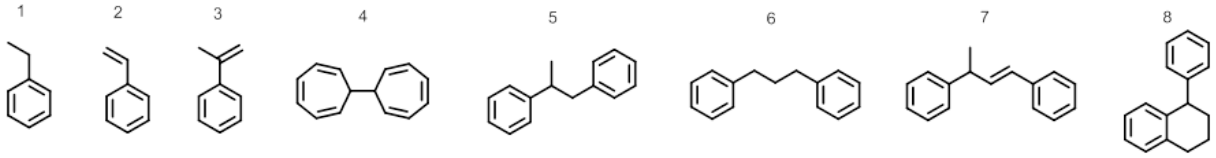

Scheme 6-1. The identified compound structures accordingly.

6.4.2 GC-EI-Orbitrap analysis of distillation fraction

The distillation process was operated at a temperature range of 25-270 ^{o}C (F1), 270-430 ^{o}C (F2) and above 430 ^{o}C (F3), resulting in a product yield of 60.1%, 12.8% and 25.4%, respectively. A total recovery of 98.3% was achieved after distillation.

The two distillation fractions, F1 and F2, were analyzed by GC-EI-Orbitrap as well. Here, the fraction F3 was not analyzed as it may contain non-volatile compounds which may contaminate the GC column. The results are shown in Table 6-1 and Scheme 6-1. The TIC signal of F1 was relative simple, containing mostly styrene whereas F2 had a much more complex TIC signal, the peaks of which were mainly assigned as styrene dimer derivatives. These styrene dimer derivatives were corresponding to [1,1'-bi(cycloheptane)]-2,2',4,4',6,6'-hexaene at 14.0 min, 1,2-diphenylpropane at 14.4 min, 1,3-diphenylpropane at 15.5 min, 1,3-diphenyl-1-butene at 16.2 min and 1-phenyl-1,2,3,4-tetrahydronaphthalene at 16.7 min). Only a total area of 84% was identified for this fraction.

After simplification of the sample through distillation, the identified compounds were limited to volatile compounds such as styrene monomer and dimer derivatives. An in-depth analysis of chemical composition in the pyrolysis oil still cannot be achieved in this stage. Pyrolysis process is a very complicated process, association with the generation of radicals, radical rearrangement, H shift, di-radical recombination et al. All these will lead to very complicated chemical compositions in the mixture, each of which may even have multiple isomers. This means the complexity of the sample is far away from what we have achieved here.

6.4.3 DI-APCI Orbitrap analysis

To further cover a broad range compositions analysis, especially for non-volatile compounds, here a non-target approach using APCI in positive mode in combination with high resolution mass spectrometry was used. In comparison with EI, ionization technique APCI is a soft ionization technique, showing to be a good choice for ionizing hydrocarbons to produce molecular ions in the previous research. In a typical APCI(+) ionization process, charge and

proton transfer reactions happen simultaneously, resulting in both radical and protonated molecular cations. Figure 6-1 depicts the mass spectra derived from pyrolysis LF, HF and distillation fractions F1, F2, F3. All five spectra exhibit a mass resolution of approximately 480,000 at *m/z* 400. The mean *m/z* values, based on the lists of the assigned masses, were also calculated for different treatment fractions giving 237 Da for LF, 251 Da for HF, 170 Da for F1, 241 Da for F2 and 404 Da for F3, respectively. The LF and HF showed almost identical distribution, occupying the same mass range of 100-250 Da, with a maxima observed at *m/z* 105.0698 Da, corresponding to the composition of protonated styrene $[C_8H_8+H]^+$. In comparison with original pyrolysis fuel LF and HF, distillation fraction F1 depicts a high intensity region with a narrower mass range of 100-150 Da. The maxima of F1 also appeared at m/z 105.0698 Da. The mass spectra of F2 shifted toward a slight higher mass range of 100-300 Da with a maxima observed at 131.0856 Da, corresponding to the composition of $[C_{10}H_{10}+H]^+$. The distillation residue, named F3 as well, had a much higher mass range with the observable peak mainly locating in the mass window of 100-700 Da, however the intensity decreased significantly after 500 Da.

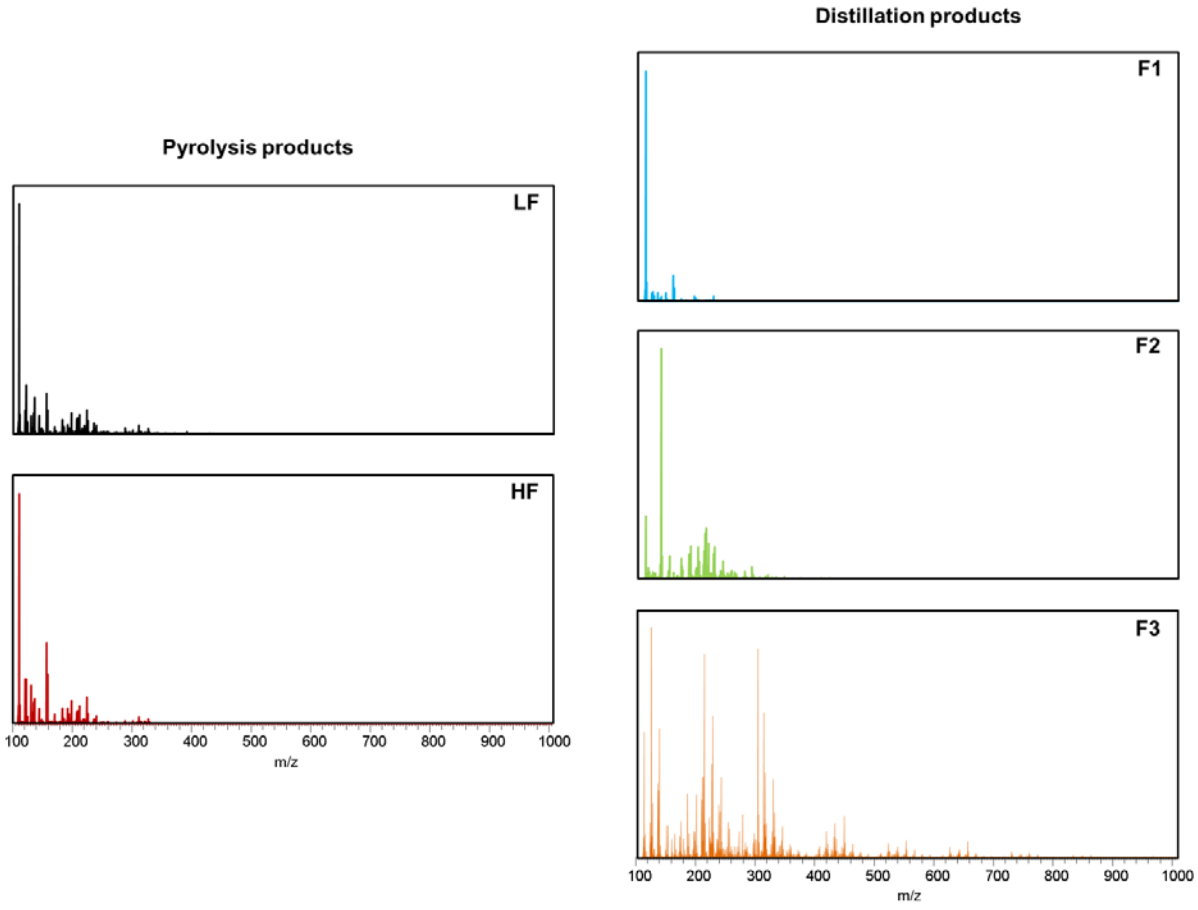

Figure 6-1. The whole mass spectra comparison in a mass range of 100-1000 Da among pyrolysis fractions (LF and HF) and distillation fractions (F1, F2 and F3).

The overall mass spectral information is summarized in class distributions, depicted in Figure 6-2. Protonated compound classes are described as [H] post the class while the radical cation form was displayed without [H]. A total of 5 different composition classes including HC, HC[H], N[H], O[H] and O_2[H] were considered to visualize the changes. As expected, the hydrocarbon class (HC[H] and HC) was the most abundant compound class, with a contribution of over 90%. The relative intensity of HC was lower than that of HC[H]. The intensity ratio of HC[H] to HC can be calculated as 6.5, 7.5, 24.6, 6.5 and 7.1, respectively. The minor existence of nitrogen or oxygen containing class compounds might be derived from pyrolysis process with incomplete air free condition or aging process.

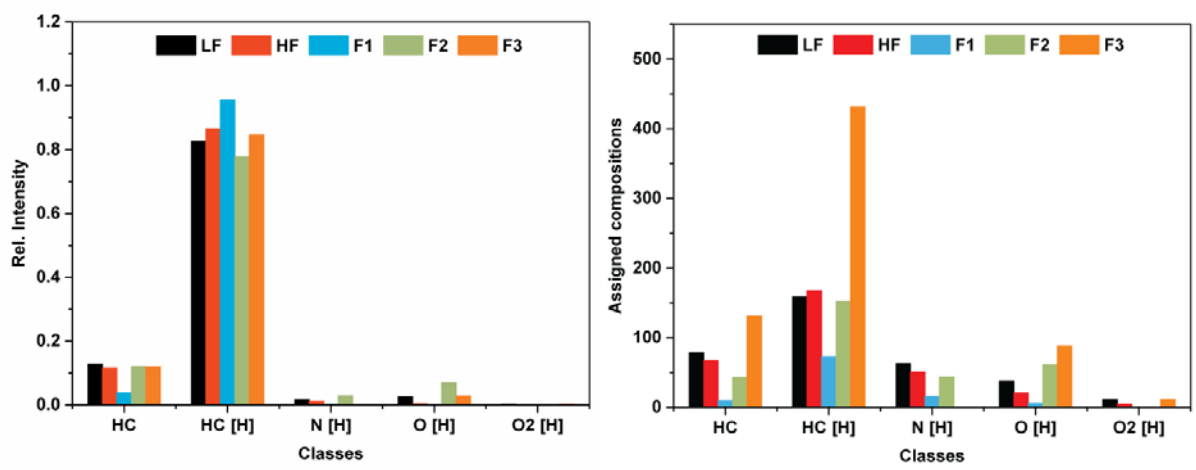

Figure 6-2. Intensity (left) and population (right) based class distribution among pyrolysis fractions (LF and HF) and distillation fractions (F1, F2 and F3).

One advantage of population-based distribution over the classic relative intensity-based distribution is the possibility to eliminate differences derived from signal intensities. As can be seen in Figure 6-2 (right graph), LF and HF had similar number of hydrocarbon compounds assignments with slightly more than 150 assigned protonated compositions. After distillation separation, the assignments differed significantly from each other. To further compare the hydrocarbon compounds' assignments, here we used the number obtained from original PS pyrolysis oil (LF and HF) as a reference. Distillation fraction F1 had the least amount of hydrocarbon compounds assigned, occupying less than half of assignments. F2 had the comparable numbers of assignments. While the heaviest distillation fraction F3 gave the highest number of assignments, roughly three times higher. This result showed that distillation process successfully accumulated those low abundance products obtained from the

pyrolysis to make them detectable and therefore expends the total number of detected compositions.

Kendrick plots give the information associated with selected properties of the different types of assigned compounds in the complex mixture after calculation of each individual signal in mass spectrum. A detailed information related with the most abundant HC[H] class was summarized in Kendrick plots of DBE against carbon atoms (left graph) and bar plots of the normalized relative intensity versus DBE (right graph), displayed in Figure 6-3.

The hydrocarbon species in LF consisted of carbon atoms 8-28, with a DBE distribution ranging from 3 to 19. The HF displayed a similar trend with carbon atoms 8-35 and DBE distribution ranging from 3 to 20. After distillation separation, F1 fraction had a low carbon atoms rang of 8 to 19 and a low DBE range of 3 to 13. As expected, F2 obtained at a higher distillation temperature range contain higher carbon atoms up to 34 and DBE value until 19. A further increase in the number of carbon atoms and DBE value can be observed in the distillation fraction F3. This fraction contained carbon atoms up to 68 and DBE value until 36.

Moreover, when observing the hydrocarbon compositions distribution among all the fractions (especially F3 fraction), a similar trend reflected by MS spectra can also be seen in the red core region which represents a high intensity region with carbon atoms and DBE differences corresponding to additional aromatic rings. For example, the molecular composition with carbon atoms 8 and DBE value 5 is supposed to be a styrene, which can be formed by tail end cutting during high temperature pyrolysis. Molecule compositions with high intensity can also be observed at DBE 10, 14, 18, 22, 26, 30 and 34 with corresponding C atoms given as 16, 25, 32, 42, 50, 58 and 66, respectively. The distinct 4-DBE-pattern increase between them is attributed to benzene related structure which extends in a separated manner. Furthermore, the compositions with an increase of DBE (e.g., 10, 11 and 12) containing the same carbon atoms (e.g., 16), can also be clearly observed with a high intensity. These compositions can be reasonably presented with structures as described in Scheme 6-2. The compound buta-1,3-diene-1,3-diyldibenzene, can be formed by the generation of di-radicals followed by dehydrogenation process. Compound 2-phenylnaphthalene can be formed by radical generation followed by cyclization and dehydrogenation process. Given the highly abundant production of styrene during high temperature process presented by GC-EI-Orbitrap measurements, a recombination of two styrene moieties can also be potential possible to form more stable condensed aromatic compound, pyrene, giving a higher DBE value of 12.

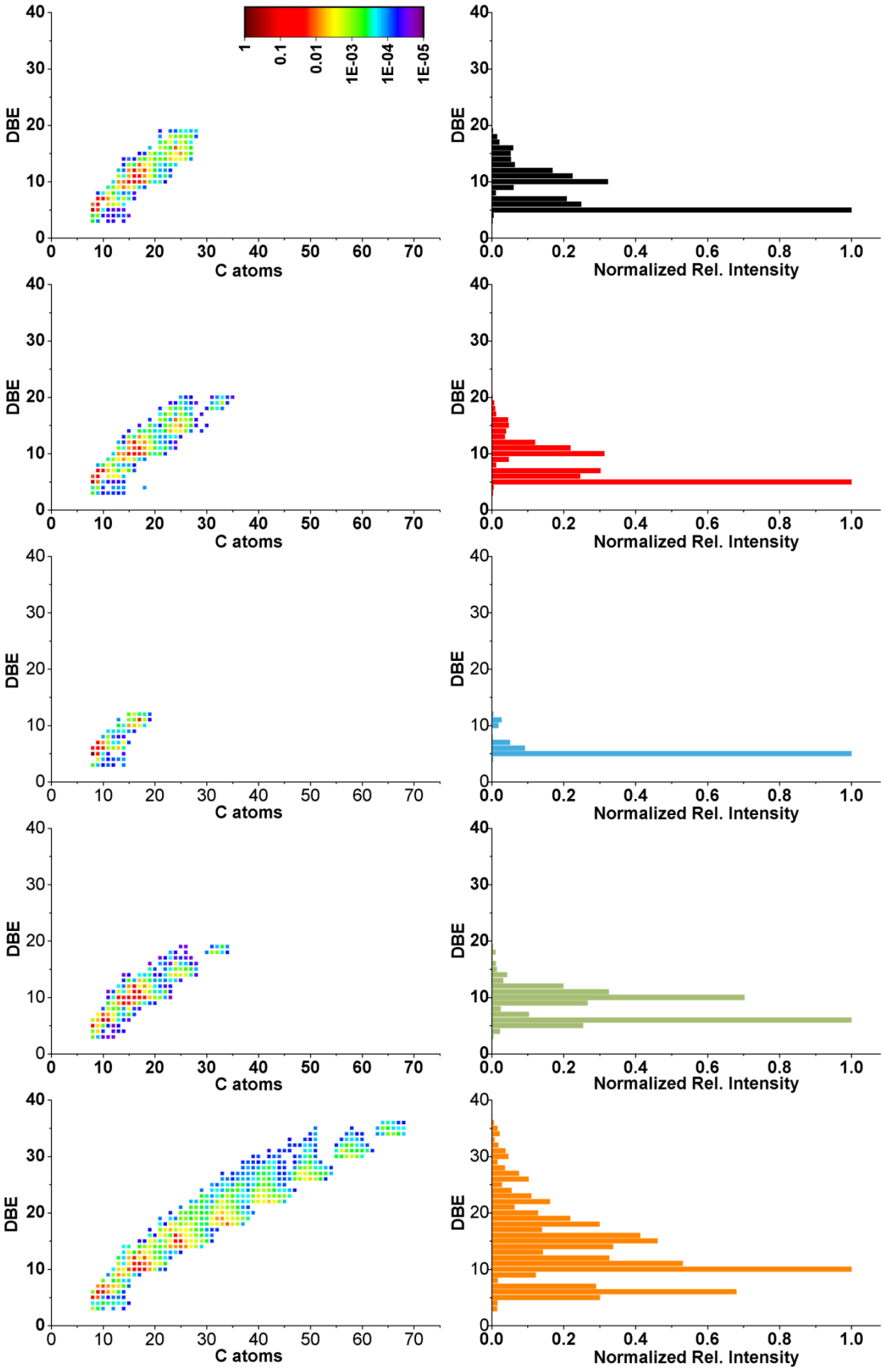

Figure 6-3. Kendrick plots of DBE against carbon atoms (left graph) and bar plots of the normalized relative intensity versus DBE (right graph) for HC[H] class.

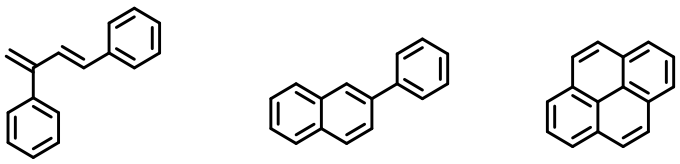

Scheme 6-2. Suggested compounds' structures for compositions of $C_{16}H_{14}$, $C_{16}H_{12}$ and $C_{16}H_{10}$, accordingly from left to right.

6.4.4 Structural elucidation by CID fragmentation

A fragmentation study is essential to gain a evidence of compound's structure. Routine GC-EI-MS allows the characterization of the compounds because of the powerful EI libraries, but is limited to small molecular weight, volatile compounds. For less volatile compounds DI-APCI Orbitrap allows a good detection of the molecular ions present in a pyrolysis fuel. Isolation of molecular ions with a small mass window shows a less complex signal for pyrolysis PS fuel mainly containing hydrocarbons. This provides an opportunity to gain a deep insight of high molecular weight compounds.

Here, zoom in mass spectra were examined within a mass range of 405-430 Da. As depicted in Figure 6-4, each 1 Da mass range is dominated by one major peak. Specifically, zoom in mass spectra were examined for the selected molecular ions *m/z* 415.2421 Da within a mass window of 0.5 Da. Compositions of $[C_{33}H_{18}+H]^+$, $[C_{31}H_{26}O+H]^+$ and $[C_{32}H_{30}+H]^+$ can be detected. The intensive signal of $[C_{32}H_{30}+H]^+$ outweighs significantly over other signals in this selected mass window.

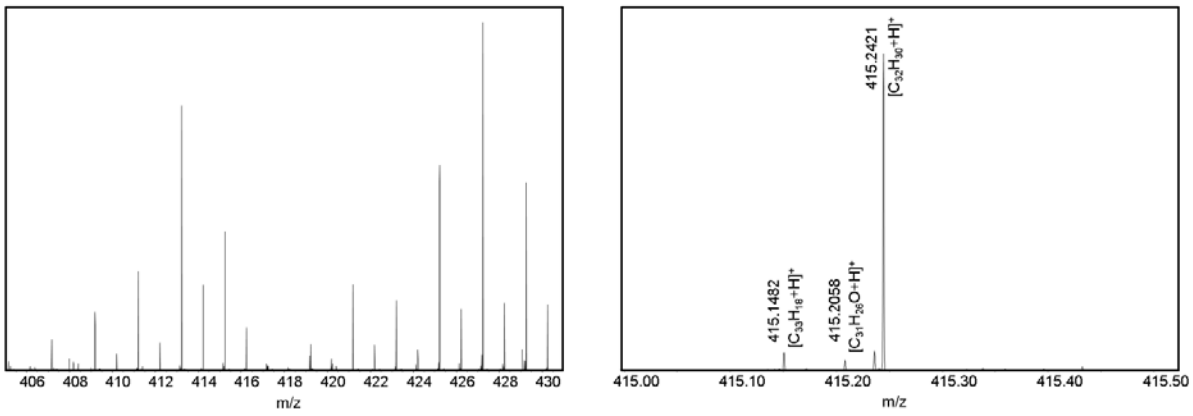

Figure 6-4. Zoom in mass spectra of distillation F3 fraction in a mass range of 405-430 Da (left graph) and 415-415.5 Da (right graph).

After the isolation of ions, a collision induced dissociation (CID) procedure was conducted. The protonated composition, $[C_{32}H_{30}+H]^+$,can be described as styrene tetramer derivatives. The fragmentation pattern can be well interpreted by the presentation of three major different isomers, octa-1,7-diene-1,3,5,7-tetrayltetrabenzene, octa-5,7-diene-1,3,5,7-tetrayltetrabenzene and octa-5,7-diene-1,1,3,7-tetrayltetrabenzene, shown in Figure 6-5. The fragmentation process can happen at various positions. And the fragmentation of such structures can possibly associates with the loss of one aromatic ring, two aromatic rings and three aromatic rings containing motifs. The loss of 78 and 104 corresponding to the loss of C_6H_6 and C_7H_8, yielding fragments ions at 337 and 311, are possible to be observed for all these isomers. The fragment ion at 311 is observed as the base peak. The difference with the loss associated with one aromatic ring motif is likely to be observed at a loss of 118 for isomer octa-1,7-diene-1,3,5,7-tetrayltetrabenzene, 92 for isomer octa-5,7-diene-1,3,5,7-tetrayltetrabenzene and 130 for isomer octa-5,7-diene-1,1,3,7-tetrayltetrabenzene, respectively. The most significant fragmentation difference differentiating with each other can be observed for the loss of two aromatic rings containing motifs. Octa-1,7-diene-1,3,5,7-tetrayltetrabenzene shows a loss of 194, 208 and 222, resulting in a formation of fragment ions at 221, 207 and 193. Octa-5,7-diene-1,3,5,7-tetrayltetrabenzene shows a loss of 196, 206, 210 and 220, resulting in a formation of fragment ions at 219, 209, 205 and 195. Octa-5,7-diene-1,1,3,7-tetrayltetrabenzene shows a loss of 168, 182, 234 and 248, resulting in a formation of fragment ions at 247, 233, 181 and 167.

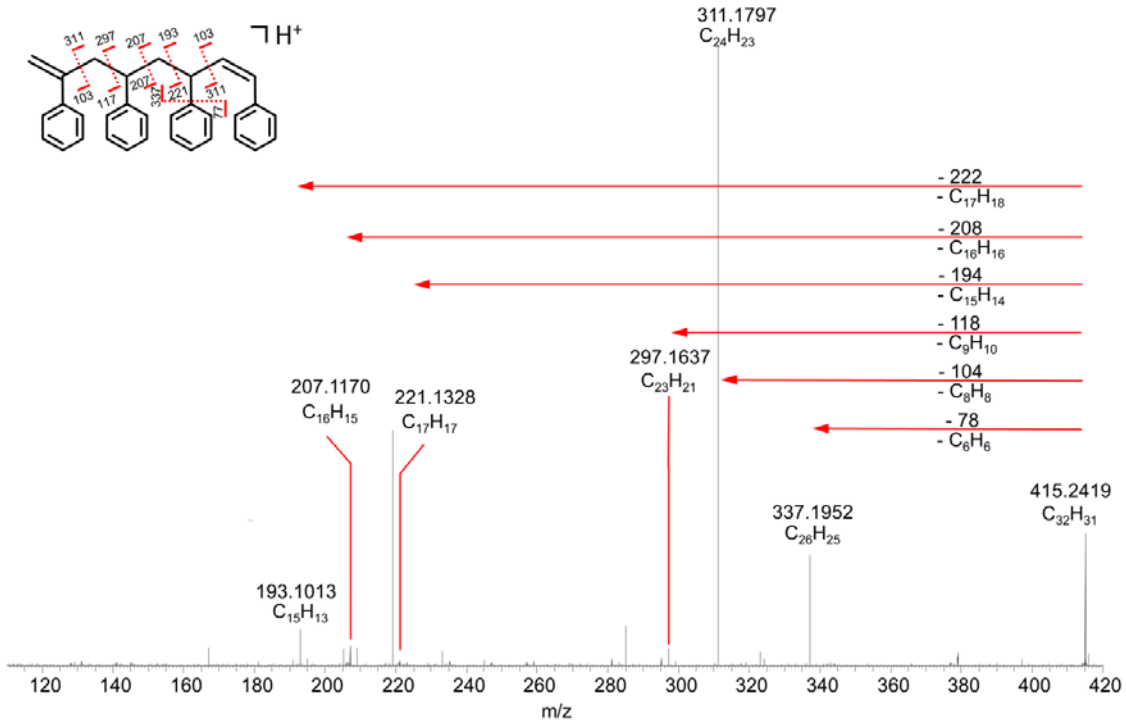

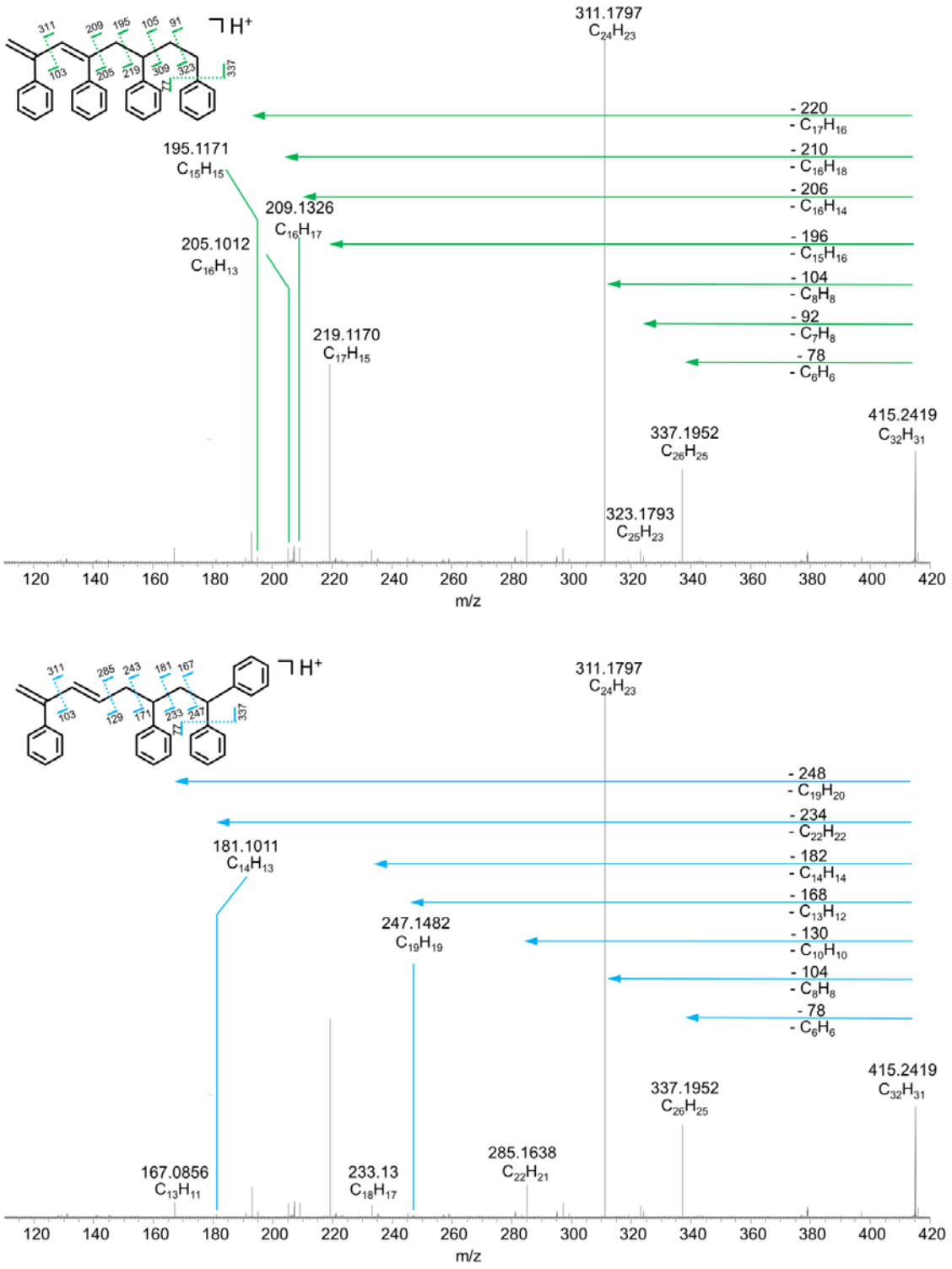

Figure 6-5. High resolution MS/MS spectrum corresponding to protonated composition $[C_{32}H_{30}+H]^+$. Three Possible isomeric structure types (octa-1,7-diene-1,3,5,7-tetrayltetrabenzene, octa-5,7-diene-1,3,5,7-tetrayltetrabenzene and octa-5,7-diene-1,1,3,7-tetrayltetrabenzene from top to down) were proposed with the assignment of corresponding fragment ions.

A pathway is suggested for the formation of these isomers and is described in Scheme 6-3. At a high temperature, polystyrene can go through two step by step radical generations followed

by the removal of a hydrogen radical to form a compound octa-1,7-diene-1,3,5,7-tetrayltetrabenzene. To form octa-1,7-diene-1,3,5,7-tetrayltetrabenzene and octa-5,7-diene-1,1,3,7-tetrayltetrabenzene, additional steps are required after the generation of the second step radical. The radical can undergo 1,5-H shift or 1,5-phenyl shift followed by hydrogen radical removal to generate octa-1,7-diene-1,3,5,7-tetrayltetrabenzene or octa-5,7-diene-1,1,3,7-tetrayltetrabenzene. The process of 1,5-phenyl shift associates the formation of cyclohexane intermediate followed by ring reopening of cyclohexane to reform the phenyl group at a different position.

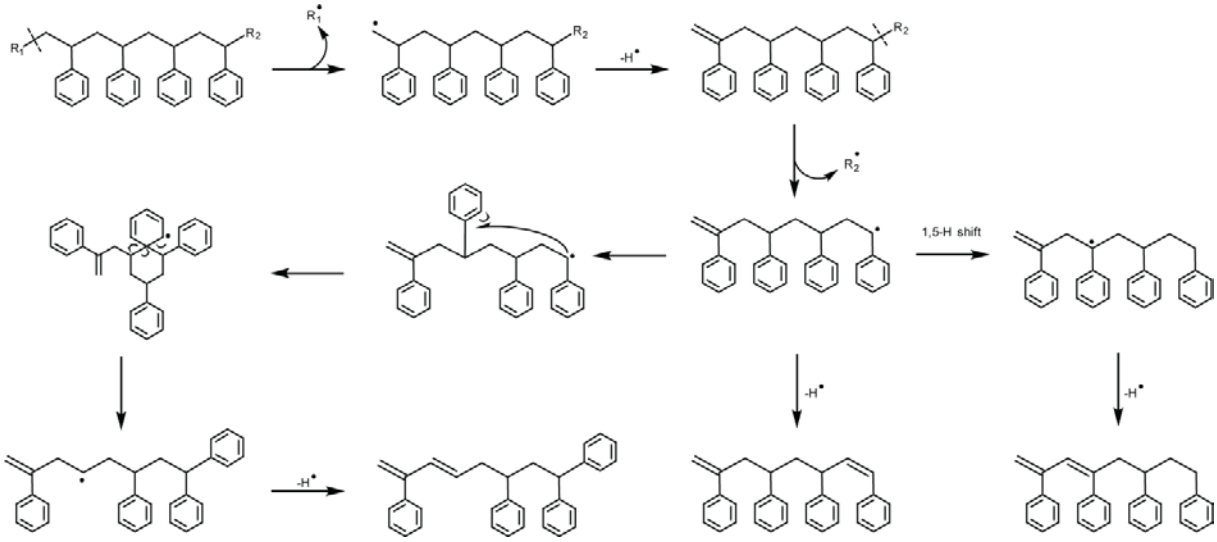

Scheme 6-3. Possible reaction pathway leads to the formation of suggested isomers for chemical composition $C_{32}H_{30}$.

6.5 Conclusion

The complexity of pyrolysis biofuel has been demonstrated previously. However, the complexity of pyrolysis fuel obtained from municipal plastic waste has not beenstudied. This research successfully demonstrates the importance of using complementary analytic techniques (GC-EI-Orbitrap and DI-APCI Orbitrap) to study the complex mixture of pyrolysis fuels from plastic materials such as polystyrene. This can further helps us to gain a deep understanding of the chemical reactions during pyrolysis process.

GC-EI-Orbitrap is suitable for studying low volatile compounds. A very limited number of compounds were revealed by GC-EI-Orbitrap. The result shows only styrene monomer derivatives can be found in both the light (LF) and the heavy fraction (HF) of pyrolysis fuel. The dominance of styrene signal in LF and HF suppresses the identification of heavier

compounds. To address this difficulty, a distillation separation was performed to separate the pyrolysis PS fuel into various fractions. Through this step, several styrene dimer derivatives were additionally revealed by GC-EI-Orbitrap. In comparison with GC-EI-Orbitrap, direct injection of sample ionized by APCI into high resolution mass spectrometry can detect a wide range of chemical compositions. The hydrocarbon compositions detected ranging from styrene monomer derivatives to octamer derivatives. Isolation of molecular ions followed by CID fragmentation allows us to investigate the structures of heavier compounds. One example is given for the structural elucidation of composition $C_{32}H_{30}$, showing three possible isomers exist. A proposed mechanism for the formation of these isomers associate with reaction steps: generation of radical, 1,5-H shift, 1,5-phenyl shift and removal of H radical.

6.6 References

1. Bridgwater, A. V.; Peacocke, G. V. C., Fast pyrolysis processes for biomass. *Renew. Sust. Energ. Rev.* **2000,** *4* (1), 1-73.
2. Azeez, A. M.; Meier, D.; Odermatt, J. r.; Willner, T., Fast pyrolysis of African and European lignocellulosic biomasses using Py-GC/MS and fluidized bed reactor. *Energy Fuels* **2010,** *24* (3), 2078-2085.
3. Duman, G.; Okutucu, C.; Ucar, S.; Stahl, R.; Yanik, J., The slow and fast pyrolysis of cherry seed. *Bioresour. Technol.* **2011,** *102* (2), 1869-1878.
4. Dickerson, T.; Soria, J., Catalytic fast pyrolysis: a review. *Energies* **2013,** *6* (1), 514-538.
5. Mortensen, P. M.; Grunwaldt, J. D.; Jensen, P. A.; Knudsen, K. G.; Jensen, A. D., A review of catalytic upgrading of bio-oil to engine fuels. *Appl. Catal. A Gen.* **2011,** *407* (1-2), 1-19.
6. Zhao, C.; Lercher, J. A., Upgrading pyrolysis oil over Ni/HZSM-5 by cascade reactions. *Angew. Chem. Int. Ed.* **2012,** *124* (24), 6037-6042.
7. Cao, Z.; Xu, Y.; Lyu, P.; Dierks, M.; Morales-García, Á.; Schrader, W.; Nachtigall, P.; Schüth, F., Flexibilization of Biorefineries: Tuning Lignin Hydrogenation by Hydrogen Partial Pressure. *ChemSusChem* **2020**.
8. de Marco Rodriguez, I.; Laresgoiti, M. F.; Cabrero, M. A.; Torres, A.; Chomón, M. J.; Caballero, B., Pyrolysis of scrap tyres. *Fuel Process. Technol.* **2001,** *72* (1), 9-22.
9. Magrinho, A.; Semiao, V., Estimation of residual MSW heating value as a function of waste component recycling. *Waste Manage.* **2008,** *28* (12), 2675-2683.
10. Miskolczi, N.; Angyal, A.; Bartha, L.; Valkai, I., Fuels by pyrolysis of waste plastics from agricultural and packaging sectors in a pilot scale reactor. *Fuel Process. Technol.* **2009,** *90* (7), 1032-1040.
11. Garcia, J. M.; Robertson, M. L., The future of plastics recycling. *Science* **2017,** *358* (6365), 870-872.
12. Al-Salem, S.; Lettieri, P.; Baeyens, J., Recycling and recovery routes of plastic solid waste (PSW): A review. *Waste Manage.* **2009,** *29* (10), 2625-2643.
13. Webb, H. K.; Arnott, J.; Crawford, R. J.; Ivanova, E. P., Plastic degradation and its environmental implications with special reference to poly (ethylene terephthalate). *Polymers* **2013,** *5* (1), 1-18.
14. O'Brine, T.; Thompson, R. C., Degradation of plastic carrier bags in the marine environment. *Mar. Pollut. Bull.* **2010,** *60* (12), 2279-2283.

15. Kale, S. K.; Deshmukh, A. G.; Dudhare, M. S.; Patil, V. B., Microbial degradation of plastic: a review. *J. Biochem. Technol* **2015,** *6* (2), 952-961.
16. da Costa, J. P.; Santos, P. S.; Duarte, A. C.; Rocha-Santos, T., (Nano) plastics in the environment–sources, fates and effects. *Sci. Total Environ.* **2016,** *566*, 15-26.
17. Thompson, R. C.; Swan, S. H.; Moore, C. J.; Vom Saal, F. S., Our plastic age. *Philos. Trans. R. Soc. B* **2009,** *364*, 1973-1976.
18. Hermabessiere, L.; Dehaut, A.; Paul-Pont, I.; Lacroix, C.; Jezequel, R.; Soudant, P.; Duflos, G., Occurrence and effects of plastic additives on marine environments and organisms: A review. *Chemosphere* **2017,** *182*, 781-793.
19. Hahladakis, J. N.; Velis, C. A.; Weber, R.; Iacovidou, E.; Purnell, P., An overview of chemical additives present in plastics: migration, release, fate and environmental impact during their use, disposal and recycling. *J. Hazard. Mater* **2018,** *344*, 179-199.
20. Hertzog, J.; Carré, V.; Le Brech, Y.; Mackay, C. L.; Dufour, A.; Mašek, O.; Aubriet, F., Combination of electrospray ionization, atmospheric pressure photoionization and laser desorption ionization Fourier transform ion cyclotronic resonance mass spectrometry for the investigation of complex mixtures – Application to the petroleomic analysis of bio-oils. *Anal. Chim. Acta* **2017,** *969*, 26-34.
21. Staš, M.; Chudoba, J.; Kubička, D.; Pospisil, M., Chemical characterization of pyrolysis bio-oil: application of Orbitrap mass spectrometry. *Energy Fuels* **2015,** *29* (5), 3233-3240.
22. Tessarolo, N. S.; Silva, R. V.; Vanini, G.; Casilli, A.; Ximenes, V. L.; Mendes, F. L.; de Rezende Pinho, A.; Romão, W.; de Castro, E. V.; Kaiser, C. R., Characterization of thermal and catalytic pyrolysis bio-oils by high-resolution techniques: 1H NMR, GC× GC-TOFMS and FT-ICR MS. *J. Anal. Appl. Pyrolysis* **2016,** *117*, 257-267.
23. Adrados, A.; de Marco, I.; Caballero, B. M.; López, A.; Laresgoiti, M. F.; Torres, A., Pyrolysis of plastic packaging waste: A comparison of plastic residuals from material recovery facilities with simulated plastic waste. *Waste Manage.* **2012,** *32* (5), 826-832.
24. Demirbas, A., Pyrolysis of municipal plastic wastes for recovery of gasoline-range hydrocarbons. *J. Anal. Appl. Pyrolysis* **2004,** *72* (1), 97-102.
25. Ma, C.; Yu, J.; Yan, Q.; Song, Z.; Wang, K.; Wang, B.; Sun, L., Pyrolysis-catalytic upgrading of brominated high impact polystyrene over Fe and Ni modified catalysts: Influence of HZSM-5 and MCM-41 catalysts. *Polym. Degrad. Stab.* **2017,** *146*, 1-12.
26. Dück, R.; Wulf, V.; Geißler, M.; Baier, H.-U.; Wirtz, M.; Kling, H.-W.; Gäb, S.; Schmitz, O. J. J. A.; chemistry, b., Combination of chemical and electron-impact ionisation with GC× GC–qMS for characterization of fatty alcohol alkoxylate polymers in the low-molecular-weight range up to 700 Da. **2010,** *396* (6), 2273-2283.
27. Li, D.-X.; Gan, L.; Bronja, A.; Schmitz, O. J., Gas chromatography coupled to atmospheric pressure ionization mass spectrometry (GC-API-MS). *Anal. Chim. Acta* **2015,** *891*, 43-61.
28. Gaspar, A.; Schrader, W., Expanding the data depth for the analysis of complex crude oil samples by Fourier transform ion cyclotron resonance mass spectrometry using the spectral stitching method. *Rapid Commun. Mass Spectrom.* **2012,** *26* (9), 1047-1052.
29. Gaspar, A.; Zellermann, E.; Lababidi, S.; Reece, J.; Schrader, W., Impact of different ionization methods on the molecular assignments of asphaltenes by FT-ICR mass spectrometry. *Anal. Chem.* **2012,** *84* (12), 5257-5267.
30. Vetere, A.; Schrader, W., Mass Spectrometric Coverage of Complex Mixtures: Exploring the Carbon Space of Crude Oil. *Chemistry Select* **2017,** *2* (3), 849-853.
31. Ayala-Cabrera, J.; Lipok, C.; Moyano, E.; Schmitz, O.; Santos, F., Atmospheric pressure ionization for gas chromatography-high resolution mass spectrometry determination of polychlorinated naphthalenes in marine sediments. *Chemosphere* **2021,** *263*, 127963.

32. Aldrich, S. Pressure-Temperature Nomograph Interactive Tool. https://www.sigmaaldrich.com/chemistry/solvents/learning-center/nomograph.html.

Chapter 7 General conclusion

The last 200 years saw an increased consumption of fossil fuel, which until now still remains to be the dominant energy source globally. Overconsumption of fossil fuel not only raises a big concern of depletion, but also causes a big issue of environment pollution and global warming. Moreover, over dependency on fossil fuel for economic growth poses a threat to energy and national security for most nations as well because fossil fuel is an unequal distributed resource and mainly concentrated on a few specific regions. Turning to renewable energy sources (e.g., biomass) or household waste as a resource for energy production and consumption helps to address these concerns in an environmentally friendly and sustainable manner and additionally leads to a reduced production of waste. Among energy production techniques, pyrolysis process raises a worldwide interest from researchers and industry as it is a simple but promising technique capable of producing transport fuels in a large scale level.

The aim of this work is to study the pyrolysis of municipal solid waste including biomass and plastic materials and to gain a detailed understanding of the transformation reaction using sophisticated analytical methods.

To understand the biofuel system, first, a highly complex mixture, biofuel derived from biomass pyrolysis process, was analyzed by using ultra high resolution mass spectrometry in combination with complementary soft ionization technique (APPI, APCI and ESI). A total number of 34472 unique compositions were detected. A wide oxygen atoms distribution can be observed, with a highest oxygen atoms value of 18, 17, 24 and 26 for APPI(+), APCI(+), ESI(+) and ESI(-), respectively. The high oxygen content contained in initial produced pyrolysis biofuel has negative effects, low heating value, high acidity, corrosiveness, instability et al. Therefore, it is generally classified as a low quality type fuel, which has to be upgraded. In this study, the limitation here is that we use the pyrolysis biofuel obtained from Aachen University. A better understanding of pyrolysis chemical change cannot be achieved in this stage.

Thus, we developed our own lab scale pyrolysis setup to obtain the pyrolysis biofuel. Lignin, one major part of biomass, was used as our starting material for pyrolysis process. The chemical compositions of lignin and its corresponding biofuel reveals that the maximum oxygen atoms per molecule decreased from 19 to 16 during the pyrolysis process, underlining the degradation of big polymers to relative smaller molecules. The loss of oxygen could be associated with the loss of water, carbon dioxide or methanol. However, the same result was

achieved as in a previous study that high oxygen content still resided in the pyrolysis biofuel. To address this problem, an upgrading process (catalytic hydrotreating reaction) was applied. The result shows a significant oxygen removal can be achieved with hydrocarbon class detected as the most abundant class. A maximum of five oxygen atoms per molecule was obtained with low intensity after upgrading process.

Later, we shift our interest to different starting materials for the pyrolysis process. Plastic waste produced from fossil fuel is a misplaced valuable energy source, which typically goes to landfilling, damping into ocean and combustion. In this part, a variety of common plastic materials, including PP, PE, PET, PVC and PS, were investigated. The pyrolysis process shows to be an efficient way to transform plastic waste into fuels. Pyrolysis products distribution of gas, condensed product and residue vary significantly depending on the plastic types and pyrolysis conditions. A further deep understanding of plastic fuel pyrolysis system can be gained by the structural studies conducted by GC-EI-Orbitrap. A corresponding mechanism was revealed, associating with the reactions such as polymer chain scission, beta-scission, beta-H abstraction, di-radical cyclization, di-radical recombination and Diels-Alder reactions. This study also demonstrates that not all plastic waste type is suitable to be used as feedstock for pyrolysis process to generate fuel as pyrolysis of PVC generates a high yield of useless, corrosive and toxic gas, HCl.

Therefore, we further focus on the energy production from only hydrocarbon containing plastics. At the same time, we not only investigate the pyrolysis process of single plastic, but complex plastic mixtures as well, both of which gave an efficient energy transformation. The obtained LDPE plastic fuel studied by GC-EI-Orbitrap shows it has a wide compounds distribution covering from gasoline, diesel to even wax range compounds. A distillation process was successfully implemented for the separation of initial pyrolysis produced plastic fuels into three different fuel types, gasoline-type, diesel-type and wax-type, indicated by semi-quantification of carbon atoms distribution.

In the last part, we address the importance of using complementary analytic techniques (GC-EI-Orbitrap and DI-APCI Orbitrap) to study the complex mixture of pyrolysis plastic PS fuel. This can further help in gaining a better understanding of the chemical reactions that occur during the pyrolysis process. GC-EI-Orbitrap is suitable for studying volatile and low molecular weight compounds with high mass resolution and accuracy. Styrene monomer and dimer derivatives were found in the original pyrolysis fuel and distillation fraction by this method. In comparison, DI-APCI Orbitrap can discover a broad range of chemical

compositions from volatile (styrene monomer derivatives) to non-volatile compounds (styrene octamer derivatives). Three isomers for non-volatile styrene tetramer derivative composition $C_{32}H_{30}$ were successfully discovered by isolation of protonated molecular ion m/z 415.2421 Da followed by CID fragmentation. A corresponding mechanism was proposed based on these isomer structures.

Overall, these results show that municipal waste is a resource that can be better used for the production of fuels instead of dumping it in landfills. It is too valuable a resource and in addition to recycling it allows a final enduse of different plastic materials.

Chapter 8 Appendix

8.1 List of abbreviations

%	Percentage
Δm	mass difference
ACEA	European automobile manufacturers association
APCI	atmospheric pressure chemical ionization
API	atmospheric pressure ionization
APPI	atmospheric pressure photo ionization
CID	collision induced dissociation
CRM	charge residue model
CV	calorific value
Da	Dalton
DBE	double bond equivalent
DSC	differential scanning calorimetry
DTG	differential thermogravimetry
e.g.	for example
EI	electron ionization
EN	European norm
ESI	electrospray ionization
et al.	and so on
eV	electron volt
FID	flame ionization detector
FT	fourier transform
FWHM	full width at half maximum

g	Gram
GC	gas chromatography
GC x GC	two-dimensional gas chromatography
h	Hour
H x W	height x width
HDO	Hydrodeoxygenation
HDPE	high density polyethylene
HRMS	high resolution mass spectrometry
ICR	ion cyclotron resonance
ID	inner diameter
IE	ionization energy
IEM	ion evaporation model
IR	Infrared
kg	Kilogram
kV	Kilovolts
L	Liter
LC	liquid chromatography
LDPE	low density polyethylene
LTQ	linear ion trap quadrupole
m	Meter
m/z	mass-to-charge ratio
mbar	Millibar
mg	Microgram
min	Minute
MJ	Megajoule

mL	Milliliter
mm	Millimeter
MPa	Megapascal
nm	Nanometer
NMR	nuclear magnetic resonance
^{o}C	degree Celsius
PAH	polycyclic aromatic hydrocarbon
PET	Polyester
PP	Polypropylene
ppm	parts per million
PS	Polystyrene
PVC	polyvinyl chloride
R	Resolution
RF	Radiofrequency
RIC	resin identification code
s	Second
SEM	scanning electron microscopy
SPI	society of plastic industry
TEM	transmission electron microscopy
TG	Thermogravimetry
TIC	total ion current
um	Micrometer
UV	Ultraviolet
W	Watt
wt%	weight percentage

XRPD	X-ray powder diffraction
μL	Microliter
ω_z	angular frequency

8.2 List of figures

8.3 List of tables

8.4 List of schemes

8.5 List of publications

Publications in peer-reviewed journals

1. Cao, Z.; **Xu, Y.**; Lyu, P.; Michael, D.; Garcia, A.; Schrader, W.; Nachtigall, P.; Schüth, F., Flexibilization of biorefineries: Tuning lignin hydrogenation by hydrogen partial pressure. *ChemSusChem* **2020**, 13, 1-7.
2. **Xu, Y.**; Schrader, W., Studying the complexity of biomass derived biofuels, will be submitted to *Energies*.
3. **Xu, Y.**; Schrader, W., Studying the thermal transformation of lignin into fuels using high solution mass spectrometry, will be submitted to *Rapid Commun. Mass Spectrom.*
4. **Xu, Y.**; Schrader, W., Converting municipal plastic waste into useful transport fuels using a pyrolysis process, will be submitted to *ChemSusChem*.
5. **Xu, Y.**; Schrader, W., *Waste-to-Fuel*: Producing gasoline and diesel type fuels derived from low value polymers by successive pyrolysis and distillation, will be submitted to *ACS Applied Energy Materials*.
6. **Xu, Y.**; Schrader, W., Comprehensive characterization of pyrolysis PS fuel by using GC-EI-Orbitrap and DI-APCI Orbitrap, will be submitted to *Fuel*.

Posters

1. **Xu, Y.**; Schrader, W., Investigation of gasoline and diesel range fuels derived from plastics using GC-EI-Orbitrap, 1 – 4 March **2020**, Münster, Germany
2. **Xu, Y.**; Schrader, W., Characterization of trash fuel using GC-EI-High resolution-MS, 52nd German mass spectrometry society annual meeting, 10. – 13. March **2019**, Rostock, Germany
3. **Xu, Y.**; Schrader, W., Ultra-high resolution mass spectrometric characterization of a pyrolysis biofuel by using different ionization techniques and spectra-stitching method, European mass spectrometry conference, 11 – 15 March **2018**, Saarbrücken, Germany
4. **Xu, Y.**; Schrader, W., Characterization of fast-pyrolysis bio-oil, 50th German mass spectrometry society annual meeting, 5 – 8 March **2017**, Kiel, Germany

Oral presentations

1. **Xu, Y.**; Schrader, W., Molecular characterization of a pyrolysis biofuel by FT MS, 2nd GDCh division meeting of chemistry and energy, 30. Septemper – 2. October **2018**, Mülheim an der Ruhr, Germany
2. **Xu, Y.**; Cao, Z.; Schüth, F.; Schrader, W., Detailed molecular characterization of the upgrading process of pyrolysis oil by ultrahigh resolution mass spectrometry, 22nd International mass spectrometry conference, 26-31 August, **2018**, Florence, Italy

8.6 Acknowledgments

I would like to express my great appreciation to my thesis supervisor Prof. Dr. Wolfgang Schrader for providing me such a precious opportunity to conduct the research in Max-Planck-Institut für Kohlenfroschung. I feel so lucky to have the great chance to learn multiple techniques of different types of mass spectrometers in his group. During the research here for my Ph.D. degree, he has endeavored so much effort and time to teach me how to develop scientific and critical thinking as well as problem-solving skills, which would be quite helpful to my future work and career. Compared to my simple while immature skills and limited knowledge, he enlightens me to manage the projects by way of a simple, while quite useful principle, which is “learning things by practical doing”. He always inspired me that if you do not take action to do it, you will never know it. At the same time, I sincerely appreciate Prof. Dr. Wolfgang Schrader for giving me freedom to conduct the research according to my own interest here. Meanwhile, I would like to express my great gratitude for my supervisor’s patience to instruct every detailed information to me during my research all these years.

I also would like to express my great appreciation to Prof Dr. Oliver J. Schmitz for being my second supervisor. I sincerely appreciate for his precious time reviewing my thesis and providing constructive suggestions for me. I also would like to appreciate Prof. Dr. Jochen Gutmann for being the Chairman of my thesis committee. Thanks very much for all your help with my thesis defense.

I want to show my thanks to the big lovely family of mass spectrometry group, Xuxiao Wang, Alessandro Vetere, Aikaterini Kondyli, Ruoji Luo, Zahra Farmani, Ilker Satilmis, Oleksandra Kuzmich, Haifa Shamseldin, David Hamacher, Robert Kalnins, Jens Dreschmann, Martin Ohrt, Andrei Jarashneli, Mrion Blumenthal, Daniel Margold, Simone Marcus, Frank Kohler, Dirk Kampen, Dino Rechter, Christopher Grundmann, Nadine Haupt, Nico Tchorz, Daniel Dotauer and Marc Strack, for bringing me so much joy (christmas parties, group travelling and activities, students’ gathering parties, cake seminars) during my PhD study in Germany. I have learned a lot from all of you, including German learning, lab safety concerns, technical skills, et al. Meanwhile, such an international group in the lab which gathers people from multiple countries has created the wonderful chance for me to experience the cultural difference, which would be valuable experience and unforgettable memory in my life, and I will always treasure the time staying together with this lovely family.

I would like to express my special gratitude to my wife, Liping Chen, who has kept accompany with me for more than five years even in the situation that we have been separating from each other and staying in different countries all these years around, which has great difficulty for normal people to sustain the relationship in the current daily lives. Despite of the lack of my accompany with her by her side, she still has great faith on me and insists on supporting my work and life in every aspect without leaving me alone, although that would be much better for her in order to live an easier life. I sincerely appreciate her absolute love, understanding and great encouragement as well as absolute belief in me during my study for my PhD degree in Germany all along these years. The special experience of separation with different time zones and long distances makes us believe that if we could make through such kind of hardship and challenges we have met during these years, we can achieve everything together in the future. I sincerely treasure every moment I spent with my wife together. And thanks to my parents, who raise me up and give me the freedom as well as respect on the choices whatever I have ever made. They are always there by my side and help me all through the years.

Last but not the least, thanks to all the others, who I might forget to mention in this thesis, but have contributed to my PhD study. I sincerely appreciate it a lot!